

UNCLASSIFIED

AD 4 2 1 5 9 0

DEFENSE DOCUMENTATION CENTER

FOR

SCIENTIFIC AND TECHNICAL INFORMATION

CAMERON STATION, ALEXANDRIA, VIRGINIA



UNCLASSIFIED

NOTICE: When government or other drawings, specifications or other data are used for any purpose other than in connection with a definitely related government procurement operation, the U. S. Government thereby incurs no responsibility, nor any obligation whatsoever; and the fact that the Government may have formulated, furnished, or in any way supplied the said drawings, specifications, or other data is not to be regarded by implication or otherwise as in any manner licensing the holder or any other person or corporation, or conveying any rights or permission to manufacture, use or sell any patented invention that may in any way be related thereto.

M R D d i v i s i o n

GENERAL AMERICAN TRANSPORTATION CORPORATION
7501 NORTH NATCHEZ AVENUE • NILES 48, ILLINOIS • NILES 7-7000



Final Technical Report
MECHANICS OF PENETRATION
VOLUME II
SINGLE AND LAMINATED PLATES

Astia Availability Notice: "QUALIFIED
REQUESTORS MAY OBTAIN COPIES OF THIS
REPORT FROM ASTIA."

Prepared for
Quartermaster Research and Engineering Command
Natick, Massachusetts

Contract DA-19-129-QM-1542

Project Nr. 7-80-05-001

Prepared by
MRD Division
General American Transportation Corporation

MR 1127

31 December 1962
MRD DIVISION
GENERAL AMERICAN TRANSPORTATION CORPORATION
7501 NORTH NATCHEZ AVENUE, NILES 48, ILLINOIS

FOREWORD

MRD Division of General American Transportation Corporation submits this final technical report on Phase III of Contract DA-19-129-QM-1542 entitled, "The Mechanics of Penetration". The work on Phases I and II was previously reported in Volume I.

The investigation was carried out under the direction of L.E. Fugelso. Acknowledgment is made to P.G. Boekhoff, D.H. Duel, H.M. Gruen, D.A. Davidson, and A.A. Arentz, Jr. of MRD for their contributions to this report and Mr. A.L. Alesi, project engineer for the Quartermaster Research and Engineering Command, for his helpful guidance.

Prepared by:

MRD Division
GENERAL AMERICAN TRANSPORTATION CORP.



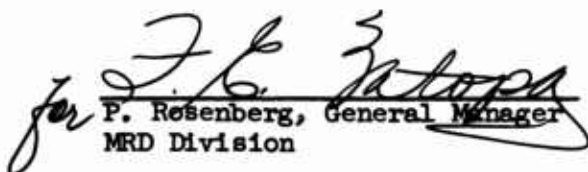
L.E. Fugelso
Research Engineer

REVIEWED BY:



G.L. Neidhardt, Group Leader
Engineering Mathematics Group

APPROVED BY:



P. Rosenberg, General Manager
MRD Division

MRD DIVISION
GENERAL AMERICAN TRANSPORTATION CORPORATION

ABSTRACT

Ballistic resistance of thin metallic plates, both single plates and laminates, to projectile impact is investigated. Two mathematical models are formulated, each emphasizing a critical aspect of the deformational process.

The first model considers failure by high tensile or shear stress in the transient stress wave that propagates across the plate, while the second model considers failure by sustained plastic shear flow.

Engineering models of fracture and flow under high speed impact are evaluated, using the continuum theory of dislocations. These models are used in the analysis of the modes of failure. Critical impact velocities for failure are calculated and characterized as a function of dynamic material properties.

The results of this study indicate that there is a need for research on the determination of high-speed properties of materials. Improved armor materials can be realized through materials research based upon theories developed herein.

Further analytic research on stress-wave propagation and failure in materials other than metals is advised. Both the present analytic work and future studies should be used to formulate and carry out an experimental program.

MRD DIVISION
GENERAL AMERICAN TRANSPORTATION CORPORATION

TABLE OF CONTENTS

<u>SECTION</u>		<u>Page</u>
	FOREWORD	11
	ABSTRACT	111
1	INTRODUCTION	1
	1.1 Objectives	2
	1.2 Previous Work	3
	1.3 The Physical Phenomena of Fracture	4
	1.4 Scope	11
2	PLASTIC DEFORMATION OF METAL UNDER TRANSIENT LOADS	12
	2.1 Constitutive Equation	12
	2.2 Dynamic Yield Stresses	25
3	FRACTURE	26
	3.1 Mathematical Model for Fracture under Transient Loading	28
	3.2 Relation of the Fracture Criteria to Plastic Strain	36
4	TRANSIENT WAVE ANALYSIS	42
	4.1 Equation of Motion	42
	4.2 Boundary Conditions	43
	4.3 Dimensionless Variables	44
	4.4 Equations in Dimensionless Form	44
	4.5 General Integral Solution	45
	4.6 Specific Integral Solution	46
	4.7 Analytic Reduction of Integral Solution	48

MRD DIVISION
GENERAL AMERICAN TRANSPORTATION CORPORATION

TABLE OF CONTENTS (Cont.)

<u>SECTION</u>		<u>Page</u>
	4.8 Numerical Integration	52
	4.9 Reflection of Stress Wave	53
	4.10 Wave Analysis for Laminated Plate	59
	4.11 Method of Solution	59
	4.12 Numerical Evaluation	60
	4.12.1 Input Data	60
	4.12.2 Outline of Computer Program	61
	4.12.3 Computational Portion of Program	63
	4.12.4 Results of Numerical Evaluation	67
	4.13 Qualitative Discussion of Results	67
	4.14 Implications on Ballistic Resistance of Plates	75
5	MODEL FOR SHEAR FAILURE OF THE PLATE	86
	5.1 Historical Background	86
	5.2 Mathematical Model	87
	5.3 Numerical Method of Solution	94
	5.4 Results	97
	5.5 Summary	126
6	COMBINATION OF RESULTS	131
7	CONCLUSIONS AND RECOMMENDATIONS	133
	7.1 Survey of Results	133
	7.2 Design Implications	135
	7.2.1 Materials	136
	7.2.2 Geometry	137

MRD DIVISION
GENERAL AMERICAN TRANSPORTATION CORPORATION

<u>SECTION</u>	<u>TABLE OF CONTENTS (Cont.)</u>	<u>Page</u>
7.2.3	Local Effects	138
APPENDIX A	FORMAL INTEGRAL SOLUTION FOR STRESSES IN A LAMINATED PLATE	
BIBLIOGRAPHY		
APPENDIX B (Bound separately)		

MRD DIVISION
GENERAL AMERICAN TRANSPORTATION CORPORATION

Section 1

INTRODUCTION

Throughout the annals of ancient history there are many references to the arms and armor which great armies bore in battle. Horner makes reference to arms and armor made of bronze and occasionally of iron. Body armor at first consisted merely of shields and, a little later, helmets. It was not too long however before breast plates and shin guards were in vogue. During the middle ages, complete body armor was the standard uniform of the equestrian knight; indeed, even his horse was protected by form-fitting metal plates. It did not take too long a period of time before the suits of armor became vehicles for artistic expression in addition to their protective purposes. Examples of this form of art are now the prizes of many art collectors. Examination of these relics of a bygone era will show why they were reserved only to horse-borne warriors. The wearer was not very mobile. It was long after the use of such armor became general that it was doomed to become obsolete. This was brought about first by the efficiency of the English long bow and finally by the coming of age of firearms.

As firearms came into increasing use and brought about a new concept of warfare, one which depended on a mobile infantryman, body armor became increasingly unpopular. The greater and greater muzzle velocities which firearms were becoming capable of were decreasing the feasibility of individualized protection. In order to stop a high-velocity bullet, the armor would have had to be so thick that it would be impossible for a man to carry and still be mobile.

The concept of body armor has not been abandoned, however. The quest for an

MRD DIVISION
GENERAL AMERICAN TRANSPORTATION CORPORATION

individual protective shield that will be effective against modern arms and yet leave its wearer completely mobile still continues. Up to very recent times, this quest has been unidirectional in approach emphasizing, almost exclusively, the experimental viewpoint. It does not come as a complete surprise that the results of this approach have not been overly gratifying.

Throughout the history of science there have been many proponents of the strictly experimental approach as well as the strictly contemplative or theoretical approach to given problems. The ultimate lesson to be learned from this is that neither is completely adequate by itself. And so it follows that a wedding of these two approaches is the best way to solve a given practical problem.

Achieving such a union is not an easy task, however. There is generally a wide gap existing between theory and experiment. This is mainly due to the difference of interests of the theoretician and experimenter in addition to at least a modicum of mutual distrust. The present study is directed toward the development of an adequate theory that will enable the experience of existing experimental studies to be given a more meaningful interpretation. In addition, and perhaps more important, the goal of the present theoretical endeavor is to provide a more fruitful basis for future experimentation.

Thus the present study is intended to be the first theoretical link in a balanced overall program directed toward the design of personnel armor that will be effective against modern firearms.

1.1 Objectives

In view of the state of the art of body-armor design that was current when the present study began, it was not difficult to determine the objectives of the

MRD DIVISION
GENERAL AMERICAN TRANSPORTATION CORPORATION

program. Indeed, the objectives were dictated by the circumstances,

First of all, a theory must be developed to describe what occurs when a bullet strikes a piece of armor. This theory must be based on the basic concepts of the physical laws which govern the behavior of materials under the conditions of impact. The role that the properties of the materials involved play must be determined. The study must ascertain which properties or combinations of properties have the greatest bearing on the adequacy of the armor to do its job. The theory developed must, wherever possible, take into account the existing results of the experimenters in order that there be communication with the realities of experience.

Finally, the theory must point out the path for future experiments. It must answer the question of the experimenter, "What area have I failed to explore?" Then, when the experimenter has responded with new experiments and the theoretician has joined him in reaching a compatible answer to the problem of penetration, the designer may, with knowledge, approach his task.

1.2 Previous Work

As may be noted from the title of this report, there has been a previous volume dealing with the mechanics of penetration. It was the task of Volume I to break the ground for the theory of penetration. Outside of a few voices that had cried in the wilderness (notably Bjork⁽⁵⁾, and Hopkins and Kolsky⁽¹⁷⁾) there had been little done in the way of theoretical work on the problem.

Volume I gave the results of the first year's study of the mechanics of

MRD DIVISION
GENERAL AMERICAN TRANSPORTATION CORPORATION

penetration. While this preparatory work took cognizance of the aspects of plastic flow involved in the problem, it did not attempt to solve the problem in terms of plasticity. This would have been too great a bite for an area in which so little work had been done. Instead, the phenomena were investigated from the viewpoint of elasticity theory. By using this approach, a framework for more advanced study was constructed. Qualitative descriptions and quantitative boundaries were established. The basic mechanism of the phenomena could be worked out without becoming entangled in the intricate niceties of plastic theory.

This volume, based on the ground work of Volume I, now attacks the full-blown problem and considers the effects of plastic flow. It investigates the effects of plastic deformation, fracture, and the two types of failure that may occur, tensile failure or shear failure. It considers the combined effect of these two types of failure when applied to a given problem. The theory developed will be applied to the penetration of laminated metallic plates. Recommendations for future work in the area of armor penetration are made based on the conclusions that may be drawn from this study.

1.3 The Physical Phenomena of Fracture

When a target is impacted by a projectile, a number of physical phenomena may occur, depending on the magnitude and direction of the impact velocity, and on the materials and geometries of the target and projectile. For prescribed impact conditions, the relative importance of these phenomena will determine the nature of the impact and, therefore, such quantitative aspects

MRD DIVISION
GENERAL AMERICAN TRANSPORTATION CORPORATION

as momentum transfer, partition of the projectiles, kinetic energy into other forms, and the type and extent of fracture. For a specific target and projectile, the impact velocity alone will determine the character of the impact, and, consequently, it is possible to divide the general impact problem into a number of regimes that depend on the impact velocity. In each of these regimes, a different phenomenon or combination of phenomena is important in controlling the physical processes that occur. There is, of course, considerable overlap between the regimes, but, nevertheless, they are a valuable way of describing the various kinds of impact. In order of increasing impact velocity, the regimes are:

1. Elastic Impact
2. Plastic Impact
3. Hydrodynamic Impact
4. Superseismic Impact
5. Explosive Impact

The first of these regimes, elastic impact, is characterized by the fact that the stresses produced by impact in the target and in the projectile are not above the elastic limit, and the impact process is, consequently, fully reversible. For this type of impact, the kinetic energy of the impinging projectile is usually converted almost entirely into elastic strain energy in the target and projectile. Elastic stress waves will be generated in the target, consisting of primary (or dilatational) waves, secondary (or distortional) waves, and Rayleigh surface waves. However, the duration of impact at the low velocities associated with elastic impact is so long that there is time for many reflections of the waves within the target and projectile, and a

MRD DIVISION
GENERAL AMERICAN TRANSPORTATION CORPORATION

quasi-static stress distribution is effectively established, with very little of the total energy converted into the kinetic energy of elastic waves. A reasonably accurate description of this type of impact can be obtained by presuming that the entire kinetic energy of the incoming projectile is converted into the strain energy of a static stress distribution as given, for instance, by the Hertz formulation for contact stresses.

When the impact velocity is increased beyond the critical velocity where the elastic limit of either the target or projectile is exceeded, the stress distribution will be partly elastic and partly plastic, which is typical of the regime of plastic impact. The critical velocity that separates the elastic and plastic regimes depends markedly on the materials and also on the geometries of the target and projectile. It has been found, for example, that the critical velocity for a 1/4-inch diameter steel ball impacting normally onto a large steel plate is only about 0.15 m/sec⁽³⁴⁾. For the normal impact of two flat-ended steel cylinders, however, the critical velocity is in excess of 60 m/sec. The critical velocity for plastic impact also depends, of course, on the elastic limit of the materials of the target and projectile, and if the materials behave in brittle rather than a ductile manner, no plastic regime will exist.

The regime of hydrodynamic impact is characterized by stresses that are far in excess of the yield strength of the materials, with the result that, for a part of the time of impact, the materials flow freely. The sequence of such an impact is depicted schematically in Figure 1.1⁽¹¹⁾. Immediately

MRD DIVISION
GENERAL AMERICAN TRANSPORTATION CORPORATION

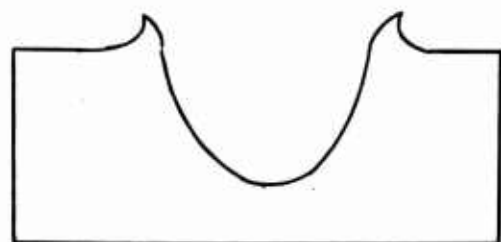
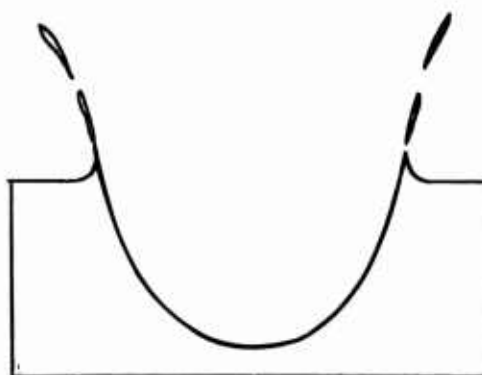
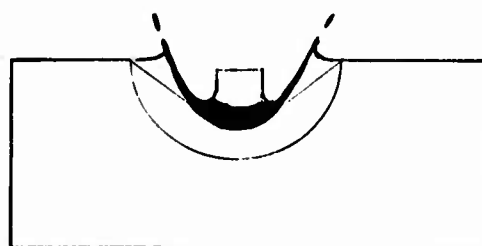
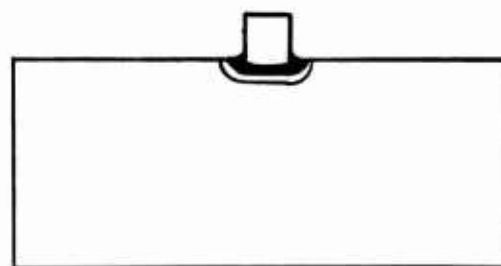
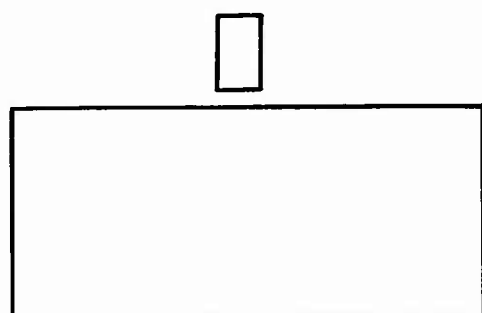


Figure 1.1 - Sequence of Hydrodynamic Impact

MRD DIVISION
GENERAL AMERICAN TRANSPORTATION CORPORATION

after contact, a region of extremely high compressive stress is created near the projectile-target interface, and a compressive wave is initiated. Shortly thereafter, the material of both target and projectile begin to flow, and the compressive wave and shear wave propagate into the body of the target. The flow of the projectile material continues until the projectile is entirely dissipated, and the flow in the target continues for a somewhat longer period because of the very high flow velocities induced by the projectile. Finally, the crater formed by the impact contracts slightly because of elastic (and some plastic) rebound. This type of impact can be described theoretically by hydrodynamic calculations, which assume that the materials behave as fluids with no effective resistance to distortion. Such calculations are accurate in determining the flow patterns and stress distribution when the stress levels are well above the yield strength of the materials, but they are not accurate in predicting the later stages of the impact (afterflow and rebound) where the yield strengths are important.

The sequence of events that comprise an impact in the superseismic regime is shown in Figure 1.2. The initial stage of high compressive stress (in the megabar range) is similar to the corresponding state of hydrodynamic impact, except for considerably higher stress levels. The next stage, however, is different in that no compressive wave will propagate away from the expanding cavity into the body of the target material, because the cavity is expanding at superseismic speed. The lateral and rearward flow of the materials continues in the same general manner as for hydrodynamic impact, except for the higher flow velocities. Most importantly, the flow can occur only within the super-

MRD DIVISION
GENERAL AMERICAN TRANSPORTATION CORPORATION

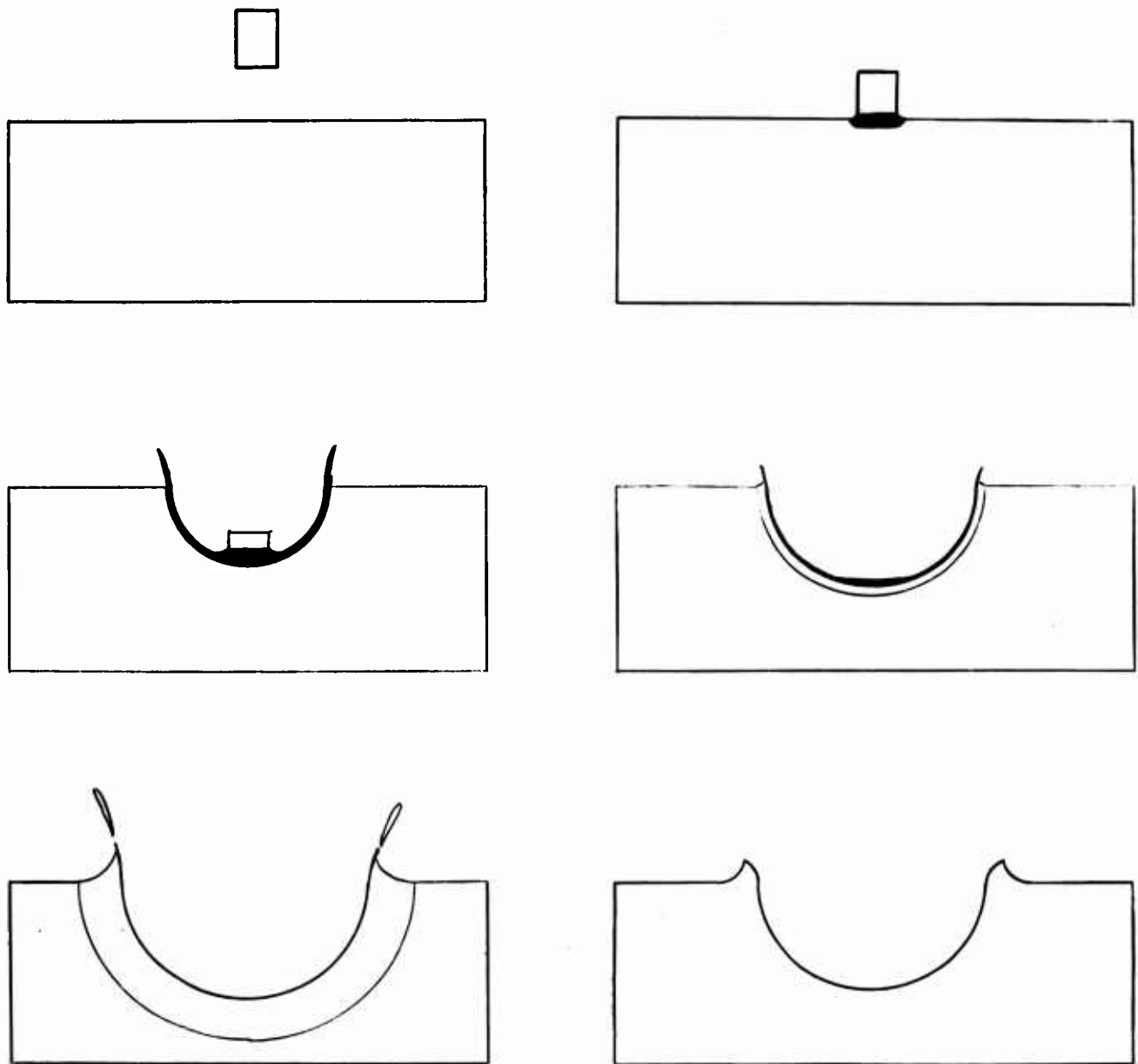


Figure 1.2 - Sequence of Superseismic Impact

MRD DIVISION
GENERAL AMERICAN TRANSPORTATION CORPORATION

seismically expanding cavity, and since the downward penetration of the projectile is limited by the seismic velocity, the flow of material is general throughout a hemispherical region. As a result, the final crater of a super-seismic impact is typically hemispherical.

The regime of explosive impact is characterized by impact velocities high enough to vaporize material of the target and projectile. Under these conditions, the impact problem is akin to a surface explosion, wherein the momentum transfer and stresses are produced by the high pressure of vaporized materials.

MRD DIVISION
GENERAL AMERICAN TRANSPORTATION CORPORATION

1.4 Scope

In Section 2, a qualitative description of plastic deformation is presented. The mathematical form of the constitutive equation is given and the evaluation of specific models is made. An interpretation of dynamic yield strength is given and discussed. The material contained in this section represents original work in this field.

The subject of fracture is treated in Section 3. The Griffith theory of fracture is explained and the growth of macro-holes is discussed for the special cases of interest. The relationship of time-to-fracture to the problem of penetration is then explored.

Sections 4, 5 & 6 deal with the subject of failure of both single and laminated plates. Both tensile and shear failure and a combination of these are investigated. The equations of motion and their solutions are presented and numerical results are given. Conclusions and recommendations are presented in Section 7.

MRD DIVISION
GENERAL AMERICAN TRANSPORTATION CORPORATION

Section 2

PLASTIC DEFORMATION OF METAL UNDER TRANSIENT LOADS

In this problem of impact deformation and penetration of metallic plates by projectiles, the stresses in the plate often exceed the static proportional limit. When the impact stress exceeds this level the constitutive relations between the stress and the strains are markedly altered.

The basic mechanism for plastic deformation in metals is by the movement and formation of dislocations under stress. The physical background for this mechanism was discussed in Vol. I⁽¹⁴⁾.

2.1 Constitutive Equation

The form of the constitutive equations for a plastic flow in crystalline and polycrystalline material specimens has been investigated quite thoroughly in view of microscopic mechanism of plastic flow⁽¹²⁾⁽²⁵⁾.

In an inelastic material, the rate of total strain may be decomposed into two parts, the strain rate corresponding to the elastic distortion or strain of the sample and to the plastic strain rate or rate of permanent deformation.

$$\dot{\epsilon}_{ij} = \dot{\epsilon}_{ij}^E + \dot{\epsilon}_{ij}^P \quad (2.1)$$

where

$$\dot{\epsilon}_{ij} = \text{total strain} = \frac{1}{2} \left(\frac{\partial u_i}{\partial x_j} + \frac{\partial u_j}{\partial x_i} \right)$$

$$\dot{\epsilon}_{ij}^E = \text{elastic strain}$$

$$\dot{\epsilon}_{ij}^P = \text{plastic or permanent strain}$$

$$(\dot{}) = \frac{d}{dt}()$$

MRD DIVISION
GENERAL AMERICAN TRANSPORTATION CORPORATION

The elastic strain is related directly to the stress. If the linear elastic relationship (Hooke's Law) holds, this component of strain rate is proportional to the stress rate.

$$\dot{\epsilon}_{ij}^E = c_{ijkl} \dot{\sigma}_{kl} \quad (2.2)$$

c_{ijkl} = elastic constants

If the mechanism of plastic deformation is the passage of a number of dislocations through the sample in response to the applied stress, the expression for the plastic strain rate component may be written⁽¹²⁾

$$\dot{\epsilon}_{ij} = \overline{\epsilon_{rqj} V_r \alpha_{rq}} \quad (2.3)$$

where

$$\epsilon_{rqj} = \begin{cases} 1 & \text{rqj even permutation of 1,2,3} \\ -1 & \text{rqj odd permutation of 1,2,3} \\ 0 & \text{otherwise} \end{cases}$$

α_{iq} is the number of dislocations per unit area having its Burger's vector in the i-direction and having its axis in the q-direction

V_r is the velocity component of the dislocation in the r direction.

The summation convention over repeated indices is used. The bar over the whole expression indicates that the average is taken over all possible orientations of the dislocation in the plane normal to its axis.

In this expression, the velocity of the dislocation is a function of the shear stress in the plane normal to the axis of the dislocation. The increase of velocity is not linear function of stress. Fugelso⁽¹²⁾ has worked out a theoretical expression for this velocity in terms of this shear stress.

$$V = V_D e^{-\frac{\Delta H}{RT}} \sinh \gamma \tau$$

$$V = V_D \quad \begin{matrix} |\tau| < |\tau_c| \\ |\tau| > |\tau_c| \end{matrix}$$

MRD DIVISION
GENERAL AMERICAN TRANSPORTATION CORPORATION

where

$$\tau_c \text{ is the solution to } \sinh \gamma \tau = e^{\frac{\Delta H}{RT}}$$

ΔH = activation energy for self-diffusion

R = gas constant

T = absolute temperature

The number of dislocations is incorporated in the definition of α_{ij} . This number may be constant or may increase by creation or regeneration mechanisms.

The behavior of several simpler problems will now be investigated. These cases will be chosen for their diagnostic value, first in checking the validity of the model for plastic flow for form, second to determine basic methods for determining the numerical value of the constants through controlled experiments.

Consider the case of uniform deformation of a rectangular block of material.

$$\epsilon_{ij} = 0, \quad i = j$$

The remaining constitutive equations may be written

$$\begin{aligned}\epsilon_{xx} &= \frac{1}{E} \sigma_{xx} - \frac{\nu}{E} (\sigma_{yy} + \sigma_{zz}) + \epsilon_{xx}^p \\ \epsilon_{yy} &= \frac{1}{E} \sigma_{yy} + \frac{\nu}{E} (\sigma_{xx} + \sigma_{zz}) + \epsilon_{yy}^p \\ \epsilon_{zz} &= \frac{1}{E} \sigma_{zz} - \frac{\nu}{E} (\sigma_{xx} + \sigma_{yy}) + \epsilon_{zz}^p\end{aligned}\tag{2.4}$$

with

E = Young's Modulus

ν = Poisson's Ratio

MRD DIVISION
GENERAL AMERICAN TRANSPORTATION CORPORATION

Since the standard tensile and compressive test apparatus set up a state of biaxial stress — this model will be restricted to biaxial symmetry

$$\dot{\epsilon}_{yy} = \dot{\epsilon}_{zz}$$

$$\sigma_{yy} = \sigma_{zz}$$

The general form of plastic components of strain have been evaluated for the case of biaxial stress⁽¹²⁾.

$$\dot{\epsilon}_{xx}^p = -2V_D Nb \quad (2.5)$$

$$\dot{\epsilon}_{yy}^p = \dot{\epsilon}_{zz}^p = V_D Nb \quad (2.6)$$

where

$$V_D = V_D^0 e^{\frac{\Delta H}{RT} \sinh \gamma \tau}$$

$$|\tau| < |\tau_c|$$

$$V_D = V_D^0$$

$$|\tau| > |\tau_c|$$

$$\tau = \frac{1}{2}(\sigma_{xx} - \sqrt{\sigma_{yy}^2 + \sigma_{zz}^2})$$

$$\tau_c \text{ is given by the solution of } \sinh \gamma \tau_c = e^{\Delta H/RT}$$

V_D is the dislocation velocity

V_D^0 is the maximum dislocation velocity

N is the number of dislocations per unit area

b is the Burger's vector of the dislocation

In the most elementary testing machine the lateral stresses are zero

$$\sigma_{yy} = \sigma_{zz} = 0 \quad (2.7)$$

MRD DIVISION
GENERAL AMERICAN TRANSPORTATION CORPORATION

Thus

$$\tau = \frac{1}{2} \sigma_{xx} \text{ and only the first equation is left}$$

$$\dot{\epsilon}_{xx} = \frac{\dot{\sigma}_{xx}}{E} = 2V_D b N \quad (2.8)$$

Inserting the value of the dislocation velocity, the constitutive equation is

$$\begin{aligned} \dot{\epsilon}_{xx} &= \frac{\dot{\sigma}_{xx}}{E} = 2V_D^0 e^{-\frac{\Delta H}{RT}} \sinh \gamma \frac{\sigma_{xx}}{2} \quad \sigma_{xx} < 2\tau_c \\ \dot{\epsilon}_{xx} &= \frac{\dot{\sigma}_{xx}}{E} = 2V_D^0 N b \quad \sigma_{xx} > 2\tau_c \end{aligned} \quad (2.9)$$

Rather than evaluating this pair of equations with the discontinuous form, we shall replace the expression for the dislocation velocity with an analytic expression over the range $0 < \tau < \infty$ which is very close approximation

$$V_D = V_D^0 e^{-A/\tau} \quad 0 < \tau < \infty$$

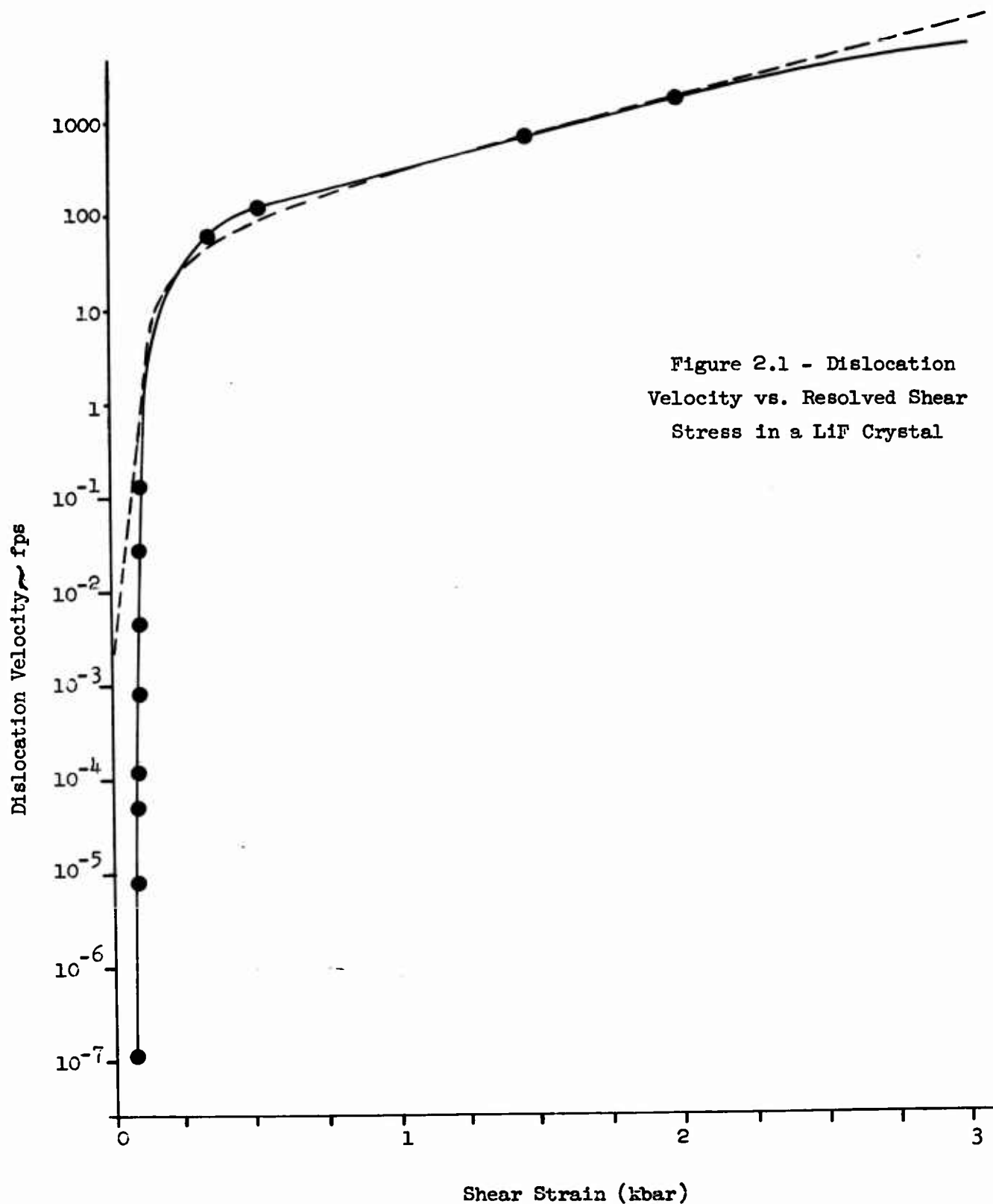
$$V_D = -V_D^0 e^{-A/\tau} \quad -\infty < \tau < 0$$

The comparison of the two expressions is given in fig. 2.1 . Only in the neighborhood of zero shear stress is there any marked deviation and in this region the contribution from this term is negligible there anyway.

The coefficient A absorbs the temperature behavior

$$A = \frac{A_0}{RT} \quad (2.10)$$

MRD DIVISION
GENERAL AMERICAN TRANSPORTATION CORPORATION



MRD DIVISION
GENERAL AMERICAN TRANSPORTATION CORPORATION

This form is preferable since we will be dealing only with solutions of problems whose stresses have the same sign during the process of deformation.

Four cases will now be considered

- | | | |
|---|---|---------------------------------|
| a) Constant strain rate | } | Constant number of dislocations |
| b) Constant strain | | |
| c) Constant stress | | |
| d) Constant strain rate - increasing number of dislocations | | |

We may drop the subscript xx as no confusion will arise.

Case a) Constant strain rate

This problem will be solved for a constant strain rate

$$\dot{\epsilon} = C = \text{constant}$$

Inserting this into the constitutive equation

$$C = \frac{\sigma}{E} + \dot{\epsilon}_p^0 e^{-2A/\sigma} \quad (2.11)$$

This equation is solved numerically by the Runge-Kutta method for several values of C, the applied strain rate. The values of C range over several orders of magnitudes from 10^{-4} /sec to 10^{-5} /sec. (Fig. 2.2)

It is found that the stress increases linearly with strain at the beginning and then very rapidly changes slope, This sharp bend occurs at a stress which is far below the maximum possible plastic flow rate. If its applied strain rate is less than the maximum plastic strain rate, the stress approaches a limiting value which is given by

$$\sigma = \frac{2A}{\ln \dot{\epsilon}_p / C} \quad (2.12)$$

MRD DIVISION
GENERAL AMERICAN TRANSPORTATION CORPORATION

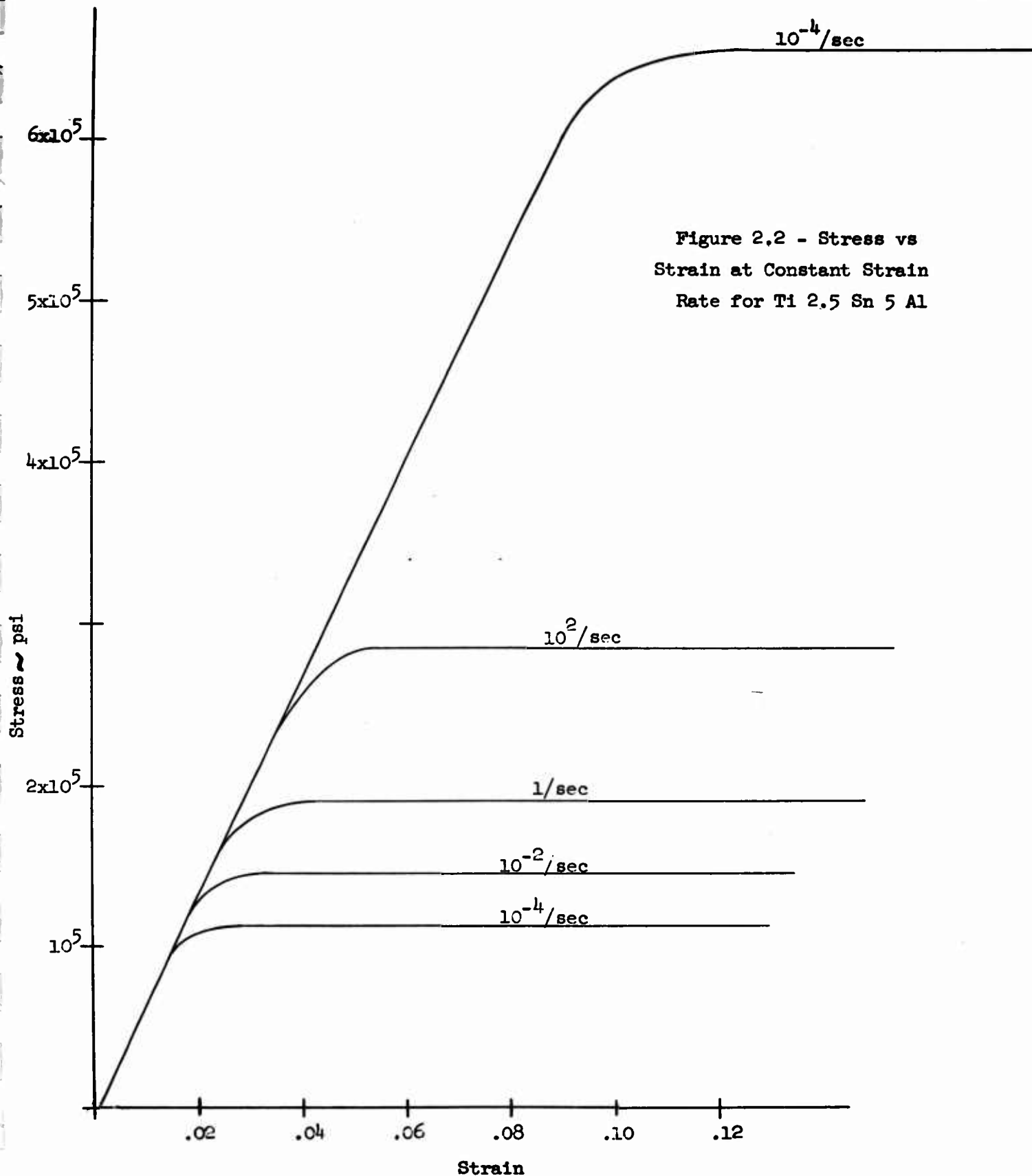


Figure 2.2 - Stress vs
Strain at Constant Strain
Rate for Ti 2.5 Sn 5 Al

MRD DIVISION
GENERAL AMERICAN TRANSPORTATION CORPORATION

The plastic flow is able to absorb the entire applied strain. This value of the stress may be considered to be the dynamic yield strength of the material at that strain rate. If, on the other hand, the critical strain rate exceeds the maximum flow rate, the plastic flow cannot respond fast enough to account for all the strain and the stress must increase indefinitely.

Case b) Constant strain, suddenly applied and held

$$\epsilon = \epsilon_0 1(t)$$

If ϵ_0 is the value of the strain at $t = 0$ and σ_0 is the stress at $t = 0$

$$\sigma_0 = E\epsilon_0 \text{ since no flow has occurred}$$

and

$$\dot{\epsilon} = 0$$

Thus

$$\frac{d\sigma}{dt} + \dot{\epsilon}_p^0 e^{-2A/\sigma} = 0 \quad (2.13)$$

Subject to the initial conditions

$$\sigma = \sigma_0 \text{ at } t = 0$$

the stress-time history is plotted in Figure 2.3.

It is seen that the stress decays from its initial value very rapidly if the initial stress is high and very gently if the initial stress is small.

Case c) Constant stress

At time $t = 0$, the stress σ_0 is suddenly applied and maintained

$$\sigma = \text{const} = \sigma_0$$

thus the constitutive equation is

$$\dot{\epsilon} = \dot{\epsilon}_p^0 e^{-2A/\sigma} \quad (2.14)$$

MRD DIVISION
GENERAL AMERICAN TRANSPORTATION CORPORATION

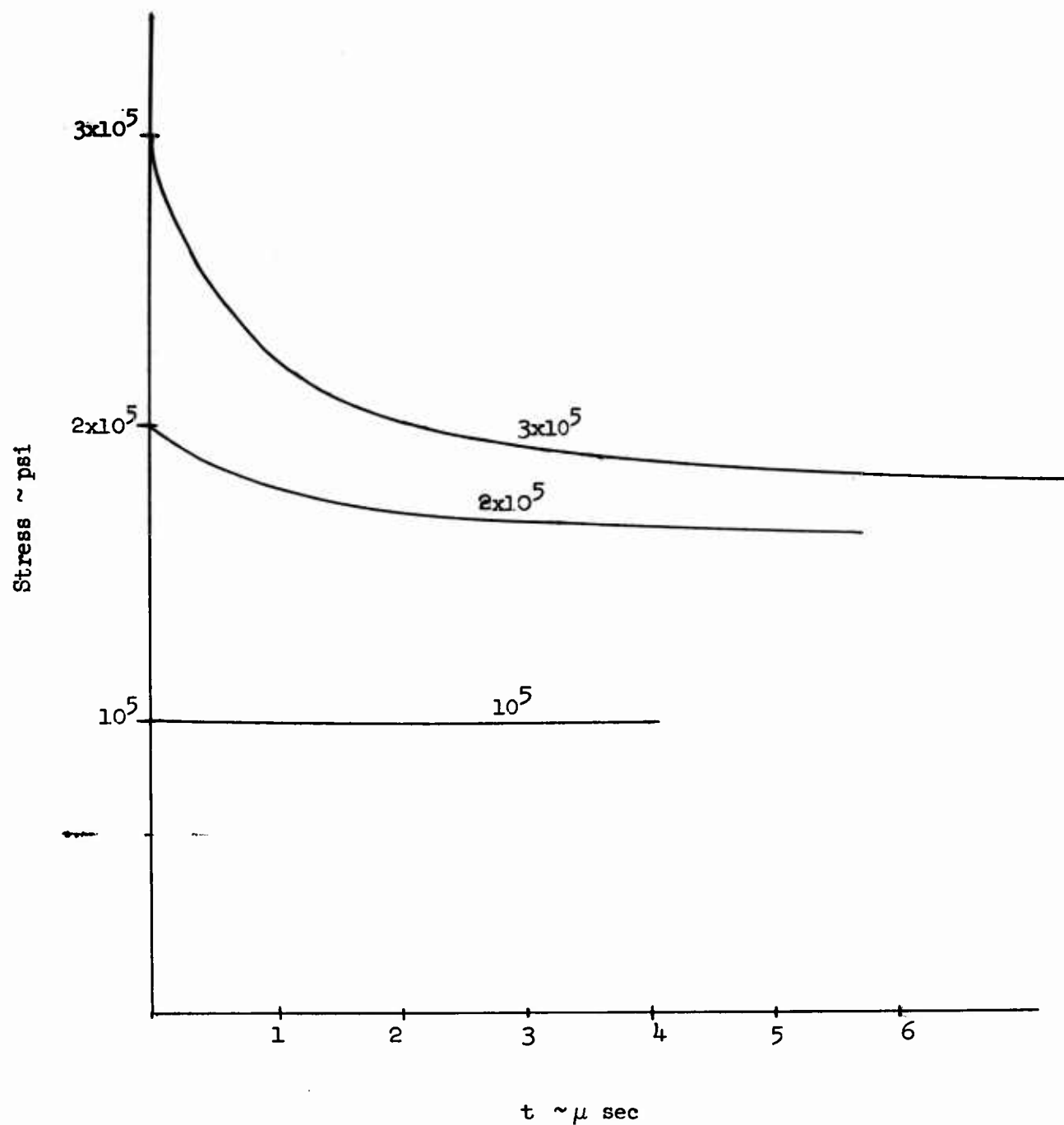


Figure 2.3 - Stress vs. Time at Constant
Strain for Ti 2.5 Sn 5 Al

MRD DIVISION
GENERAL AMERICAN TRANSPORTATION CORPORATION

The solution to this equation is

$$\epsilon = \frac{\sigma_0}{E} + \dot{\epsilon}_p^0 e^{-\frac{2A}{\sigma_0} t} \quad (2.15)$$

The strain starts at its elastic value and increases linearly with time. The rate of increase of strain approaches a limiting value, as the stress becomes very large.

Case d) Constant strain rate - increasing number of dislocations

In materials the number of dislocations may increase by a variety of microscopic mechanisms. Fugelso⁽¹³⁾ has evaluated the behavior of the stress-strain curves if the number of dislocations increases by the Frank-Read dislocation log mechanism. In terms of macroscopic variables the constant term in the expression for strain rate is replaced by

$$\dot{\epsilon}_p^0 = \dot{\epsilon}_p^0 \int_0^t \frac{V_D(\tau, s)}{V_D^0} ds \quad (2.16)$$

The equation for stress-strain at constant rate becomes

$$\sigma = \frac{\partial \sigma}{\partial t} + \dot{\epsilon}_p^0 e^{-\frac{2A}{\sigma} t} \int_0^t e^{-\frac{2A}{\sigma(s)}} ds \quad (2.17)$$

This equation was solved numerically for several values of the applied strain rate, fig. 2.4.

In this case the stress-strain curve is altered. The stress rises rapidly along its elastic values, passes through a maximum as the plastic flow becomes dominant, decays rapidly and finally reaches a plateau where the decay is very slow.

MRD DIVISION
GENERAL AMERICAN TRANSPORTATION CORPORATION

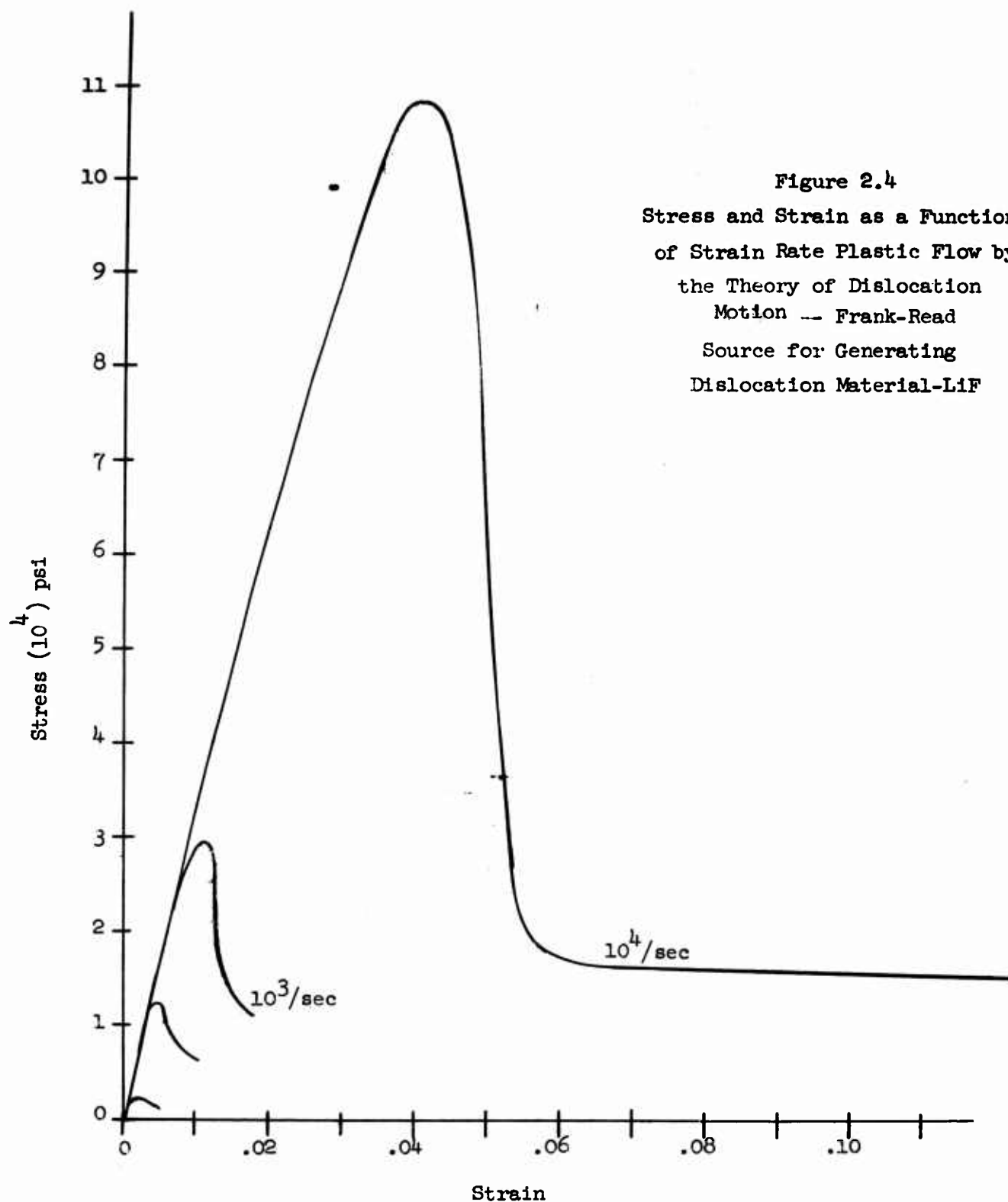


Figure 2.4
Stress and Strain as a Function
of Strain Rate Plastic Flow by
the Theory of Dislocation
Motion -- Frank-Read
Source for Generating
Dislocation Material-LiF

MRD DIVISION
GENERAL AMERICAN TRANSPORTATION CORPORATION

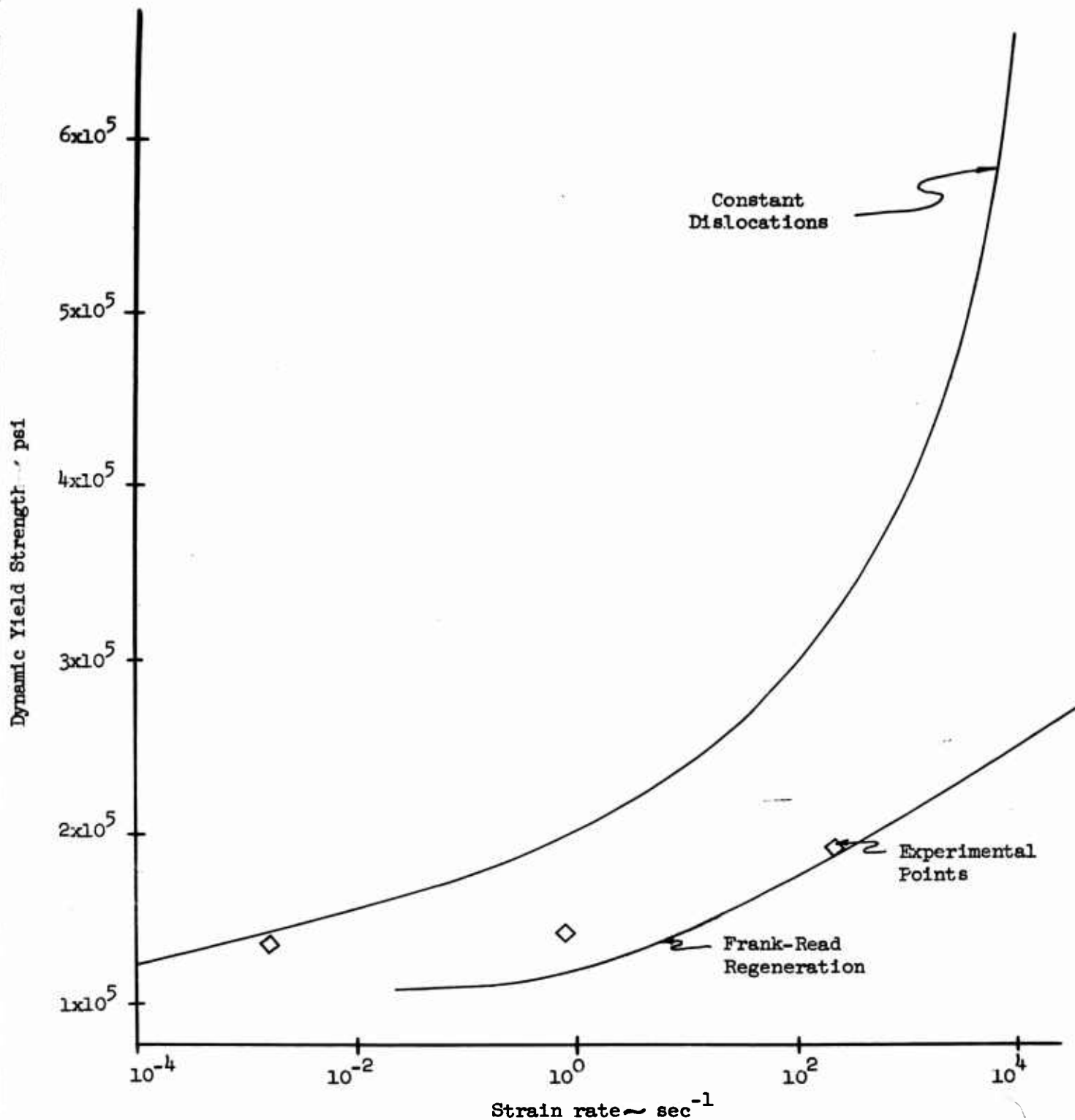


Figure 2.5 - Dynamic Yield Strength as a Function of Strain-Rate for a Ti 2.5 Sn 5 Al Target

MRD DIVISION
GENERAL AMERICAN TRANSPORTATION CORPORATION

2.2 Dynamic Yield Stresses

Consider the resulting stress-strain curves at constant strain rate. For any applied strain rate below the maximum rate, the stress rapidly levels off to a constant value which is characteristic of the strain rate. This stress is then maintained throughout the remainder of the deformational sequence. This level of stress may be termed the dynamic yield stress of the metal in plane stress at constant strain rate. For this case the dynamic strength of the material has a simple algebraic expression as a function of strain rate.

$$\tau_{\text{dynamic yield}} = \frac{A}{\ln\left(\frac{\epsilon_p^0}{\dot{\epsilon}_\tau}\right)} = \frac{A}{\ln \epsilon_p^0 - \ln \dot{\epsilon}_\tau}$$

This expression is valid only for strain rates such that

$$\epsilon_p^0 > \dot{\epsilon}_\tau$$

These values of the dynamic yield strength for a titanium alloy Ti 2.5 Sn 5 Al are plotted in fig. 2.5 along with the plateau stresses reached in the Frank-Read model (case d). Also plotted are the experimental values for the yield stress at constant strain rate⁽¹³⁾. The constant dislocation model gives dynamic yield strengths which are too high. The regeneration model gives reasonable agreement with the experimental data.

MRD DIVISION
GENERAL AMERICAN TRANSPORTATION CORPORATION

Section 3

FRACTURE

In the perforation of metallic plates by projectiles, it is rather obvious that the plate will fracture if perforation is to occur. To determine when a metal specimen will break under rapidly applied short-duration loads, some relationship between fracture and stress must be set forth.

It is obvious that some combination of finite stresses will cause a solid specimen to break up since the solid has only a finite bonding energy. It is observed however that the work done to break up a solid is much less than the bonding energy.

In 1920 A.A. Griffith⁽¹⁵⁾ advanced the postulate that the strength of a solid material could be explained by the presence and subsequent growth of cracks within the specimen. (That this theory is fundamentally correct has been long since verified experimentally). Griffith's postulate was that the crack would grow if the rate of release of elastic strain energy surrounding the crack was greater than the increase in the surface energy.

It is observed in the fracture of metal that the crack will grow under applied stresses if the stress is large enough. The stresses in the region near the crack are very large. Even for so-called brittle metals substantial plastic flow is noted next to the growing crack.

Thompson et al.⁽²⁹⁾ have qualitatively described the fracture process for polycrystalline copper. This description might well be an excellent starting point for a thorough discussion. In their stressed specimen, the first cracks developed in the glide bands that formed. The length of these

MRD DIVISION
GENERAL AMERICAN TRANSPORTATION CORPORATION

cracks then increased, accompanied by plastic deformation in the neighborhood of the crack. Then several cracks that were formed joined together. The entire process of fracture under applied stresses may then be broken into 3 distinct phases:⁽²⁰⁾

Phase I - Formation of the crack

Phase II - Growth of the crack

Phase III - Joining of the cracks to cause macroscopic fracture

Phase I or the formation of the cracks themselves within a good crystal matrix has not been overly considered in the theory of fractures. In the first place, the normal metallic specimen already has the microcracks in it. Second, the formation of the microcracks is tied up with plastic deformation on the crystalline level, a subject which is not well understood.

Almost all subsequent fracture theories of solid specimens have followed this basic model and have concentrated on phase II. Sneddon⁽²⁶⁾ and Westergaard⁽³⁰⁾ calculated the elastic strain energy for various shaped cracks. Irwin⁽²¹⁾ postulated that the rate of energy given up by the solid comes from plastic strains near the crack.

Rather than try energy approaches to this problem of the growing crack, we shall ask one simple question. Given a crack, where does it get the empty space necessary to grow? This question may be answered in two ways. First, there is the possibility of straining or displacing the walls outward. However, if the stress is relieved, the volume of the crack will return to its original position. To extend the volume covered by the crack, either bonds must be broken at the edge of the crack or dislocations must enter into the crack from

MRD DIVISION
GENERAL AMERICAN TRANSPORTATION CORPORATION

the surrounding matrix. To break a bond requires a great deal more energy than to move a dislocation.

The model that will be developed formally in the next section then assumes phase I complete, that the growth of a crack is caused by dislocations moving into it and that the cracks will grow into and overlay each other.

The dislocations however have a direct role to the plastic strain of the crack region and to the specimen as a whole. Through this feature, the relationship between fracture and external forces is sought.

3.1 Mathematical Model for Fracture under Transient Loading

Consider an elementary volume of some metal. This elementary volume contains initially mostly little volumes of perfect crystalline material and some imperfections. These imperfections fall into several categories.

1. Interstitial atoms and vacancies
2. Intracrystalline dislocations
3. Intercrystalline dislocations and grain boundaries
4. Foreign or solute atoms

In addition to these atomic level imperfections there are imperfections on a larger scale,

This elementary volume will contain many individual crystals of the metal. These crystals will have a random orientation with respect to any set of Cartesian axes. (In many cases, however, this may not necessarily be so. The following arguments would then have to be altered to account for this anisotropy). The main result of this assumption is that local variations of imperfection movement will be cancelled out by averaging,

MRD DIVISION
GENERAL AMERICAN TRANSPORTATION CORPORATION

Let the elementary volume be placed under a uniform stress from external forces. The stress field within this volume will be composed of the external stress and the local stresses due to the various imperfections.

In an elementary volume V_o denote the volume of one of the macro-holes by V_m . Two factors must now be established. First, given the rate of growth of a single macro-hole, the rate of growth of the total volume V of the macro-hole must be computed. Second, the rate of growth of a single macro-hole must be established.

Assume that at some time the volume of metal is divided into two volumes, a volume of remaining good crystal $V_o - V$ and the volume V of the holes. The volume V_m associated with each elementary hole grows at some rate.

$$\frac{dV_m}{dt} = k(t) \quad (3.1)$$

The rate at which the elementary hole grows is dependent on external variables as much as stress and temperature and will, in general, vary with time.

The increment in the volume occupied by all the holes is proportional to the remaining volume of good crystal and to the rate at which an elementary hole increases

$$dV = (V_o - V) dV_m = (V_o - V) k dt \quad (3.2)$$

or expressed in terms of rates

$$\frac{dV}{dt} = (V_o - V) \frac{dV_m}{dt} = k(V_o - V) \quad (3.3)$$

Integrating the equation for the increment in total volume occupied by holes

MRD DIVISION
GENERAL AMERICAN TRANSPORTATION CORPORATION

$$V = V_0 \left(1 - e^{-\int_0^t \frac{dV_m}{dt} dt} \right) \quad (3.4)$$

or

$$V = V_0 (1 - e^{-V_m}) \quad (3.5)$$

The next step is to determine an expression for V_m . This is the portion of the problem that will have many possible variants, i.e. dependence on crystal structure, stress pattern, temperature, etc. An outline of the procedure used in determining this rate will be given and only one of the many possibilities will be used in further calculations.

The hole with volume has some shape. It lies wholly within a region of fairly good crystal containing several types of atomic-level imperfections (Fig. 3.1). Under a uniform external stress field, some of these dislocations will move toward the hole. When they intersect the hole, they will cause the hole to increase in size. (A dislocation or a vacancy is just a very small hole or empty space. What is happening here is that the volume of very small holes within the matrix of the good crystal are being transferred to the large hole).

To simplify further discussion, the only imperfection to be considered will be edge dislocations, which is the dominant mode of inelastic behavior. The author has previously characterized the behavior of these imperfections under transient external loads⁽¹²⁾. Because of the initial assumption of random orientation, we need only to consider the average motion of the dislocations.

The growth of the micro-holes requires that dislocations move through the body or matrix. The dislocations will move in patterns relative to the local stress field. The stress in the matrix is composed of stresses from two sources, the applied stress and the stress concentration around the holes.

MRD DIVISION
GENERAL AMERICAN TRANSPORTATION CORPORATION

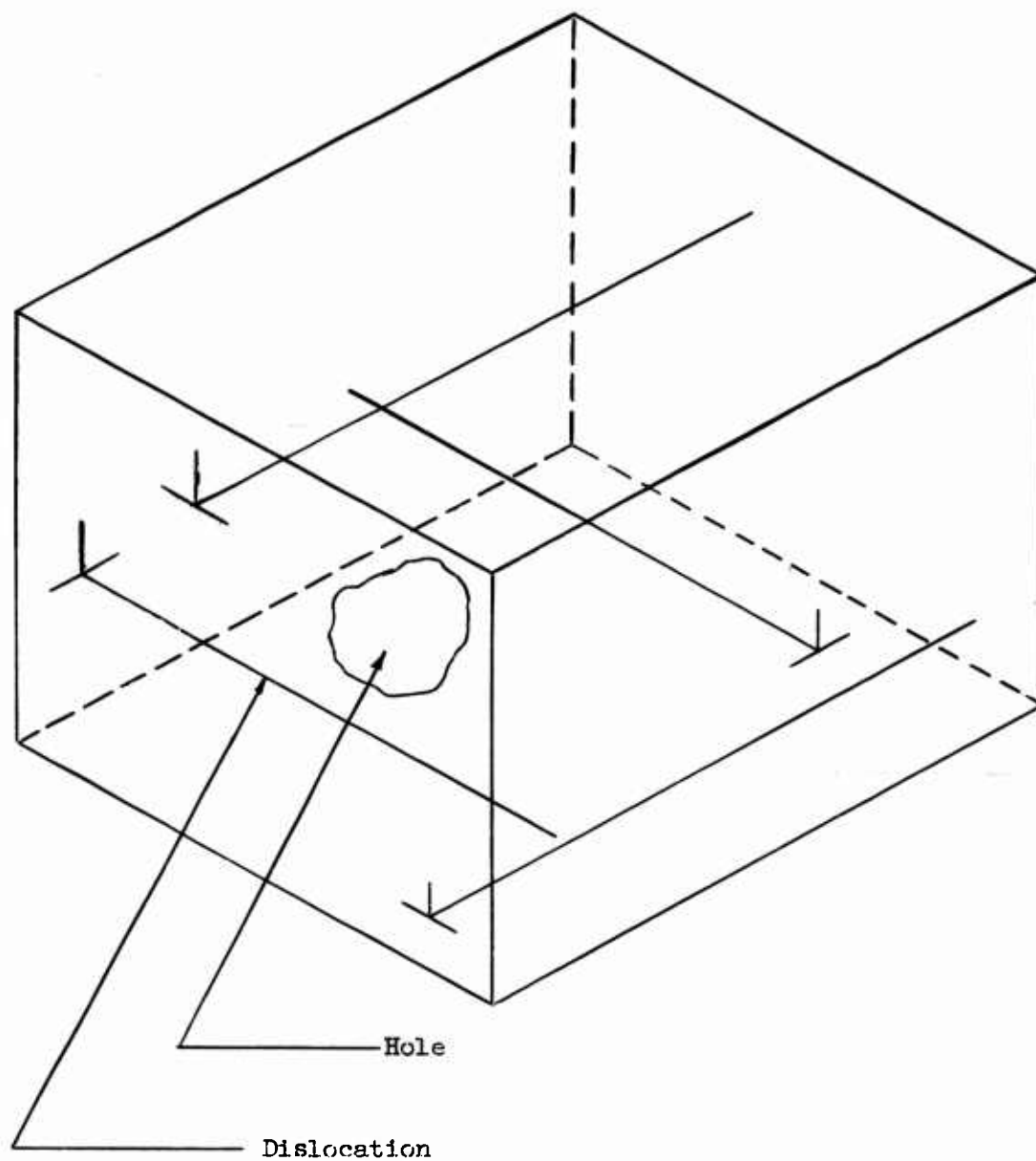


Figure 3.1 - Initial Configuration of Microhole

MRD DIVISION
GENERAL AMERICAN TRANSPORTATION CORPORATION

If the dislocations have to move for any appreciable distance within the crystal before striking a hole, the majority of its motion will be determined by the applied field. We shall assume that is the case.

The geometry of the stress pattern determines the directions from which the dislocations approach the holes. For example, in uniform compression, the dislocations will approach the hole in a 45° cone above or around axis of largest principal stress⁽¹²⁾ (Fig. 3.2). For simple shear, edge dislocations will come only from one direction (parallel to the shear in traction) Fig. 3.3.

The hole will grow at a rate proportional to the surface area exposed to oncoming dislocation. The hole will grow at a rate proportional to the number of dislocations that cross this area per unit time. It is also proportional to the volume increment of each single dislocation

$$\frac{dV_m}{dt} = k_1 A_s \frac{dN}{dt} \Delta V \quad (3.6)$$

A_s = surface area of hole exposed to oncoming dislocations

N = number of dislocation per unit area

ΔV is volume associated with a single dislocation

If a dislocation has a velocity V_D it will reach the hole in unit time if it is close enough. This requirement defines a length λ such that all of the dislocations in the volume of good material

$$v_1 = \lambda A_s \quad (3.7)$$

will reach the macro-hole.

Thus the rate of dislocations crossing into the hole may be written as

$$\frac{dN}{dt} = \frac{V_D N}{\lambda} \quad (3.8)$$

MRD DIVISION
GENERAL AMERICAN TRANSPORTATION CORPORATION

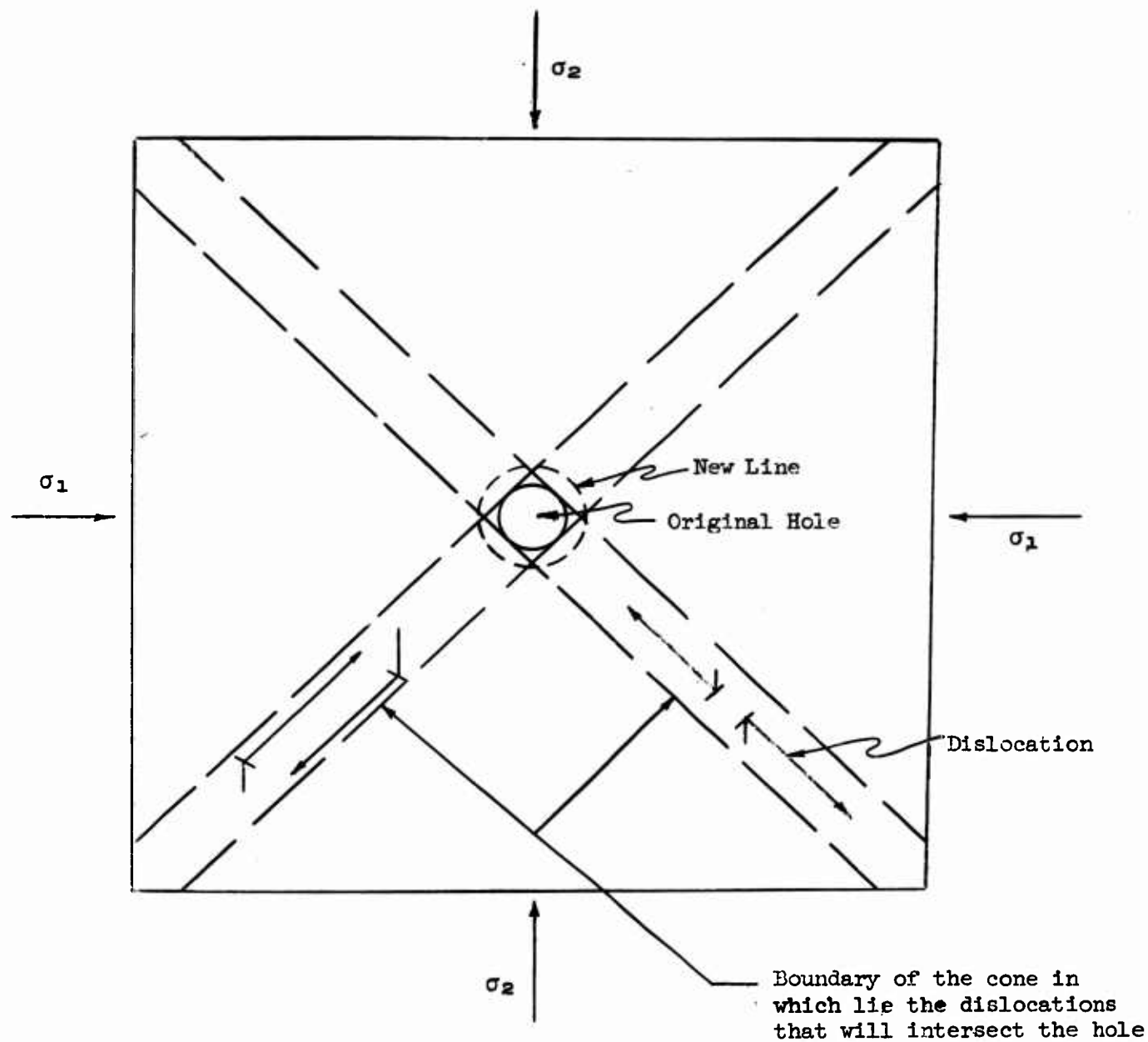


Figure 3.2

Growth of the Microhole under Triaxial Compressive Stress
(Spherical Growth)

MRD DIVISION
GENERAL AMERICAN TRANSPORTATION CORPORATION

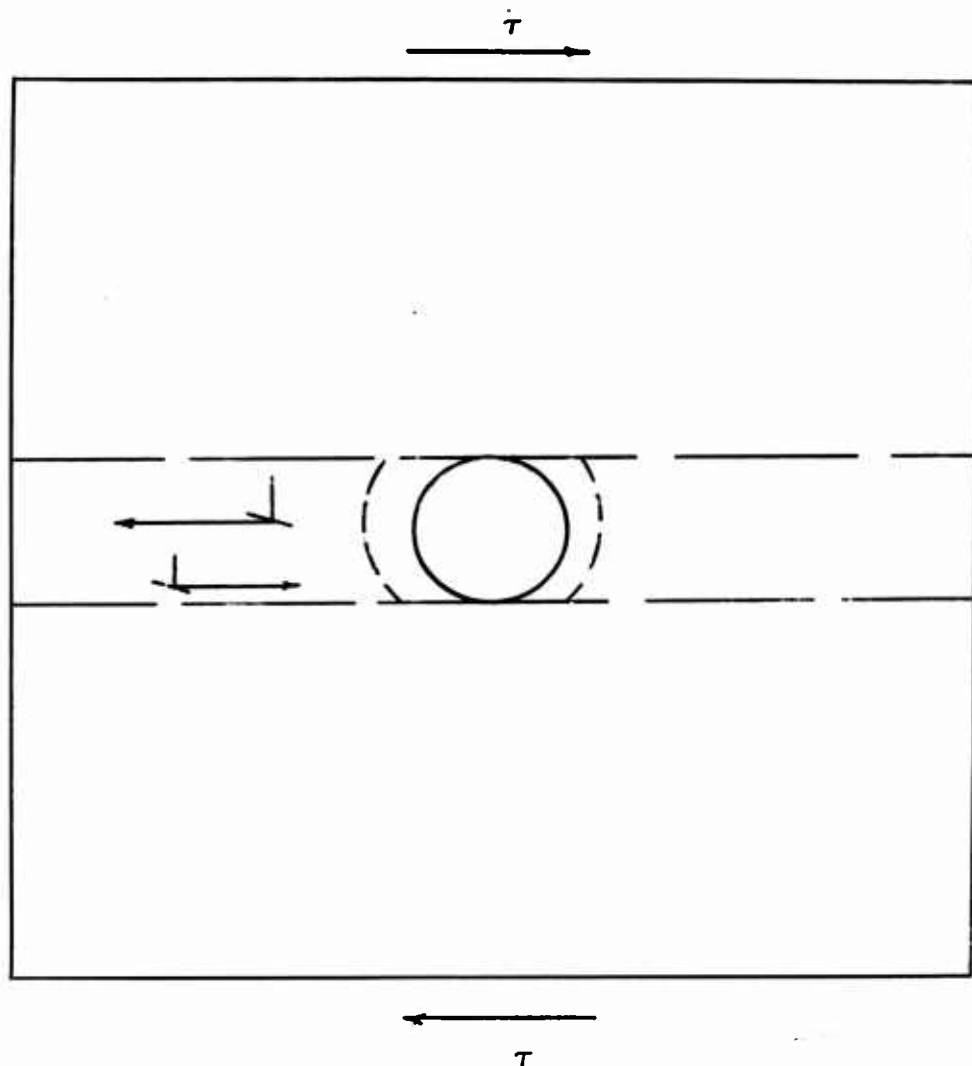


Figure 3.3

Growth of the Microhole under Single Shear
(Rod-like Growth)

MRD DIVISION
GENERAL AMERICAN TRANSPORTATION CORPORATION

For the compression case, the expansion of V_m is spherical

$$\frac{dV_m}{dt} = 4\pi k_2 r^2 A \frac{V_D^N}{\lambda} \quad (3.9)$$

or

$$\frac{dr}{dt} = k_2 \frac{V_D^N}{\lambda} \quad (3.10)$$

$$r - r_o = \int_0^t k_2 \frac{V_D^N}{\lambda} dt$$

$$k_2 = k_1 \Delta V_{dis}$$

The volume of the hole at any later time is

$$V_m = \frac{4\pi}{3} \left[\int_0^t k_2 \frac{V_D^N}{\lambda} dt \right]^3 + V_m^o \quad (3.11)$$

with V_m^o the initial volume of the hole.

For simple shear case the growth is rod-like. The linear rate of growth is

$$\frac{dx}{dt} = A_s \frac{V_D^N}{\lambda} \quad (3.12)$$

The volume of the hole at any later time is

$$V_m = A_s \left[\int_0^t k_3 \frac{V_D^N}{\lambda} dt \right] + V_m^o \quad (3.13)$$

Inserting these expressions into the equation for total volume of holes

$$V = V_o \left[1 - e^{-\left(\int_0^t \frac{k_2}{\lambda} V_D^N dt \right)^3} \right] \quad \text{spherical or compressive}$$

$$V = V_o \left[1 - e^{-\int_0^t \frac{k_3}{\lambda} V_D^N dt} \right] \quad \text{Rod-like or simple shear}$$

MRD DIVISION
GENERAL AMERICAN TRANSPORTATION CORPORATION

If the stress is very high, V_D is very nearly constant and the integrals may be evaluated explicitly

$$V = V_0 (1 - e^{-k_4 t^3}) \quad \text{Compressive stress}$$

$$V = V_0 (1 - e^{-k_5 t}) \quad \text{Simple Shear}$$

$$\text{with } k_4 = k_2 \frac{V_D^0 N}{\lambda} \quad k_5 = k_3 \frac{V_D^0 N}{\lambda}$$

A schematic picture of the rate of growth of the total volume occupied by the micro-holes is shown in fig. 3.4.

These two curves may cross each other. It is quite likely that the two coefficients k_4 and k_5 are different functions of temperature. Thus, at one temperature of one of the mechanisms may grow much faster than the other, while at a different temperature the order may be reversed.

3.2 Relation of the Fracture Criteria to Plastic Strain

The postulate for fracture of the elementary volume is very simple. If the volume occupied by the assemblage of macro-holes is greater than a certain percentage of the total volume the structures can no longer hold together and the volume falls apart — or in other words, fractures. This critical volume ratio may be different for different crystal structures.

This critical volume concept holds only in the region of the specimen wherein the shear stresses are high. The growth of the elementary volumes is dependent on the level of the resolved shear stress. In any large specimen these shear stresses are not uniform throughout. At the beginning of the

MRD DIVISION
GENERAL AMERICAN TRANSPORTATION CORPORATION

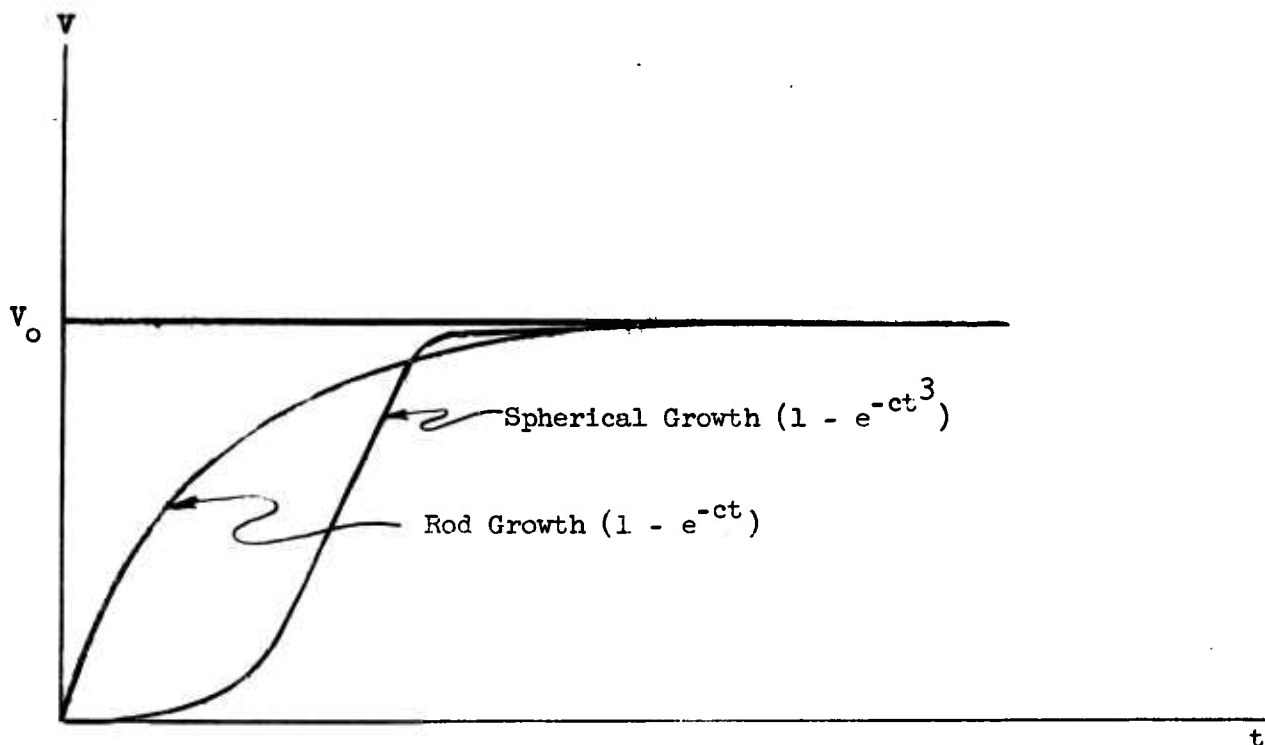


Figure 3.4

Stress vs. Time-to-Fracture at Constant Stress
 Compared to Plastic Strain-Rate at Constant Stress

MRD DIVISION
GENERAL AMERICAN TRANSPORTATION CORPORATION

deformation process when all the stresses are elastic, this stress pattern is not uniform. As plastic deformation of the specimen proceeds this non-uniformity of stress distribution and concentration can become altered. In particular, the high shears can localize in or near the area of greatest plastic flow (for a numerical example of this, see ref. 12). The shear stress pattern must be solved as a part of the boundary value problem involving the elastic strain and flow pattern.

The critical volume for fracture may be quite different for different types of crack growth, for example, the crack that grows in a disk shape will require only a small volume before fracture occurs.

This critical volume will be essentially the volume of holes in a region wherein the shear stress is uniform and will not pertain to the volume of holes in the entire specimen.

Denote by V_c the ratio of V to V_0 when fracture occurs. At fracture

$$V_c = 1 - e^{-V_m}$$

$$= 1 - e^{-\int_0^t \frac{dV_m}{dt} dt}$$

Inserting the expression for $\frac{dV_m}{dt}$

$$V_c = 1 - e^{-(\int_0^t \frac{k_1 V_D}{\lambda} N dt)^n} \quad (3.14)$$

where

$n = 1$ for simple shear

$n = 3$ for biaxial compression

MRD DIVISION
GENERAL AMERICAN TRANSPORTATION CORPORATION

Solve this equation for the integral

$$k_1 \int_0^t \frac{V_D N}{\lambda} dt = [\ln(1-V_c)]^{-1/n} \quad (3.15)$$

This integral expression may be compared to the expression for total plastic strain of the previous chapter.

$$\epsilon_p = b \int_0^t V_D N dt \quad (3.16)$$

where b is the Burger's vector defined in Sec. 2.

Thus

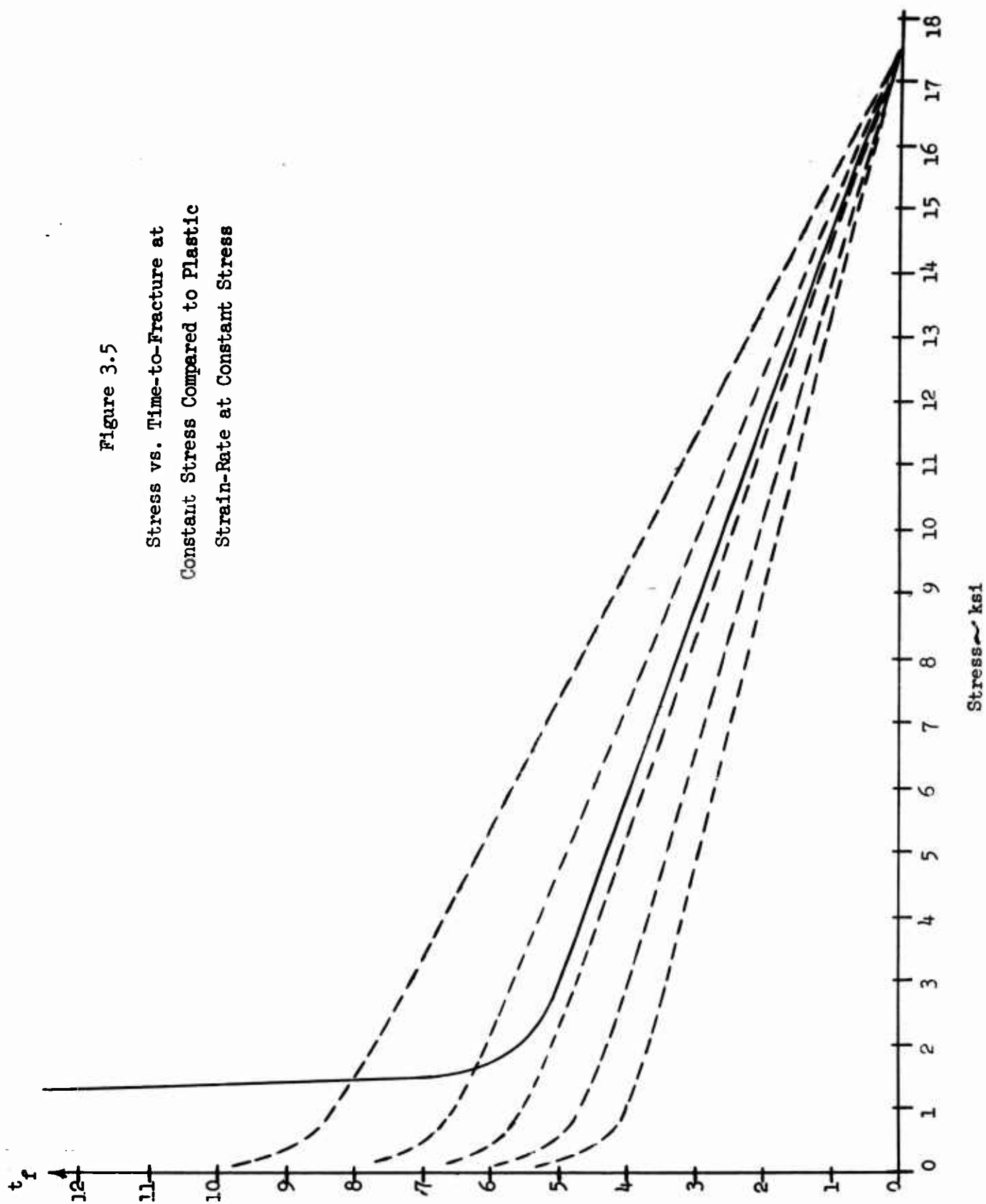
$$\epsilon_p \Big|_{\text{fracture}} = \frac{n}{\lambda k_n} [\ln(1-v_c)]^{-1/n} \quad (3.17)$$

Thus at fracture a certain amount of plastic strain has occurred which is an indicator of fracture. The magnitude of this critical strain is one measure of whether the metal is ductile or brittle.

Since the plastic strain rate for simple compression or tensile stress specimens is a function of the applied stress, experiments carried out at constant stress should give some indication as to the validity of the theory.

Figure 3.5

Stress vs. Time-to-Fracture at
Constant Stress Compared to Plastic
Strain-Rate at Constant Stress



MRD DIVISION
GENERAL AMERICAN TRANSPORTATION CORPORATION

At some constant stress level, the plastic strain rate is constant and using the form for this strain rate as in Section 2.

$$\dot{\epsilon}_p = V_D N b e^{-A/\sigma} \quad (3.18)$$

where σ is the applied stress.

Integrate the plastic strain from zero to the critical strain

$$\epsilon_p^c = \dot{\epsilon}_p(\sigma) t_f \quad (3.19)$$

where t_f is the time at which fracture occurs.

Thus

$$t_f = \frac{\epsilon_p^c}{\dot{\epsilon}_p(\sigma)} \quad (3.20)$$

$$= \frac{\epsilon_p^c}{V_D N b} e^{A/\sigma} \quad (3.21)$$

This time-to-fracture curve is very similar to the data on aluminum and the noble metals measured by Zhurkov⁽³²⁾⁽³³⁾. The results of the theory and the experiment are shown in Fig. 3.5.

The time-to-fracture of metallic specimen under a given stress loading can be related to the plastic strain in the region of the fracture under the same stress history. This criteria will be used to determine the penetration.

This criterion is $\int_0^{t_f} \dot{\epsilon}_p^o \sim \epsilon_p^c$

To use this criterion in a boundary value problem, the deformational process must be solved for the dynamic elastic plastic case and the fracture will occur at the point or surface in the material where first the plastic strain exceeds its maximum value.

MRD DIVISION
GENERAL AMERICAN TRANSPORTATION CORPORATION

Section 4

TRANSIENT WAVE ANALYSIS

In this section we shall investigate the propagation of stress waves through an elastic medium. First we consider an axially symmetric half-space under an arbitrary axially-symmetric load. The general integral solution for this problem is then examined for the specific case of a unit load over a unit circle, and expressions are derived for the stresses along the axis under this load, as functions of time and depth. A numerical integration is programmed and carried out on the IBM 1620 to find the values of these stresses.

A second program is then developed which, from the numerical values just found, computes the stresses as the waves are reflected through a plate. This computation is performed for two cases, a Fe plate and a Ti plate. The results are presented as contour drawings, which show the time, depth, and duration of maximum stress components in the radial and axial directions; the tangential stress along the axis will have been shown to be identically equal to the radial, and the shear to be identically zero.

4.1 Equations of Motion

Stress-wave propagation is defined by the equations of motion

$$\frac{\partial \sigma_{rr}}{\partial r} + \frac{\partial \tau_{rz}}{\partial z} + \frac{\sigma_{rr} - \sigma_{\theta\theta}}{r} = \mu \frac{\partial^2 u_r}{\partial t^2} \quad (4.1)$$

$$\frac{\partial \tau_{rz}}{\partial r} + \frac{\tau_{rz}}{r} + \frac{\partial \sigma_{zz}}{\partial z} = \mu \frac{\partial^2 u_z}{\partial t^2} \quad (4.2)$$

MRD DIVISION
GENERAL AMERICAN TRANSPORTATION CORPORATION

where σ_{rr} , σ_{zz} , $\sigma_{\theta\theta}$ and τ_{rz} are the radial, axial (vertical), tangential, and shear stresses given by the stress-strain relations

$$\sigma_{rr} = (\lambda + 2G) \frac{\partial u_r}{\partial r} + \lambda \left(\frac{u_r}{r} + \frac{\partial u_z}{\partial z} \right) \quad (4.3)$$

$$\sigma_{\theta\theta} = (\lambda + 2G) \frac{u_r}{r} + \lambda \left(\frac{\partial u_r}{\partial r} + \frac{\partial u_z}{\partial z} \right) \quad (4.4)$$

$$\sigma_{zz} = (\lambda + 2G) \frac{\partial u_z}{\partial z} + \lambda \left(\frac{\partial u_r}{\partial r} + \frac{u_r}{r} \right) \quad (4.5)$$

$$\tau_{rz} = G \left(\frac{\partial u_r}{\partial z} + \frac{\partial u_z}{\partial r} \right) \quad (4.6)$$

with u_r and u_z denoting the radial and axial components of displacement, and μ , λ , G the density, uniaxial strain modulus, and shear modulus of the medium.

4.2 Boundary Conditions

The condition of axial symmetry is assumed in the above relations; the further boundary conditions for this problem are that the surface $z = 0$ (taking the axis to be vertical) is free from shear and that the pressure history on the surface is given by some function f . Then, considering the stresses as functions of r , z , and t , we have for our boundary conditions:

$$\sigma_{zz}(r, 0, t) = f(r, t)$$

$$\tau_{rz}(r, 0, t) = 0$$

4.3 Dimensionless Variables

The variables in the problem can be reduced to dimensionless form by introducing a characteristic pressure p and characteristic distance R . The characteristic distance will be taken as the radius of the bullet. The characteristic pressure is the normal pressure generated at impact⁽¹⁴⁾

$$p = \frac{\mu_1 c_1 \mu_2 c_2}{\mu_1 c_1 + \mu_2 c_2} V_S \quad (4.7)$$

where

$\mu_1 \mu_2$ are densities of the plate and bullet

$c_1 c_2$ are longitudinal sonic velocities of the plate and bullet

V_S is the impact velocity

Then letting $c_1^2 = \frac{\lambda + 2G}{\mu}$ and $c_2^2 = \frac{G}{\mu}$, we have

$$\begin{aligned} \rho &= \frac{r}{R} & \sigma_{\rho\rho} &= \frac{\sigma_{rr}}{p} \\ \zeta &= \frac{z}{R} & \sigma_{\zeta\zeta} &= \frac{\sigma_{zz}}{p} \\ u_\rho &= \frac{\mu c_1^2}{p R} u_r & \sigma_{\phi\phi} &= \frac{\sigma_{\theta\theta}}{p} \\ u_\zeta &= \frac{\mu c_1^2}{p R} u_z & \tau_{\rho\zeta} &= \frac{\tau_{rz}}{p} \\ & & \tau &= \frac{c_1 t}{R} \end{aligned}$$

and we define $\beta^2 = \frac{c_1^2}{c_2^2} = \frac{\lambda + 2G}{G}$, $p = p_1$ (4.8)

R = radius of bullet

4.4 Equations in Dimensionless Form

In terms of the dimensionless variables defined above, the equations of motion become:

MRD DIVISION
GENERAL AMERICAN TRANSPORTATION CORPORATION

$$\beta^2 \left(\frac{\partial^2 u}{\partial \rho^2} + \frac{1}{\rho} \frac{\partial u}{\partial \rho} - \frac{u}{\rho^2} + \frac{\partial^2 u}{\partial \zeta \partial \rho} \right) - \frac{\partial^2 u}{\partial \zeta \partial \rho} + \frac{\partial^2 u}{\partial \zeta^2} = \beta^2 \frac{\partial^2 u}{\partial \tau^2} \quad (4.9)$$

$$\frac{\partial^2 u}{\partial \rho^2} + \frac{1}{\rho} \frac{\partial u}{\partial \rho} + (\beta^2 - 1) \frac{\partial}{\partial \zeta} \left(\frac{\partial u}{\partial \rho} + \frac{u}{\rho} \right) + \beta^2 \frac{\partial^2 u}{\partial \zeta^2} = \beta^2 \frac{\partial^2 u}{\partial \tau^2} \quad (4.10)$$

And the boundary conditions are:

$$\sigma_{\zeta\zeta}(\rho, 0, \tau) = -\psi(\rho, \tau)$$

$$\tau_{\rho\zeta}(\rho, 0, \tau) = 0$$

4.5 General Integral Solution

The Hankel-Laplace transform solutions for arbitrary ψ are given by⁽¹⁴⁾⁽¹⁶⁾

$$\begin{aligned} \sigma_{\rho\rho} = \frac{1}{2\pi i} \int_{Br} e^{s\tau} \left[\frac{1}{\rho} \int_0^\infty \frac{\xi^2 \bar{\psi}}{g} \left[m n e^{-n\zeta} - \left(\xi^2 + \frac{\beta^2 s^2}{2} \right) e^{-m\zeta} \right] J_1(\rho\xi) d\xi \right. \\ \left. + \int_0^\infty \frac{\xi \bar{\psi}}{g} \left[\left(m^2 + \frac{\beta^2 s^2}{2} \right) \left(\xi^2 + \frac{\beta^2 s^2}{2} \right) e^{-m\zeta} - \xi^2 m n e^{-n\zeta} \right] J_0(\rho\xi) d\xi \right] ds \end{aligned} \quad (4.11)$$

$$\sigma_{\zeta\zeta} = - \frac{1}{2\pi i} \int_{Br} e^{s\tau} \int_0^\infty \frac{\xi \bar{\psi}}{g} \left[\left(\xi^2 + \frac{\beta^2 s^2}{2} \right)^2 e^{-m\zeta} - \xi^2 m n e^{-n\zeta} \right] J_0(\rho\xi) d\xi ds \quad (4.12)$$

$$\sigma_{\rho\rho} + \sigma_{\phi\phi} = \frac{1}{2\pi i} \int_{Br} e^{s\tau} \int_0^\infty \frac{\xi \bar{\psi}}{g} \left[\left(\xi^2 - (\beta^2 - 2)s^2 \right) \left(\xi^2 + \frac{\beta^2 s^2}{2} \right) e^{-m\zeta} - \xi^2 m n e^{-n\zeta} \right] J_0(\rho\xi) d\xi ds \quad (4.13)$$

$$\tau_{\rho\zeta} = - \frac{1}{2\pi i} \int_{Br} e^{s\tau} \int_0^\infty \frac{m \xi^2 \bar{\psi}}{g} \left[(2\xi^2 + \beta^2 s^2) e^{-m\zeta} - (n^2 + \xi^2) e^{-n\zeta} \right] J_1(\rho\xi) d\xi ds \quad (4.14)$$

where

$$m^2 = \xi^2 + s^2$$

$$n^2 = \xi^2 + \beta^2 s^2$$

$$g = \left(\xi^2 + \frac{\beta^2 s^2}{2} \right)^2 - \xi^2 m n$$

$$\bar{\psi} = \int_0^\infty \int_0^\infty e^{-s\tau} \psi(\rho, \tau) \rho J_0(\rho\xi) d\rho d\tau$$

MRD DIVISION
GENERAL AMERICAN TRANSPORTATION CORPORATION

4.6 Specific Integral Solution

If the pressure function is a unit pressure (p) applied instantaneously and held constant over a circular area of unit radius (R), we have

$$\begin{aligned}\bar{\psi} &= \int_0^{\infty} e^{-s\tau} \int_0^1 \rho J_0(\rho\xi) d\rho d\tau \\ &= \int_0^{\infty} \frac{J_1(\xi)}{\xi} e^{-s\tau} d\tau \\ \bar{\psi} &= \frac{J_1(\xi)}{\xi s}\end{aligned}$$

We seek the stresses generated along the axis ($\rho=0$) by this pressure. Since $J_1(0) = 0$, we have from (4.14)

$$\tau_{\rho\xi}(0, \xi, \tau) \equiv 0 \quad (4.15)$$

In evaluating $\sigma_{\rho\rho}$ we note the factor $\frac{J_1(\rho\xi)}{\rho}$ in the first term of (4.11).

Since $\lim_{\rho \rightarrow 0} J_1(\rho\xi) = 0$, we apply L'Hospital's rule:

$$\begin{aligned}\lim_{\rho \rightarrow 0} \frac{J_1(\rho\xi)}{\rho} &= \lim_{\rho \rightarrow 0} \frac{\frac{d}{d\rho} J_1(\rho\xi)}{\frac{d}{d\rho} \rho} \\ &= \lim_{\rho \rightarrow 0} \xi \frac{d}{d\rho} J_1(\rho\xi) \\ &= \lim_{\rho \rightarrow 0} \xi \frac{J_0(\rho\xi) - J_2(\rho\xi)}{2} \\ &= \frac{\xi}{2} J_0(\rho\xi)\end{aligned}$$

wherein we retain this Bessel function for later use.

MRD DIVISION
GENERAL AMERICAN TRANSPORTATION CORPORATION

Thus we have

$$\begin{aligned}\sigma_{\rho\rho}(0, \zeta, \tau) &= \frac{1}{2\pi i} \int_{Br} e^{s\tau} \int_0^\infty \frac{\xi \bar{\psi}}{g} \left[\frac{\xi^2}{2} m n e^{-n\zeta} - \frac{\xi^2}{2} \left(\xi^2 + \frac{\beta^2 s^2}{2} \right) e^{-m\zeta} - \xi^2 m n e^{-n\zeta} \right. \\ &\quad \left. + \left(m^2 - \frac{\beta^2 s^2}{2} \right) \left(\xi^2 + \frac{\beta^2 s^2}{2} \right) e^{-m\zeta} \right] J_0(\rho \xi) d\xi ds \\ &= \frac{1}{2\pi i} \int_{Br} e^{s\tau} \int_0^\infty \frac{\xi \bar{\psi}}{2g} \left[\left(\xi^2 - (\beta^2 - 2)s^2 \right) \left(\xi^2 + \frac{\beta^2 s^2}{2} \right) e^{-m\zeta} - \xi^2 m n e^{-n\zeta} \right] J_0(\rho \xi) d\xi ds\end{aligned}$$

And hence at $\rho = 0$

$$\sigma_{\rho\rho} = \sigma_{\phi\phi} \frac{1}{2} (\sigma_{\rho\rho} + \sigma_{\phi\phi})$$

Then recalling that $\bar{\psi} = \frac{J_1(\xi)}{\xi \zeta}$ we must evaluate the two integrals

$$2\sigma_{\rho\rho} = 2\sigma_{\phi\phi} = \frac{1}{2\pi i} \int_{Br} \frac{e^{s\tau}}{s} \int_0^\infty \frac{(\xi^2 - (\beta^2 - 2)s^2) \left(\xi^2 + \frac{\beta^2 s^2}{2} \right) e^{-m\zeta} - \xi^2 m n e^{-n\zeta}}{g} J_0(\rho \xi) J_1(\xi) d\xi ds \quad (4.16)$$

$$\sigma_{\zeta\zeta} = - \frac{1}{2\pi i} \int_{Br} \frac{e^{s\tau}}{s} \int_0^\infty \frac{\left(\xi^2 + \frac{\beta^2 s^2}{2} \right)^2 e^{-m\zeta} - \xi^2 m n e^{-n\zeta}}{g} J_0(\rho \xi) J_1(\xi) d\xi ds \quad (4.17)$$

We can evaluate the three integrals

$$\left. \begin{aligned}I_1 &= \frac{1}{2\pi i} \int_{Br} \frac{e^{s\tau}}{s} \int_0^\infty \frac{\left(\xi^2 + \frac{\beta^2 s^2}{2} \right)^2}{g} e^{-m\zeta} J_0(\rho \xi) J_1(\xi) d\xi ds \\ I_2 &= \frac{1}{2\pi i} \int_{Br} \frac{e^{s\tau}}{s} \int_0^\infty \frac{(\xi^2 - (\beta^2 - 2)s^2) \left(\xi^2 + \frac{\beta^2 s^2}{2} \right)}{g} e^{-m\zeta} J_0(\rho \xi) J_1(\xi) d\xi ds \\ I_3 &= \frac{1}{2\pi i} \int_{Br} \frac{e^{s\tau}}{s} \int_0^\infty \frac{\xi^2 m n}{g} e^{-n\zeta} J_0(\rho \xi) J_1(\xi) d\xi ds\end{aligned} \right\} \quad (4.18)$$

MRD DIVISION
GENERAL AMERICAN TRANSPORTATION CORPORATION

and we have

$$\left. \begin{aligned} \sigma_{\zeta\zeta}(0, \zeta, \tau) &= I_3 - I_1 \\ \sigma_{\rho\rho}(0, \zeta, \tau) &= \sigma_{\phi\phi}(0, \zeta, \tau) = \frac{1}{2}[I_2 - I_3] \end{aligned} \right\} \quad (4.19)$$

4.7 Analytic Reduction of Integral Solution

We shall deal simultaneously with the three integrals of (4.18). Let us define a new variable x as follows: on the Bromwich contour $s = \epsilon + i\delta$. For $\delta < 0$ let $\xi = sx$; for $\delta \geq 0$ let $\xi = -sx$. This gives $d\xi = sdx$ and $d\xi = -sdx$ respectively. Since $\lim_{\epsilon \rightarrow 0} \operatorname{Re}(x) = 0$, we can consider the path of integration for x to be the imaginary axis, and our choice for the sign makes the limits 0 and $i\infty$ for both integrals. Then taking I_1 for example,

$$\begin{aligned} I_1 &= \frac{1}{2\pi i} \int_{\epsilon - i\infty}^{\epsilon} e^{s\tau} ds \int_0^{i\infty} \left[\frac{(x^2 + \beta^2/2)^2}{(x^2 + \beta^2/2)^2 - x^2 \sqrt{(x^2+1)(x^2+\beta^2)}} \right] \\ &\quad [e^{-s\zeta \sqrt{x^2+1}} J_0(\rho sx) J_1(sx) dx] + \left\{ \frac{1}{2\pi i} \int_{\epsilon + i\infty}^{\epsilon} e^{s\tau} ds \right\} \\ &\quad \left\{ \int_0^{i\infty} \left[\frac{(x^2 + \beta^2/2)^2}{(x^2 + \beta^2/2)^2 - x^2 \sqrt{(x^2+1)(x^2+\beta^2)}} \right] [e^{-s\zeta \sqrt{x^2+1}} \right. \\ &\quad \left. [J_0(-\rho sx) J_1(-sx)(-dx)] \right\} \end{aligned}$$

Since $J_0(\rho sx)$ and $J_1(sx)$ are even and odd functions respectively, the minus signs will drop out. Reasoning similarly for I_2 and I_3 : $k = 1, 2, 3$

$$I_k = \frac{1}{2\pi i} \int_{Br} e^{s\tau} ds \int_0^{i\infty} \frac{f_k(x)}{F(x)} e^{-s\zeta \sqrt{x^2 + a_k^2}} J_0(\rho sx) J_1(sx) dx \quad (4.20)$$

MRD DIVISION
GENERAL AMERICAN TRANSPORTATION CORPORATION

where

$$f_1(x) = \left(x^2 + \frac{\beta^2}{2}\right)^2$$

$$f_2(x) = (x^2 - \beta^2 + 2)\left(x^2 + \frac{\beta^2}{2}\right)$$

$$f_3(x) = x^2 \sqrt{(x^2 + 1)(x^2 + \beta^2)}$$

$$F(x) = \left(x^2 + \frac{\beta^2}{2}\right)^2 - x^2 \sqrt{(x^2 + 1)(x^2 + \beta^2)}$$

$$\alpha_1 = \alpha_2 = 1$$

$$\alpha_3 = \beta$$

Now we make the substitution $J_1(sx) = \frac{1}{2}(H_1^{(1)}(sx) + H_1^{(2)}(sx))$ and let $x=iv$,

$dx=idv$:

$$I_k = \frac{1}{2\pi i} \int_{Br} e^{s\tau} ds \int_0^\infty \frac{g_k(v)}{G(v)} e^{-s\sqrt{\alpha_k^2 - v^2}} \left[\frac{H_1^{(1)}(isv) + H_1^{(2)}(isv)}{2} \right] J_0(i\rho sv) dv$$

where

$$g_1(v) = \left(\frac{\beta^2}{2} - v^2\right)^2$$

$$g_2(v) = (2 - \beta^2 - v^2)\left(\frac{\beta^2}{2} - v^2\right)$$

$$g_3(v) = -v^2 \sqrt{(1 - v^2)(\beta^2 - v^2)}$$

$$G(v) = \left(\frac{\beta^2}{2} - v^2\right)^2 + v^2 \sqrt{(1 - v^2)(\beta^2 - v^2)}$$

MRD DIVISION
GENERAL AMERICAN TRANSPORTATION CORPORATION

Splitting the integral into two terms and changing the second to the negative half of the axis gives

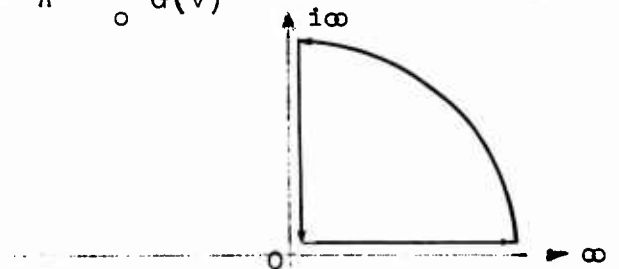
$$I_k = \frac{1}{2\pi i} \int_{Br} e^{s\tau} ds \left[\frac{1}{2} \int_0^{\infty} \frac{g_k(v)}{G(v)} e^{-s\zeta\sqrt{a_k^2 - v^2}} H_1^{(1)}(1sv) J_0(1\rho sv) dv \right. \\ \left. + \frac{1}{2} \int_0^{-\infty} \frac{g_k(v)}{G(v)} e^{-s\zeta\sqrt{a_k^2 - v^2}} H_1^{(2)}(1sv) J_0(1\rho sv) dv \right]$$

Noting that $H_1^{(1)}(ix) = -\frac{2}{\pi} k_1(x)$, $H_1^{(2)}(ix) = -\frac{2}{\pi} k_1(-x)$, and that $I_0(x) = J_0(ix)$, we have

$$I_k = -\frac{1}{2\pi i} \int_{Br} e^{s\tau} ds \left[\frac{1}{\pi} \int_0^{\infty} \frac{g_k(v)}{G(v)} e^{-s\zeta\sqrt{a_k^2 - v^2}} K_1(sv) I_0(\rho sv) dv \right. \\ \left. + \frac{1}{\pi} \int_0^{-\infty} \frac{g_k(v)}{G(v)} e^{-s\zeta\sqrt{a_k^2 - v^2}} K_1(-sv) I_0(\rho sv) dv \right]$$

which by Bateman's theorem on conjugate integrals⁽⁴⁾ reduces to

$$I_k = -\frac{1}{2\pi i} \int_{Br} e^{s\tau} ds \frac{2i}{\pi} \int_0^{\infty} \frac{g_k(v)}{G(v)} e^{-s\zeta\sqrt{a_k^2 - v^2}} K_1(sv) I_0(\rho sv) dv \quad (4.21)$$



Complex
V-plane

MRD DIVISION
GENERAL AMERICAN TRANSPORTATION CORPORATION

Considering the inner integration as integration in the complex v plane, we note that there are no singularities in the right half; let us consider the integration over the path indicated above, from 0 to ∞ , thence to $i\infty$ and back to zero along the right side of the imaginary axis. The integral over the closed path is zero, and since the integrand vanishes on the portion of the path from ∞ to $i\infty$, we have $\int_0^\infty + \int_{i\infty}^0 = 0$ or $\int_0^\infty = \int_0^{i\infty}$. Hence (4.21) can be written as

$$I_k = - \frac{1}{2\pi i} \int_{Br} e^{s\tau} ds \frac{2i}{\pi} \int_0^{i\infty} \frac{g_k(v)}{G(v)} e^{-s\zeta\sqrt{\alpha_k^2 - v^2}} K_1(sv) I_0(\rho sv) dv$$

or inverting the order of integration

$$I_k = - \frac{2i}{\pi} \int_0^{i\infty} \frac{g_k(v)}{G(v)} dv \frac{1}{2\pi i} \int_{Br} e^{s(\tau - \zeta\sqrt{\alpha_k^2 - v^2})} K_1(sv) I_0(\rho sv) ds$$

We now let $v = ix$, $s = -iy$, yielding

$$I_k = \frac{2i}{\pi^2} \int_0^\infty \frac{f_k(x)}{F(x)} dx \int_0^\infty e^{-iy\eta_k} K_1(xy) I_0(\rho xy) dy$$

where $\eta_k = \tau - \zeta\sqrt{\alpha_k^2 + x^2}$, and $f_k(x)$ and $F(x)$ are defined as in (4.20).

But $e^{-iy\eta} = \cos y\eta - i \sin y\eta$, so the real part of the integral is

$$\text{Re}(I_k) = \frac{1}{\pi} \int_0^\infty \frac{f_k(x)}{F(x)} dx \frac{2}{\pi} \int_0^\infty \sin y\eta K_1(xy) I_0(\rho xy) dy$$

Now by a theorem of Sneddon⁽¹⁰⁾

$$\frac{2}{\pi} \int_0^\infty \sin y\eta K_1(xy) I_0(\rho xy) dy = \int_0^\infty e^{-y\eta} J_1(xy) J_0(\rho xy) dy$$

MRD DIVISION
GENERAL AMERICAN TRANSPORTATION CORPORATION

for $\eta \neq 0$. This sets an upper limit of $x = \sqrt{\frac{\tau^2}{\zeta^2} - \alpha_k^2}$ for the outer integral,

and at $\rho = 0$ we have

$$\text{Re}(I_k) = \frac{1}{\pi} \int_0^{\sqrt{\frac{\tau^2}{\zeta^2} - \alpha_k^2}} \frac{f_k(x)}{F(x)} dx \int_0^{\infty} e^{-s(\tau - \zeta \sqrt{\alpha_k^2 + x^2})} J_1(sx) ds$$

The inner integral is a standard form; evaluating it gives us the desired solution

$$\text{Re}(I_k) = \frac{1}{\pi} \int_0^{\sqrt{\frac{\tau^2}{\zeta^2} - \alpha_k^2}} \frac{f_k(x)}{F(x)} \frac{\sqrt{(\tau - \zeta \sqrt{\alpha_k^2 + x^2})^2 + x^2} - (\tau - \zeta \sqrt{\alpha_k^2 + x^2})}{x \sqrt{(\tau - \zeta \sqrt{\alpha_k^2 + x^2})^2 + x^2}} dx \quad (4.22)$$

4.8 Numerical Integration

The integrals (4.22) were evaluated numerically on the IBM 1620. Values of τ ran from .1 to 3.0 at intervals of .1, and values of ζ were from .1 to $\tau - .1$, also at .1 intervals. The integration was also performed for $\zeta = \tau - .05$, $\tau - .02$, $\tau - .01$ and $\tau - .005$, to give an approximation to the shape of the peak and the value at the wave front. The parameter β^2 was taken to be 3.

For each point in the τ - ζ mesh, the upper limits $\frac{\tau^2}{\zeta^2} - 1$ and $\frac{\tau^2}{\zeta^2} - \beta^2$ were computed and designated as UL1 and UL2 respectively (UL2 was set equal to zero for $\frac{\tau^2}{\zeta^2} < \beta^2$). The program then defined $DX1 = \frac{UL1}{20}$ and $DX2 = \frac{UL2}{20}$. The values of the integrand were found at the points $x = n \cdot DX1$ ($n=1, \dots, 20$) for the first two integrals and $x = n \cdot DX2$ for the third. The integrals were then approximated by Simpson's rule, and the stresses found by adding the appropriate integrals.

MRD DIVISION
GENERAL AMERICAN TRANSPORTATION CORPORATION

The results of this computation are shown in Figure 4.1, for selected values of τ , with $\sigma_{\rho\rho}$ and $\sigma_{\zeta\zeta}$ plotted as functions of ζ .

4.9 Reflection of Stress Waves

The radial and axial stress components have now been computed for waves propagating in a half-space. To apply these results to a plate of finite thickness, a computer program was developed to find the stresses reflected in the plate from the stresses mentioned above. That is, the half-space stress previously computed were used as inputs for this program which for each point in the time-depth mesh calculates the sum of the stresses from all reflected stress waves which have passed the point, after multiplying each of these stresses by the product of the appropriate reflection coefficients to account for the reflections undergone by the wave in question. Since the stresses are calculated initially in terms of a unit pressure input, the final step in the computation is to multiply the stress sum by the coefficient of transmission from the projectile into the plate. The materials considered here are Fe for the projectile and Fe and Ti for the plate. The transmission and reflection coefficients for these media are as follows (6)(22)

		Incident Wave in	
Transmitted into	Fe	Fe	Ti
	T = 1 R = 0	T = .735 R = .265	
	Ti	T = .735 R = -.265	
	Vacuum	T = 0 R = -1	
		Ti	Ti
		T = 1 R = 0	T = 0 R = -1

MRD DIVISION
GENERAL AMERICAN TRANSPORTATION CORPORATION

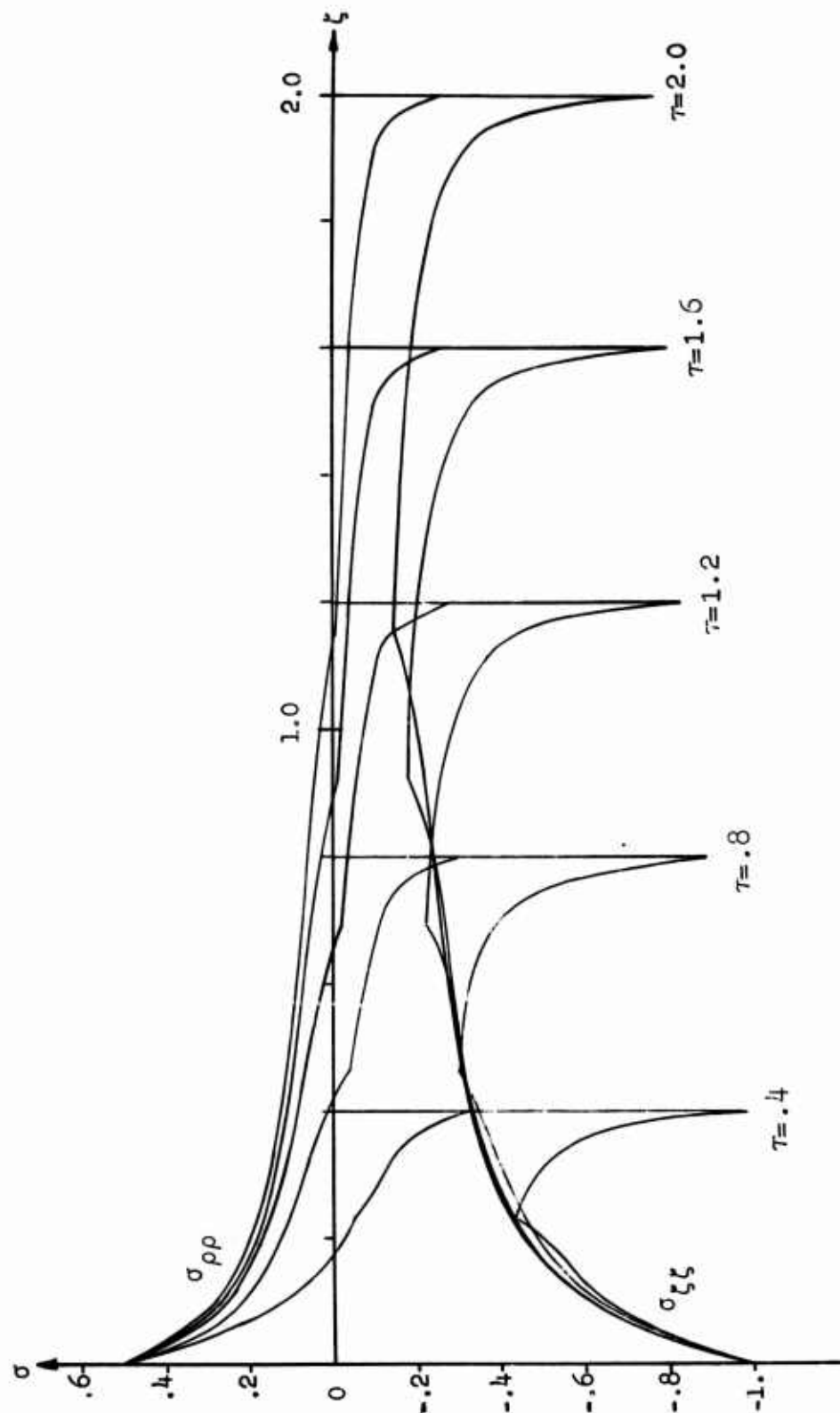


Figure 4.1 - Radial and Axial Stresses as Functions of Time and Depth (Dimensionless)

MRD DIVISION

GENERAL AMERICAN TRANSPORTATION CORPORATION

where transmission into a vacuum corresponds to our assumption that the back of the plate is free. The dimensionless plate thickness ζ is taken as 0.8 for each plate, and stresses are computed for $0 \leq \tau \leq 2$ at intervals of .10. In the case of the Fe plate (Figure 4.2), only the incident wave from the projectile and the first reflection from the back of the plate appear, since

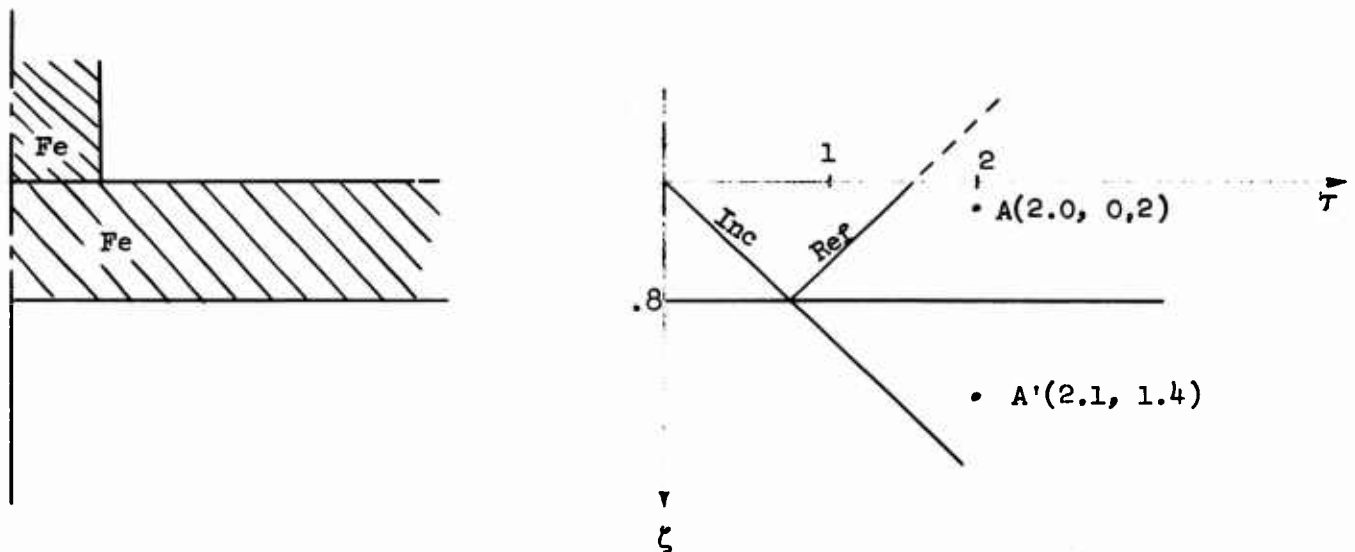


Figure 4.2 - Reflection of Stress Waves in Fe Plate

the latter, upon reaching the front of the plate, is entirely transmitted into the projectile. Let us consider for example the axial stress at point A. Since this point lies behind both the incident wave front and the reflected wave front, there will be two terms: first, the direct stress at A; second, the product of the Fe \rightarrow Vac reflection coefficient by the stress at the reflection A' of A about the rear of the plate. The sum is then multiplied by the projectile \rightarrow plate transmission coefficient:

$$\sigma_{\zeta\zeta}(2.0, 0.2) = [\sigma'_{\zeta\zeta}(2.0, 0.2) + (-1) \cdot \sigma'_{\zeta\zeta}(2.0, 1.4)] \cdot 1$$

MRD DIVISION
GENERAL AMERICAN TRANSPORTATION CORPORATION

where $\sigma'_{\zeta\zeta}$ denotes the stress computed on the half-space.

For the corresponding point Ti plate, there are three waves to consider (Figure 4.3), since the reflection from the back of the plate is not entirely transmitted into the projectile when it reaches the front surface, but is partly reflected back into the plate.

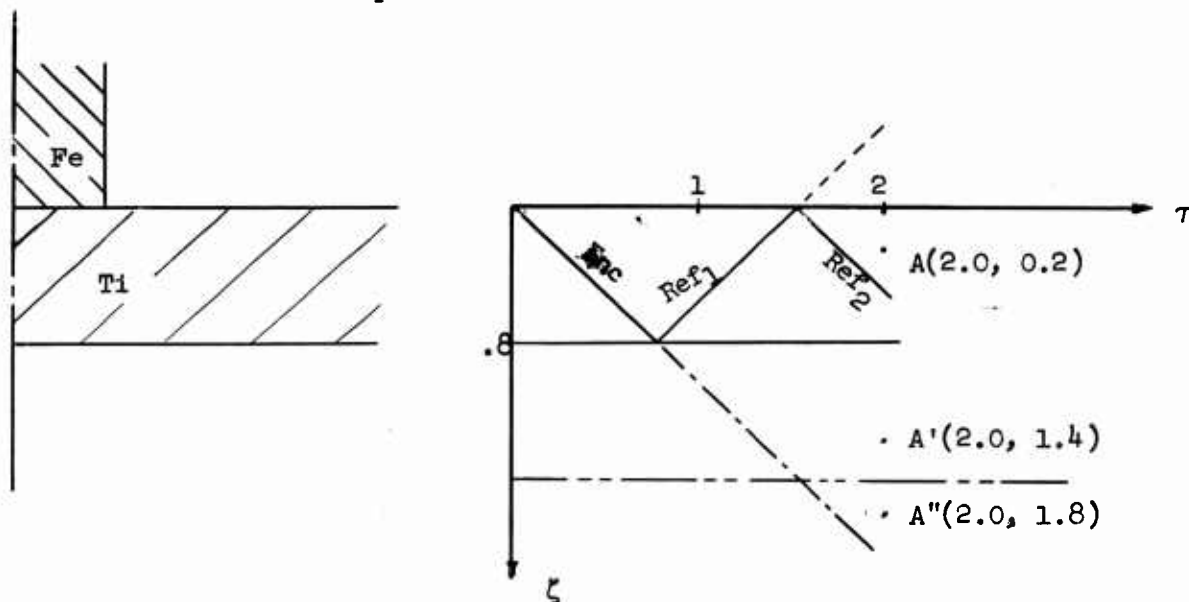


Figure 4.3 - Reflection of Stress Waves in Ti Plate

Thus we have in this case

$$\sigma_{\zeta\zeta}(2.0, 0.2) = [\sigma'_{\zeta\zeta}(2.0, 0.2) + (-1) \cdot \sigma'_{\zeta\zeta}(2.0, 1.4) + (-1) \cdot (R_{Ti \rightarrow Fe}) \cdot \sigma'_{\zeta\zeta}(2.0, 1.8)] T_{Fe \rightarrow Ti}$$

where T and R are the transmission and reflection coefficients as indicated by the subscripts.

The results of this computation are shown as stress contours in Figures 4.4 and 4.5, plotted in the τ - ζ plane. The heavy diagonal lines in these two figures show the fronts of the incident and reflected waves. The shaded areas indicate regions of tensile stress.

MRD DIVISION
GENERAL AMERICAN TRANSPORTATION CORPORATION

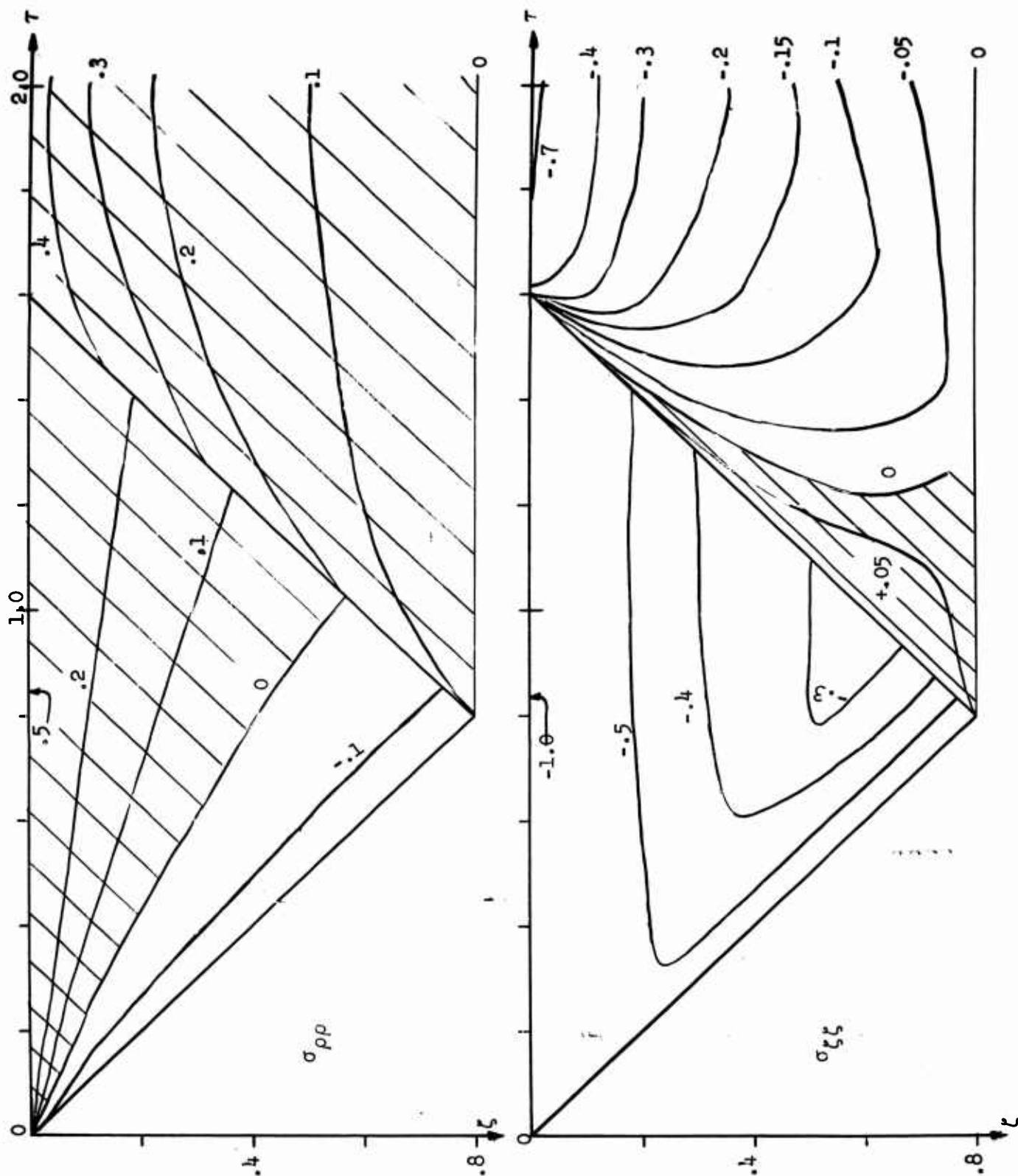


Figure 4.4 - Stress Distribution in Fe Plate

MRD DIVISION
GENERAL AMERICAN TRANSPORTATION CORPORATION

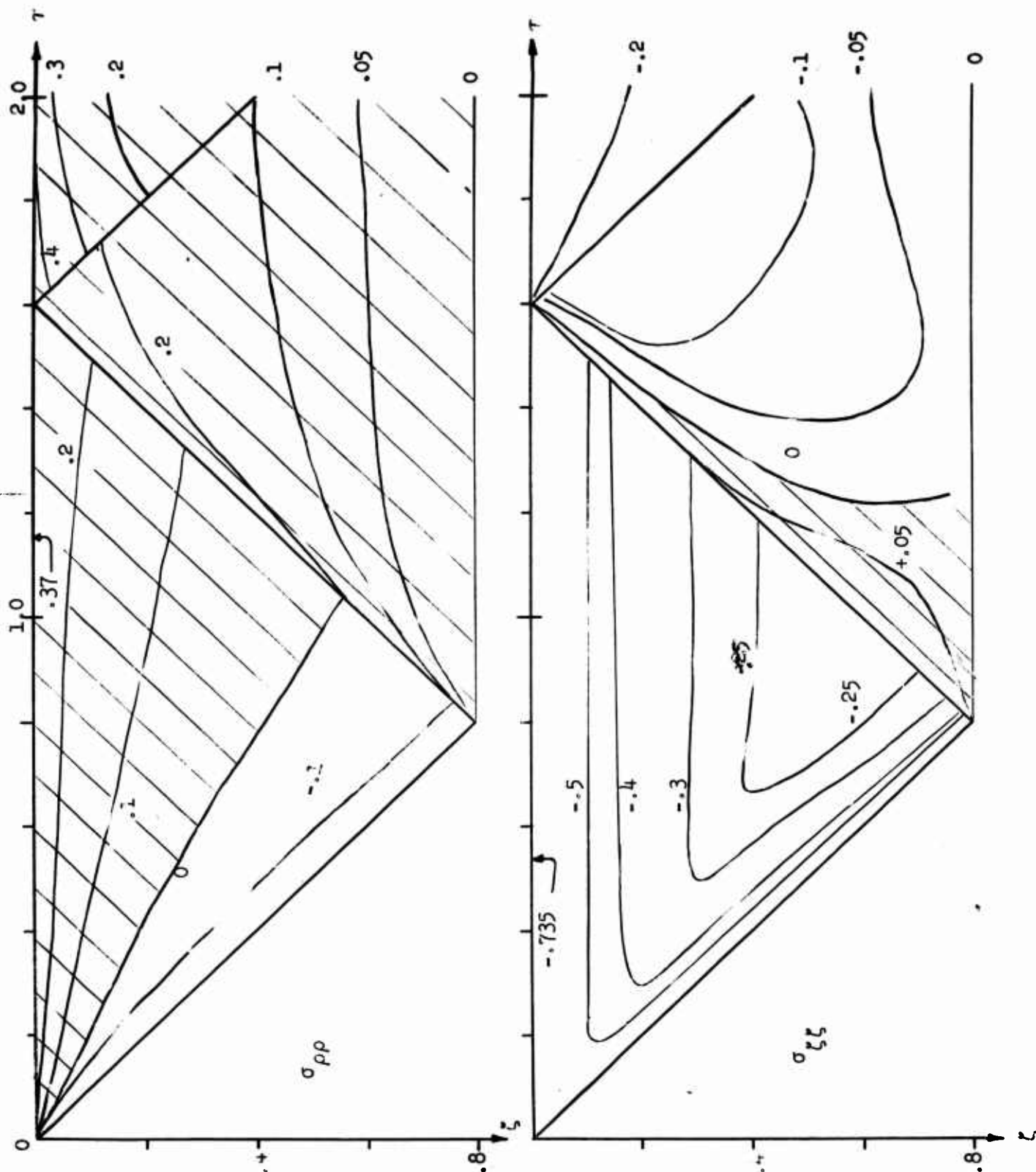


Figure 4.5 - Stress Distribution in Ti Plate

MRD DIVISION
GENERAL AMERICAN TRANSPORTATION CORPORATION

4.10 Wave Analysis for Laminated Plate

The analysis discussed above is extended here to provide a solution for the stresses in a laminated plate; we consider plates consisting of a layer of Fe and a layer of Ti, in both orders and various relative thicknesses.

The necessity for a somewhat simplified approach can be seen by referring to Appendix A, where the formal integral solution for a laminated plate is derived under a set of rather artificial boundary conditions chosen largely for the relative simplicity they provide while still retaining some resemblance to the physical situation. Even under these conditions, it can be seen that the formal solution is of an inordinate degree of complexity: evaluation requires that 8 equations similar to (A.38) be solved, and each of these, in order to be solved, must be further complicated by substitution of the defined values of the variables m_i , n_i , p_i , q_i , and by the insertion of an expression for the transform of the pressure history. Clearly, the practical value of this formal solution is somewhat limited.

4.11 Method of Solution

As stated above, the approach used is the same as that previously discussed for a single plate. The half-space stresses computed there were again used as input data for determination of the plate stresses. The computation was carried out for six cases: the two plate materials considered were again Fe and Ti, and in each order of the two, the stresses were computed for component-plate thickness ratios of 1:3, 1:1, and 3:1.

7

MRD DIVISION
GENERAL AMERICAN TRANSPORTATION CORPORATION

4.12 Numerical Evaluation

Detailed discussion of the program for the second phase of the problem, the composition of the stresses, has been reserved for this section because the same program was used here as for the single plates; the program was actually written for the laminated plates and the single plates treated as a special case.

4.12.1 Input Data

There are two types of data for the program; first, the half-space stresses computed in the first phase of this problem; second, the characteristics of the plate. They are handled in this order; first, the stress data are read (in the part of the program enclosed on the block diagram in dashed lines), consisting simply of a list of either all radial or all axial stresses. Then the plate data are read. We assume that the transmission and reflection of the stress waves is described by the transmission and reflection coefficients for plane waves as derived by Kolsky⁽²²⁾.

Incident Wave in			
Transmitted into	Fe	Ti	
	Fe	T = 1 R = 0	T = .735 R = .265
	Ti	T = .735 R = -.265	T = 1 R = 0
	Vacuum	T = 0 R = -1	T = 0 R = -1

MRD DIVISION
GENERAL AMERICAN TRANSPORTATION CORPORATION

The R and T read in are simply the reflection and transmission coefficients indicated by the subscripts 0 for the projectile, 1 for the upper plate, and 2 for the lower; e.g., R_{21} is the reflection coefficient for a wave in the lower plate reflecting from the upper. It is noted that the reflection coefficient at the bottom surface of the plate is -1 for either plate material. The code number KHL is 3, 5, 7, or 9 for an upper plate thickness of .2, .4, .6, or .8 respectively; the total plate thickness is .8 in all cases.

4.12.2 Outline of Computer Program

The program for this phase is diagramed in Figures 4.6 - 4.8. After the data are read as described above, the numbers H1, H2 and KH are computed. The first two of these are the thicknesses of the top and bottom plates, and are computed only to be printed so that the output can be identified. The actual values of time, depth, and plate thickness are not used in the computations nor in the logical decisions, which can be performed more conveniently by working with the fixed-point indices corresponding to these, defined by

$$I = 10T + 1$$

$$J = 10Z + 1$$

$$KHL = 10H1 + 1$$

The additional constant KH is defined because of the convenience of having a set of values 1, 2, 3, 4 corresponding to the values of H1.

The first step in the program after the data and required constants are all available is to initialize $I = 2$. T is then computed (initially .1) and printed. Determination of NK corresponds to the statement that, for

MRD DIVISION
GENERAL AMERICAN TRANSPORTATION CORPORATION

The R and T read in are simply the reflection and transmission coefficients indicated by the subscripts 0 for the projectile, 1 for the upper plate, and 2 for the lower; e.g., R_{21} is the reflection coefficient for a wave in the lower plate reflecting from the upper. It is noted that the reflection coefficient at the bottom surface of the plate is -1 for either plate material. The code number KHL is 3, 5, 7, or 9 for an upper plate thickness of .2, .4, .6, or .8 respectively; the total plate thickness is .8 in all cases.

4.12.2 Outline of Computer Program

The program for this phase is diagramed in Figures 4.6 - 4.8. After the data are read as described above, the numbers H1, H2 and KH are computed. The first two of these are the thicknesses of the top and bottom plates, and are computed only to be printed so that the output can be identified. The actual values of time, depth, and plate thickness are not used in the computations nor in the logical decisions, which can be performed more conveniently by working with the fixed-point indices corresponding to these, defined by

$$I = 10T + 1$$

$$J = 10Z + 1$$

$$KHL = 10H1 + 1$$

The additional constant KH is defined because of the convenience of having a set of values 1, 2, 3, 4 corresponding to the values of H1.

The first step in the program after the data and required constants are all available is to initialize $I = 2$. T is then computed (initially .1) and printed. Determination of NK corresponds to the statement that, for

MRD DIVISION
GENERAL AMERICAN TRANSPORTATION CORPORATION

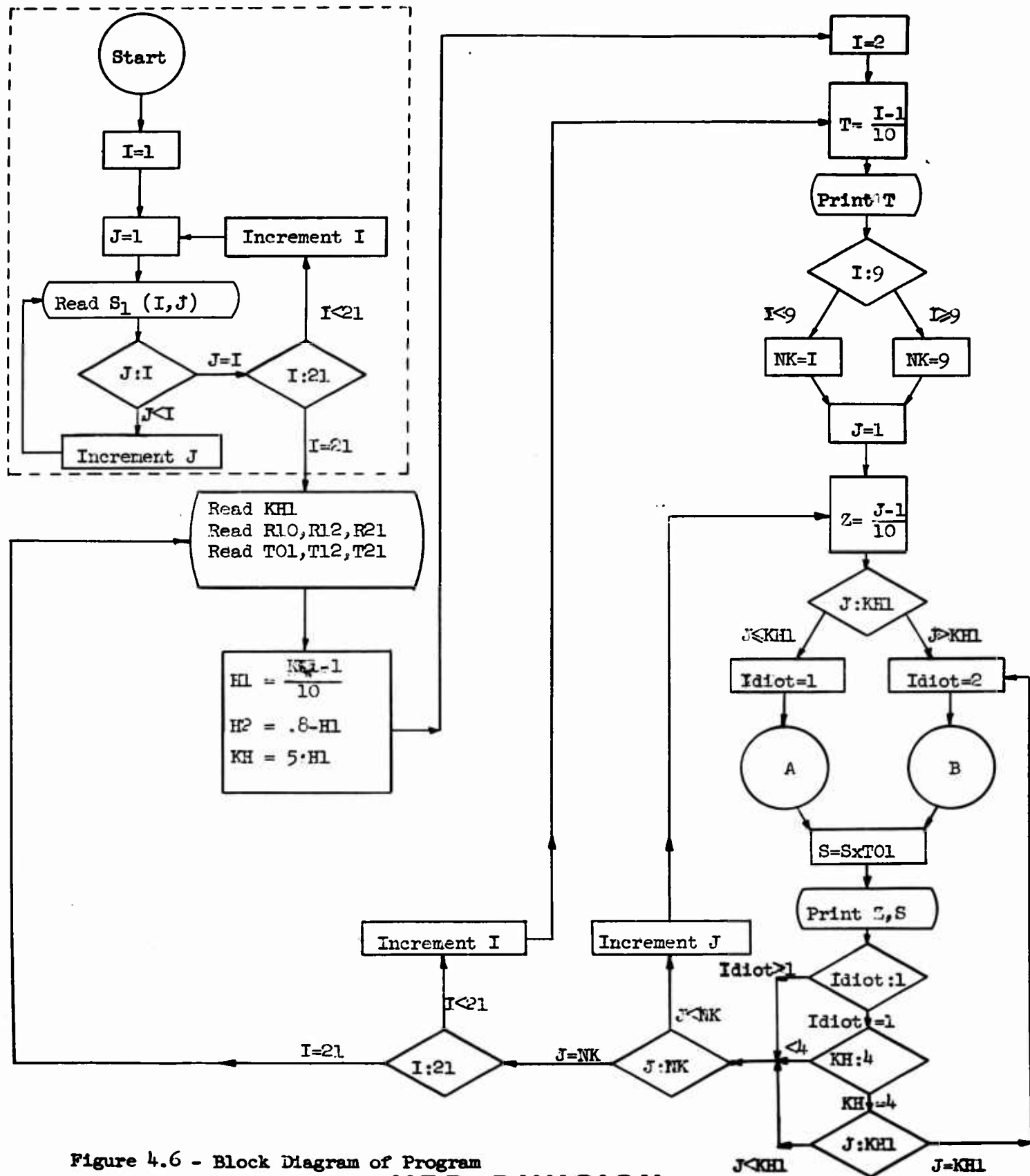


Figure 4.6 - Block Diagram of Program

MRD DIVISION

GENERAL AMERICAN TRANSPORTATION CORPORATION

any T , Z will not exceed $\min(T, .8)$. Then J is set to 1 ($Z=0$), and J is compared to KHL and the dummy variable $IDIOT$ given the value 1 or 2 depending on whether the point being considered is in the upper or lower plate (at the interface $J = KHL(Z=HL)$, the stress is computed first for a point in the upper plate approaching the interface). The actual stress computation for points in the upper and lower plates is carried out in the routines labelled (A) and (B) respectively. The sum of the stresses, S , is then multiplied by TOL , since the half-space stresses are for a unit stress input, and Z and S are printed. The three tests shown just below this in the lower right corner of Figure 4.6 are to determine whether the stress just computed was for the upper plate at the interface. If so, the next computation is for the lower plate at the same point. In any other case, J is tested to see if Z has reached its maximum value. If not, J is incremented and the computation is repeated; if so, I is incremented and J reset to 1. When I is found to have reached its maximum, the computation has been completed for the entire plate, and the data for the next plate are read and the program (except for reading the stress data) repeated. It should be noted that the program does not have a logical end. After all the plate data desired have been read and processed, the computer stops and is then instructed manually to return to the beginning and read the other set of stresses, then go on to reread each set of plate data and compute the other set of plate stresses.

4.12.3 Computational Portion of Program

As has been mentioned, the composition of stresses is performed in routines (A) and (B) of the program, shown in Figures 4.7 and 4.8. Here

MRD DIVISION
GENERAL AMERICAN TRANSPORTATION CORPORATION

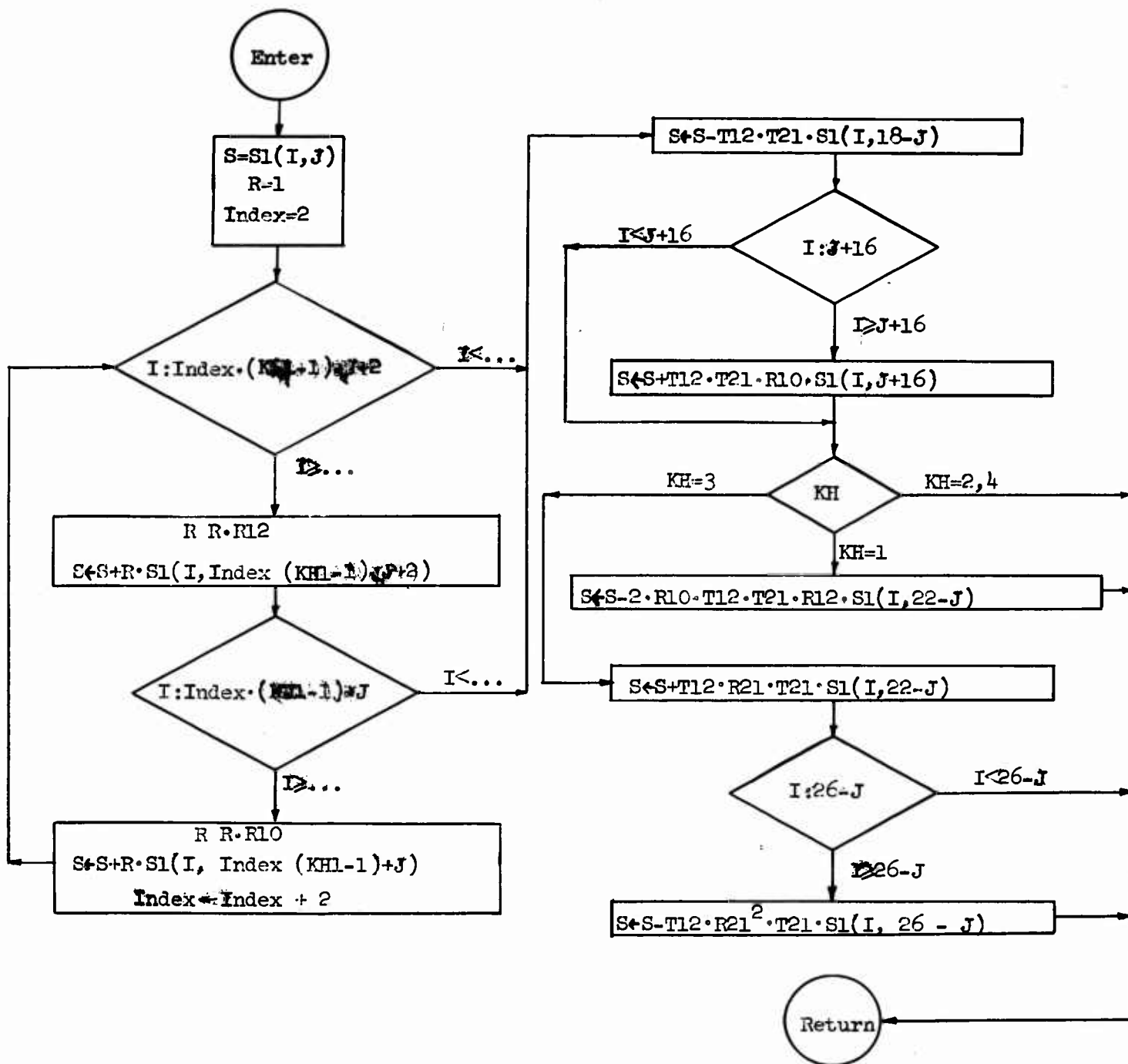


Figure 4,7 - Detail (A) of Block Diagram

MRD DIVISION
GENERAL AMERICAN TRANSPORTATION CORPORATION

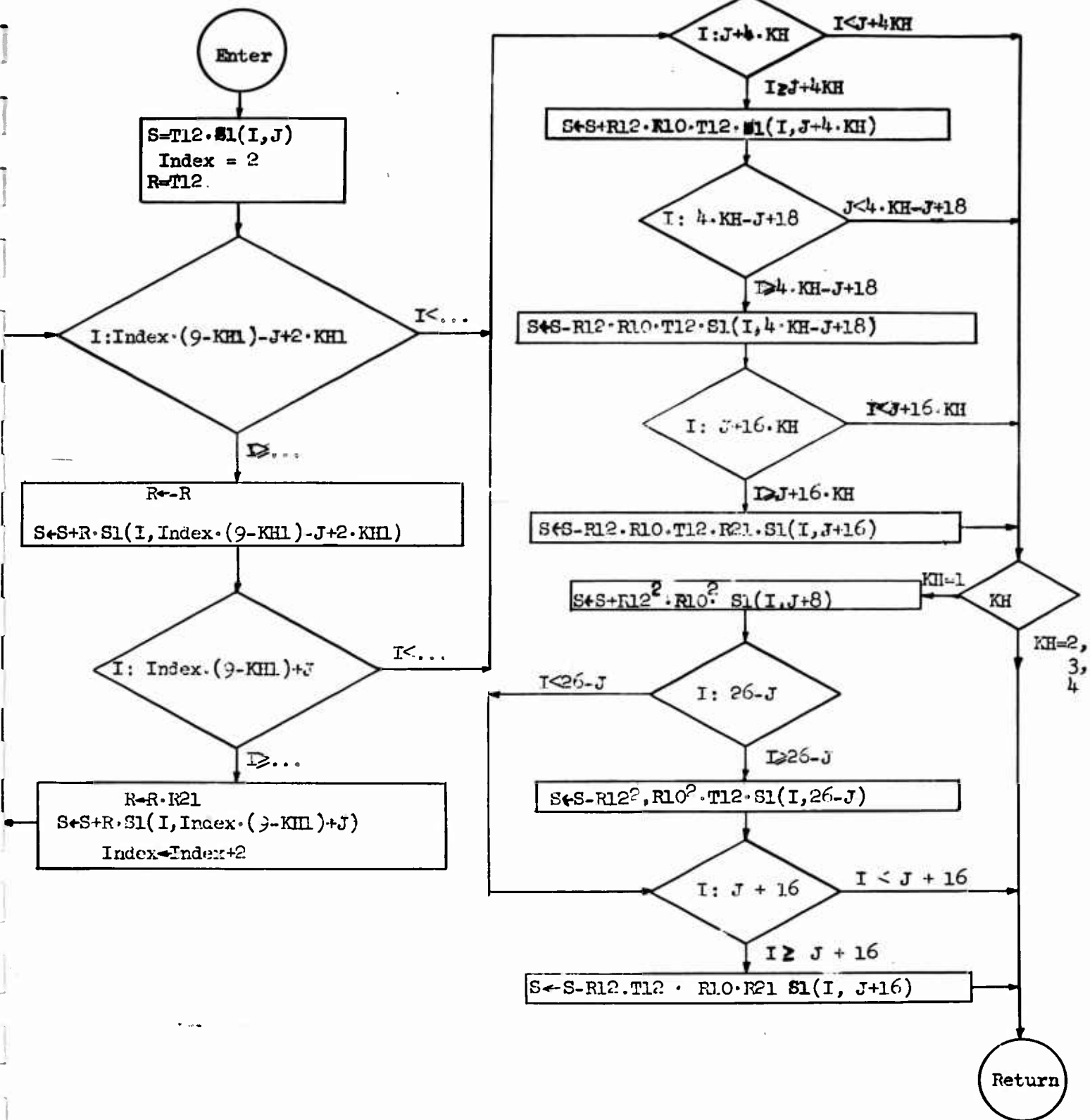


Figure 4.8 - Detail (B) of Block Diagram

MRD DIVISION
GENERAL AMERICAN TRANSPORTATION CORPORATION

we shall briefly explain (A) ; (B) , though slightly more complex, is analogous thereto.

Initially, the stress (radial or vertical) is set equal to the corresponding half-space stress; this accounts for the initial stress wave. Each test in this part of the program, with the exception of the test on KH, is to determine whether a relation between I and J (and hence between T and Z) is such that the point (I,J) lies behind the front of a particular wave. If so, a stress component, consisting of the product of the half-space stress at an appropriate point by the appropriate coefficients to account for the reflections and transmissions undergone by the particular wave reflection in reaching (I,J), is added to the sum of stresses, S, already computed for (I,J), and the computation proceeds to the next step; viz., testing to see whether the succeeding reflection has reached (or passed)(I,J). If not, the computation goes on to the next cycle; it having been found that a given reflection has not yet reached a given point, there is no reason to test for succeeding waves.

The cycle on the left-hand side of Figure 4.7, and the first three steps on the right, are common to all four thickness ratios ($\frac{.2}{.6}$, $\frac{.4}{.4}$, $\frac{.6}{.2}$, $\frac{.8}{.0}$); the computation goes through these steps for all plates. In addition, there is one reflection peculiar to the $\frac{.2}{.6}$ plate (KH=1), and two to the $\frac{.6}{.2}$ plate (at the corresponding stage in the lower plate (part (B)), there are three for the $\frac{.2}{.6}$ plate), so here the program branches according to the value of KH, and the indicated computation performed.

Now the return is made to the main program, the stress multiplied by

MRD DIVISION
GENERAL AMERICAN TRANSPORTATION CORPORATION

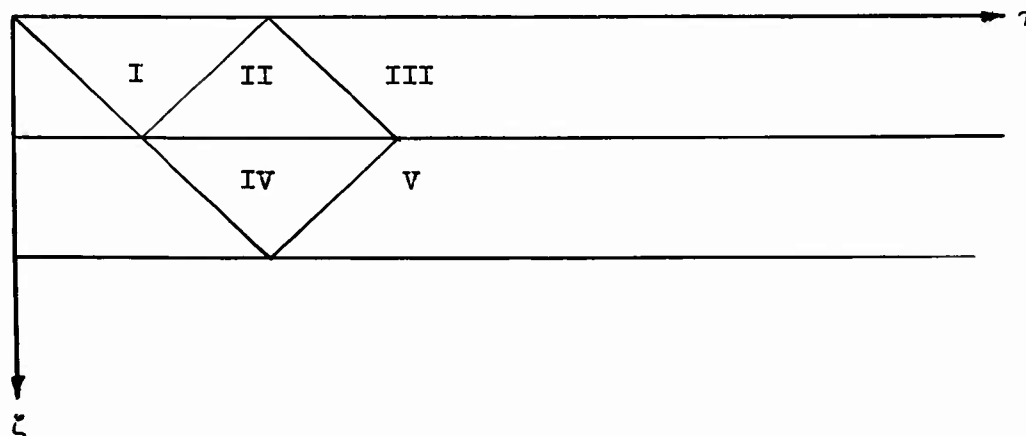
T01 (the last step in the computation, which, however, being common to (A) and (B), is placed in the main program) and printed, and the remainder of the program executed.

4.12.4 Results of Numerical Evaluation

The results of this phase of the program, as with the single plates, are presented in the form of stress contours, figures 4.9 - 4.14, with the tensile areas shaded and the wave fronts indicated as in Figures 4.4 and 4.5. The absence of contours at the lower right in several of the figures is due to the uncertainty resulting from the necessity of using the relatively coarse mesh (.1 x .1) in order to avoid exceeding the capacity of the computer; however, the values of the stresses in these areas were small, in general not in excess of .05.

4.13 Qualitative Discussion of Results

In order to consider the relative merits of the six laminated plates under consideration, they were each divided into five sections as shown:



MRD DIVISION
GENERAL AMERICAN TRANSPORTATION CORPORATION

The plates are assigned numbers in the same order as that in which they appear in the figures:

1	.2 Fe,	.6 Ti
2	.4 Fe,	.4 Ti
3	.6 Fe,	.2 Ti
4	.2 Ti,	.6 Fe
5	.4 Ti,	.4 Fe
6	.6 Ti,	.2 Fe

Then for each of the five sections, corresponding to the first few wave reflections, the plates were ordered according to the maximum tensile stresses found in the section. The results are as follows:

Section	$\sigma_{\rho\rho}$	$\sigma_{\xi\xi}$
I	1 = 2 = 3 > 4 = 5 = 6	(No tensile stresses)
II	1 > 2 > 3 > 5 > 6 > 4	(None)
III	3 > 1 > 2 > 5 > 4 > 6	(None)
IV	1 > 4 > 5; None for 2,3,6	(None)
V	1 > 2 > 3 > 4 > 5 > 6	3 > 2 > 1 > 5 > 4 = 6

In general, we may make the following observations regarding the various laminated plates: first, that those with the Fe component on top are subjected to higher stresses; and second, that those with the thinner top plate are also higher.

Taking the optimum plate to be that with the lowest maximum tensile stress, then, we would rate #6 first, then #4 and #5, followed by #2 and #3, and finally #1, which shows the highest maximum stresses.

MRD DIVISION
GENERAL AMERICAN TRANSPORTATION CORPORATION

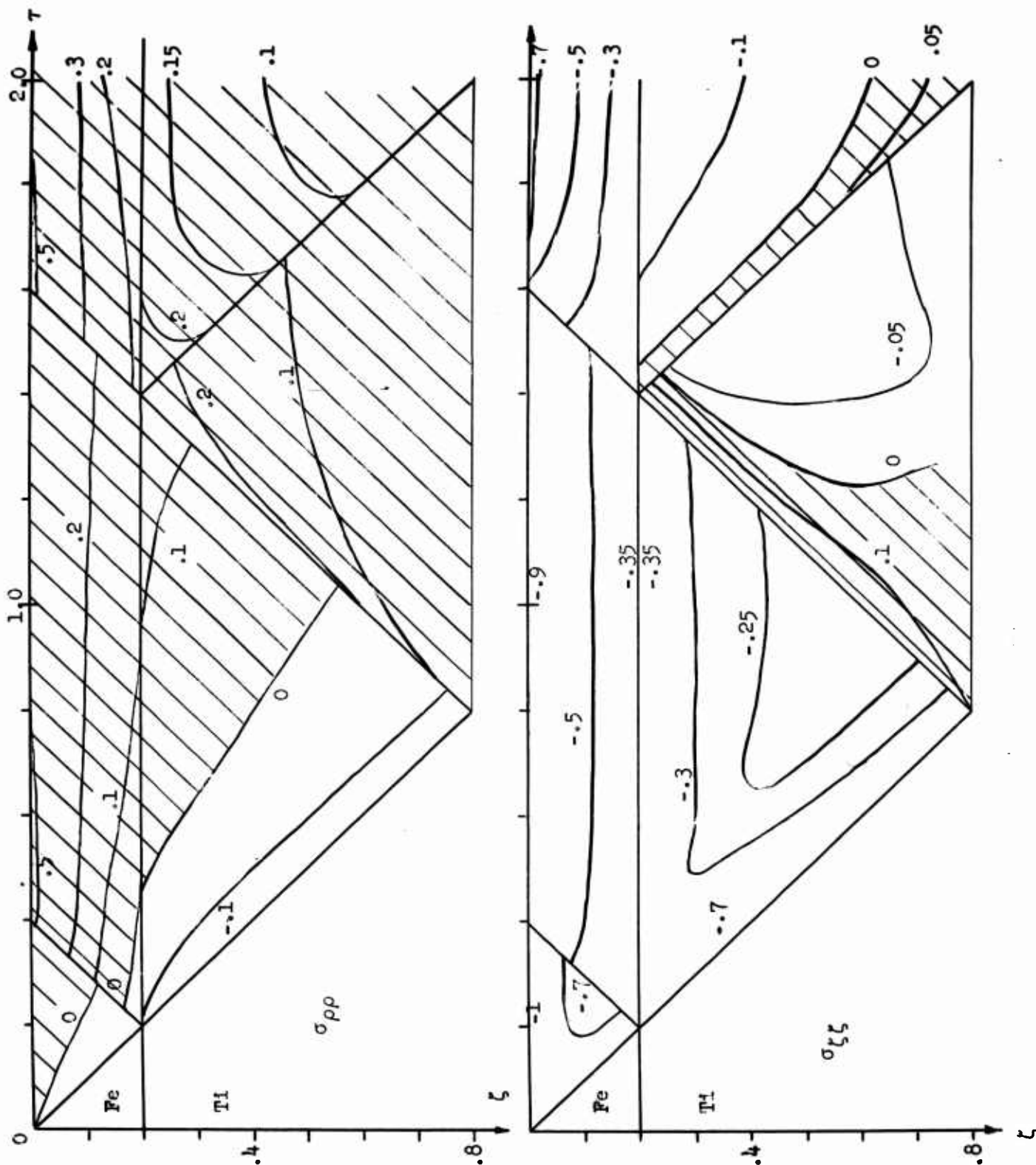


Figure 4.9 - Stresses in Laminated Plate: .2 Fe; .6 Ti

MRD DIVISION
GENERAL AMERICAN TRANSPORTATION CORPORATION



70

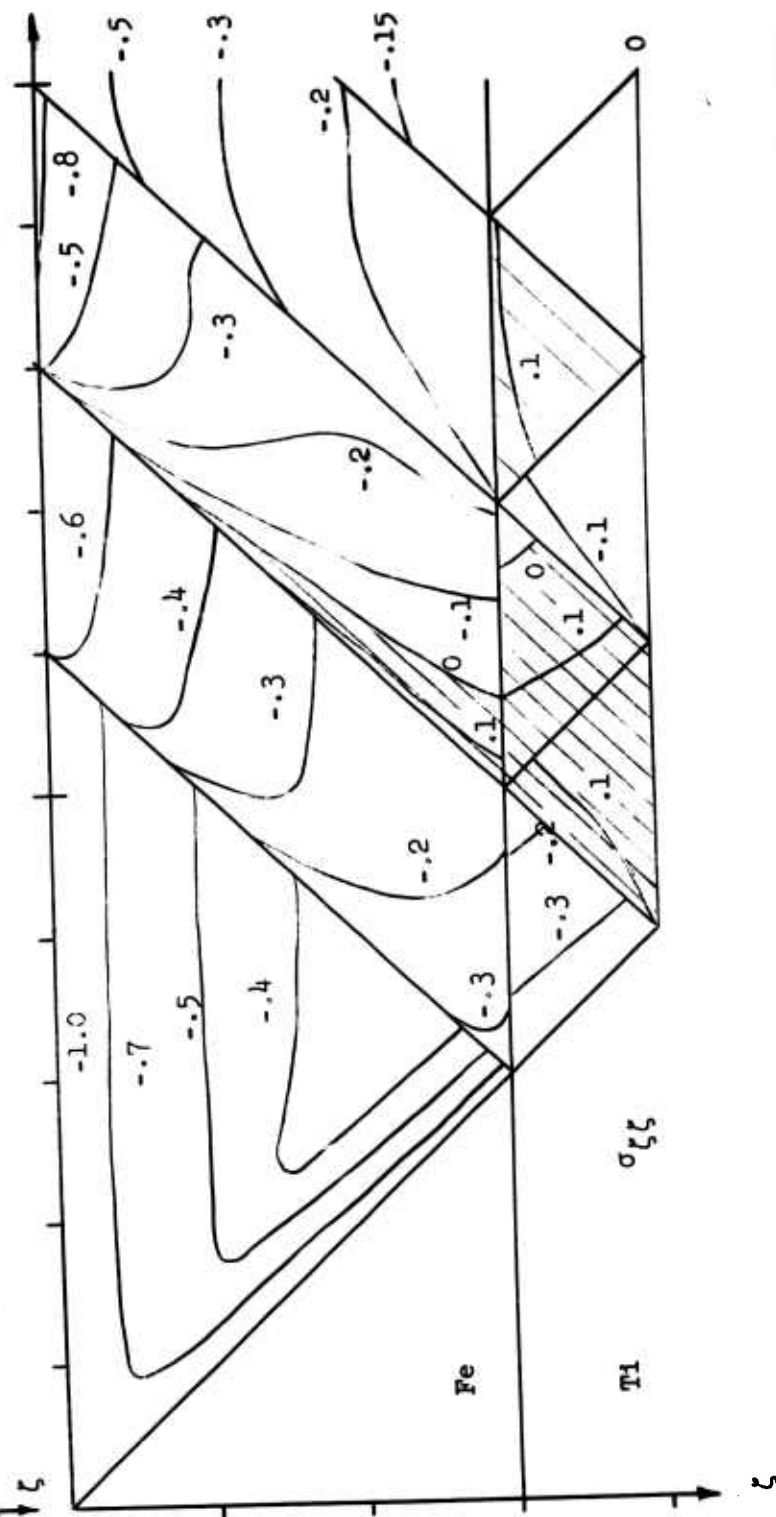
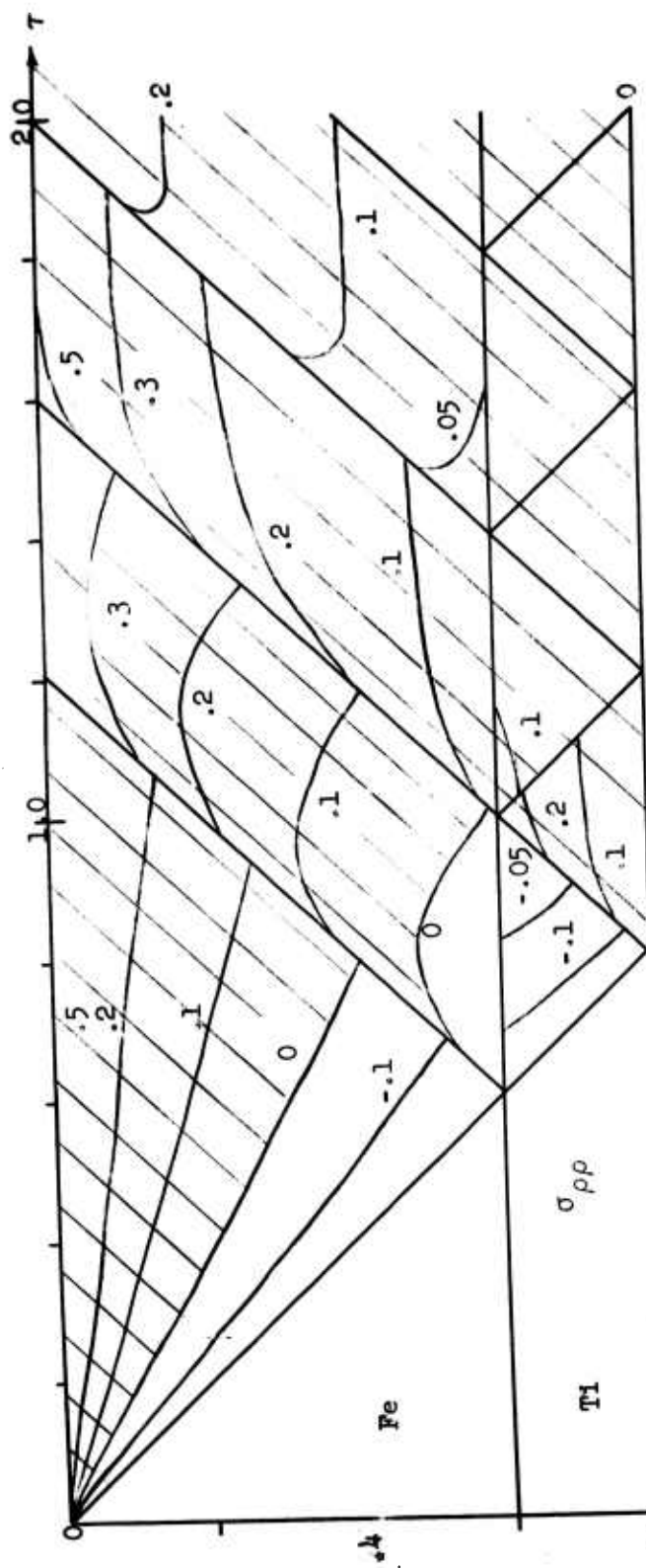


Figure 4.11 - Stresses in Laminated Plate: .6 Fe; .2 T1

MRD DIVISION
GENERAL AMERICAN TRANSPORTATION CORPORATION

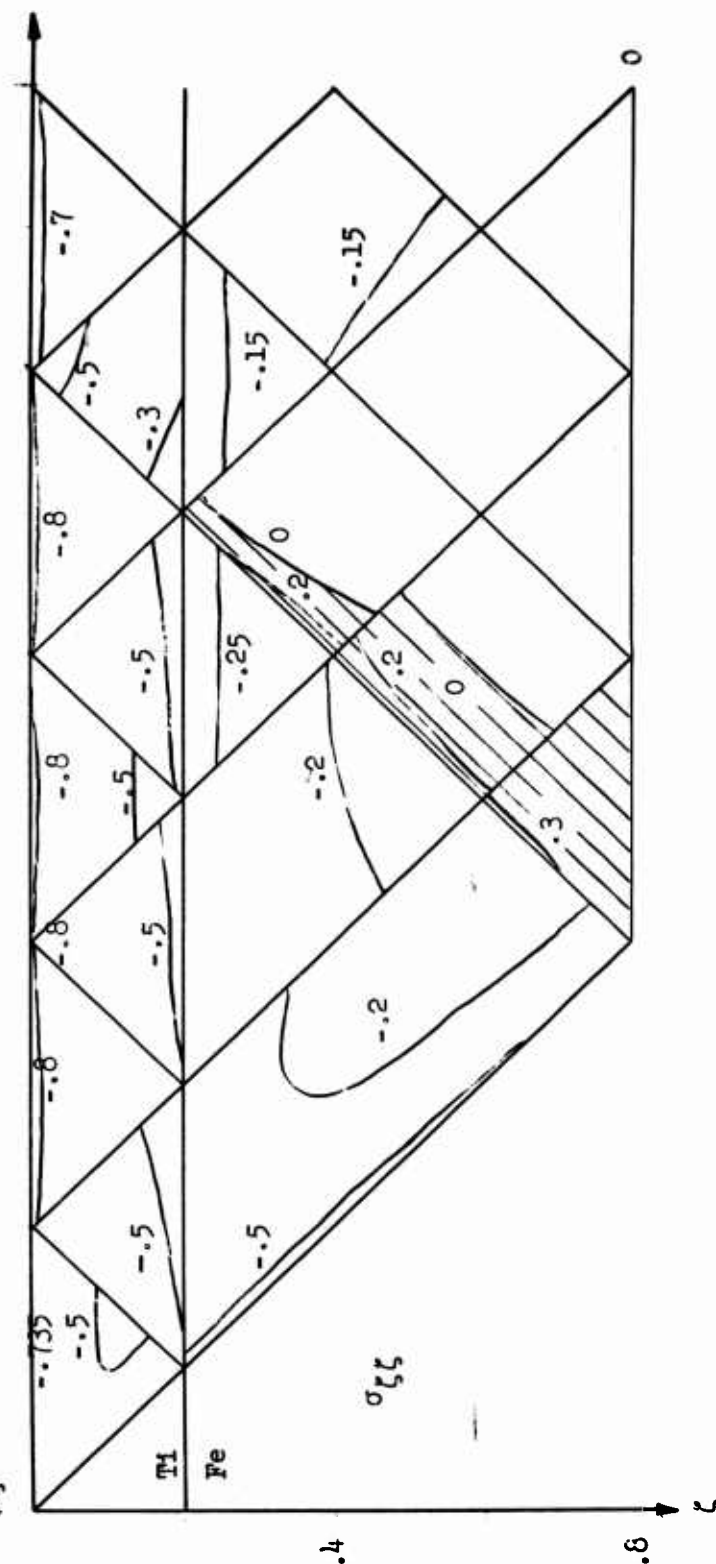
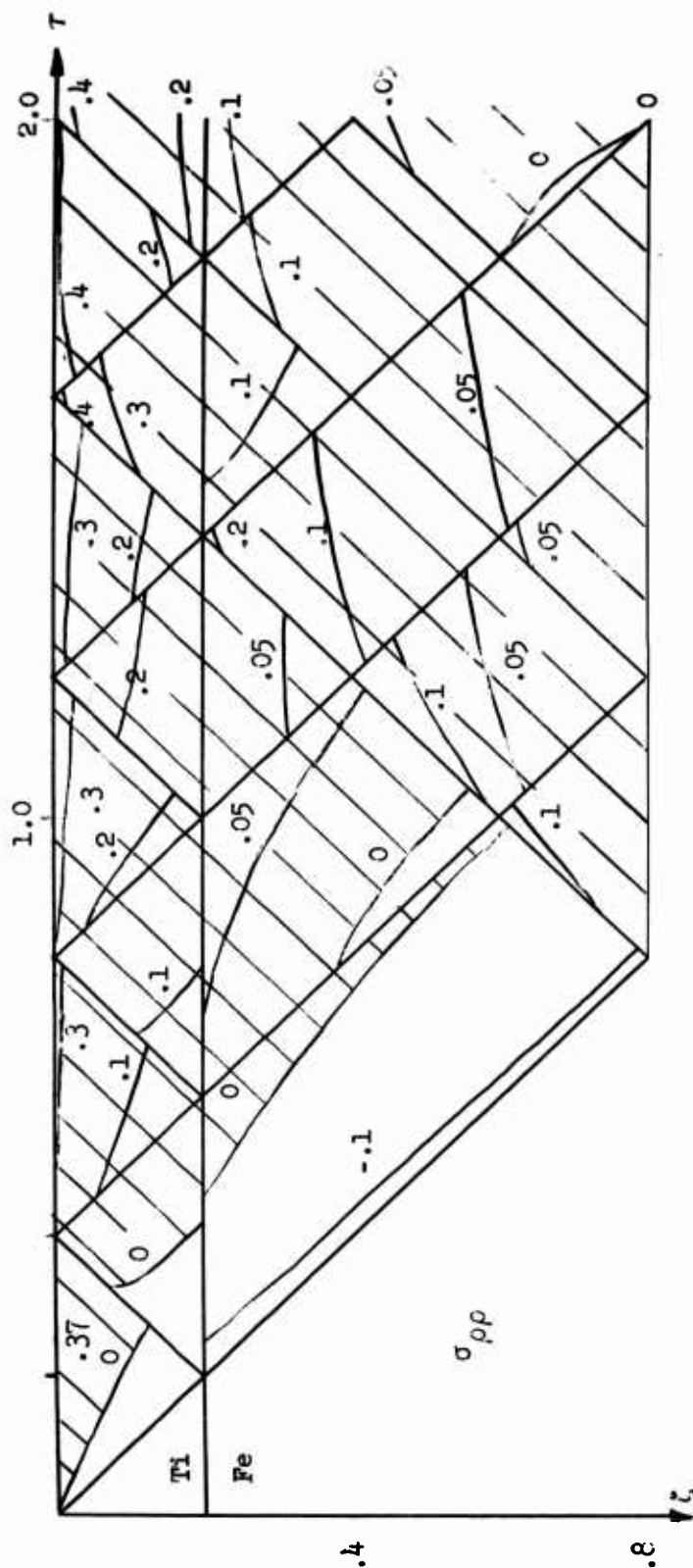


Figure 4.12 - Stresses in Laminated Plate: .2 Ti; .6 Fe

MRD DIVISION
GENERAL AMERICAN TRANSPORTATION CORPORATION

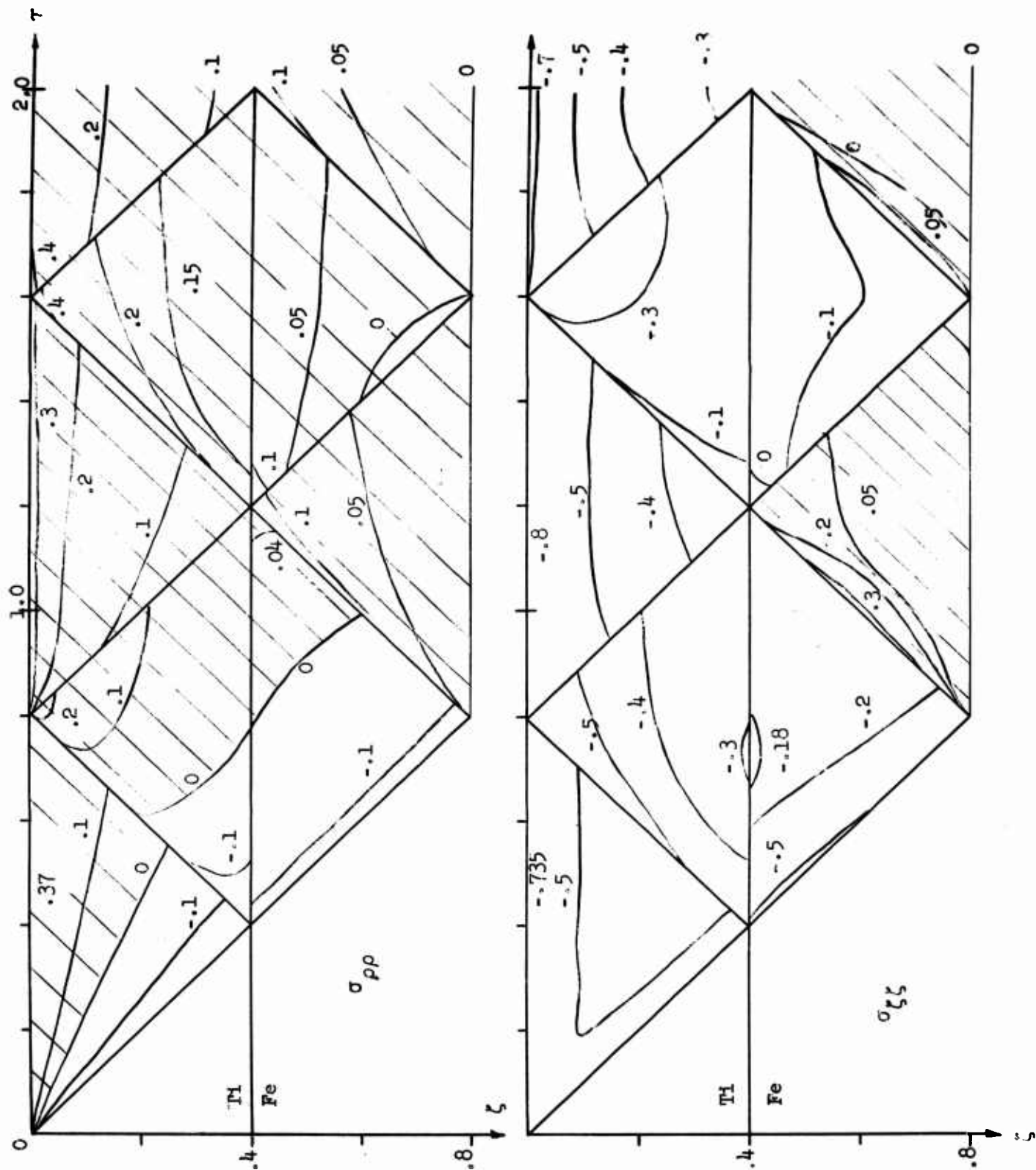


Figure 4.13 - Stresses in Laminated Plate: .4 T1; .4 Fe

MRD DIVISION
GENERAL AMERICAN TRANSPORTATION CORPORATION

4.14 Implications on Ballistic Resistance of Plates

In the previous paragraphs of this section the transient stress wave that crosses the plate system has been analyzed. The two stress components, radial (equivalent to tangential) and vertical have been numerically determined.

In a plate composed of a single material, the two stress components are compressive at the wave front. The magnitude of these stresses is quite large and for plates of thickness less than the bullet radius ($h/a < 1$) the vertical stress is of the order of magnitude of the impact pressure.

The transient spikes decay very quickly. The decay time is of the order

$$\Delta t \sim \frac{.1a}{c}$$

where a = radius of bullet

c = longitudinal sonic velocity

The stress components decay to a very steady stress configuration. The vertical stress is compressive and the radial stress is tensile. These stresses decay with depth much faster than the spikes.

Let us make a quick estimate of the decay time of a .1" steel plate for $h/a = .5$ ($a \sim 0.05$ ft). The sonic velocity for steel is about 17,000 ft/sec. Thus

$$\Delta t \sim \frac{.1(.05)}{17000} \sim 3 \times 10^{-8} \text{ sec.}$$

This time is very nearly the minimum to fracture observed by Zhurkov⁽⁸⁾.

Since this spike is held for such a short time, fracturing will not occur unless the stress level exceeds the stress at the wave front.

MRD DIVISION
GENERAL AMERICAN TRANSPORTATION CORPORATION

There are three regions in which the transient spike is analyzed for fracture:

1. As the wave crosses the plate, the first time, the sheer stress or the difference between the compressive stresses may become large.
2. The reflected transient vertical stress is tensile and the resulting vertical stress may be tensile.
3. The reflected radial stress is tensile and the total radial will be tensile.

In the first wave the stresses are compressive near the wave front. The fracture here will be dependent on the resolved shear stress. The Mohr's circle diagram of the fracture criterion is shown in Fig. 4.15. The critical shear stress will be taken as twice the tensile yield stress.

The shear stress in the directed wave is

$$\tau = \frac{1}{\beta^2} f_1(z/a)$$

$f_1(z/a)$ is the geometrical decay of the wave front and is shown in Fig. 4.16.

The maximum radial and vertical tensile stresses in the reflected wave are computed graphically by adding the value of the static stress at z/a to the negative of the stress at the wave front at position $(\frac{h}{a} + z/a)$.

The resulting maximum tensile stresses are plotted as a function of z/a parameterized by h/a . The maximum radial stresses are shown in Fig. 4.17 and the maximum tensile vertical stresses in 4.18.

MRD DIVISION
GENERAL AMERICAN TRANSPORTATION CORPORATION

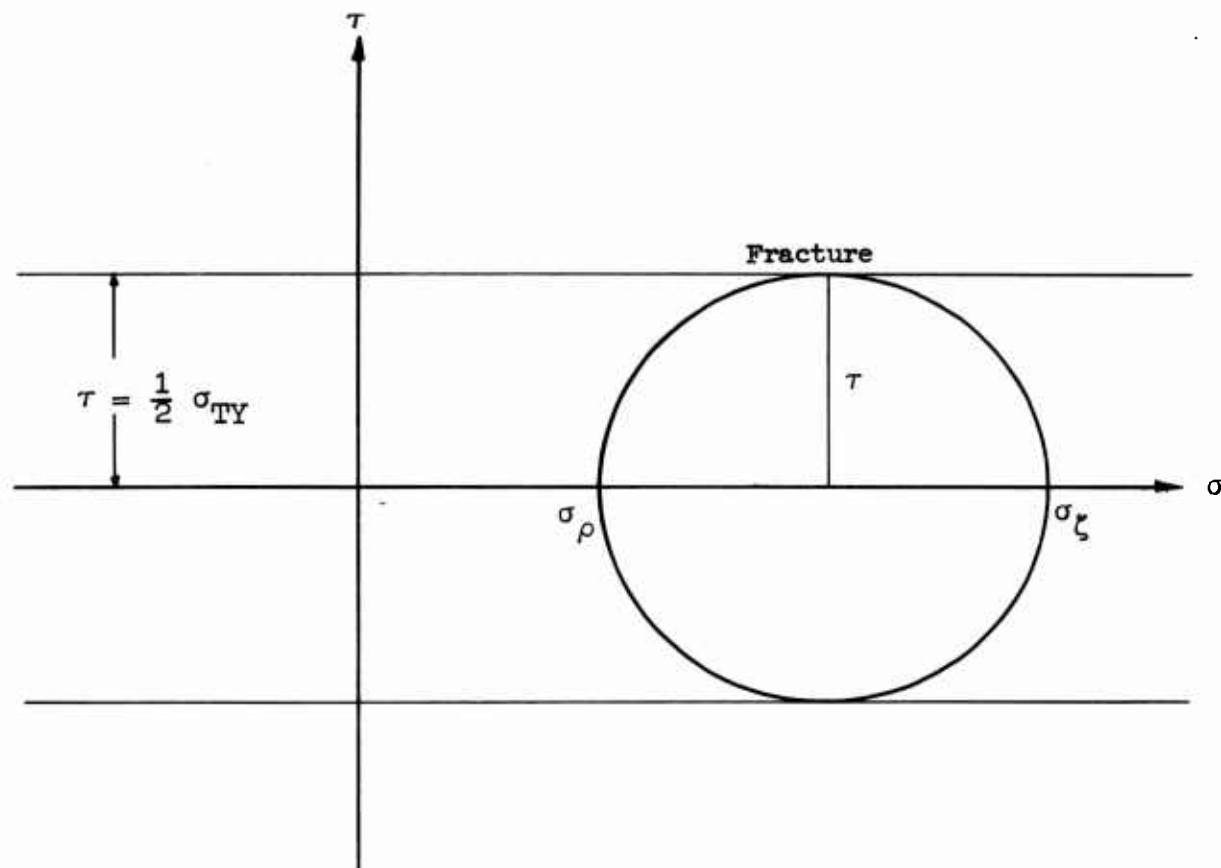


Figure 4.15 - Mohr's Diagram Showing Fracture Criterion
in Compressive Wave Front

MRD DIVISION
GENERAL AMERICAN TRANSPORTATION CORPORATION

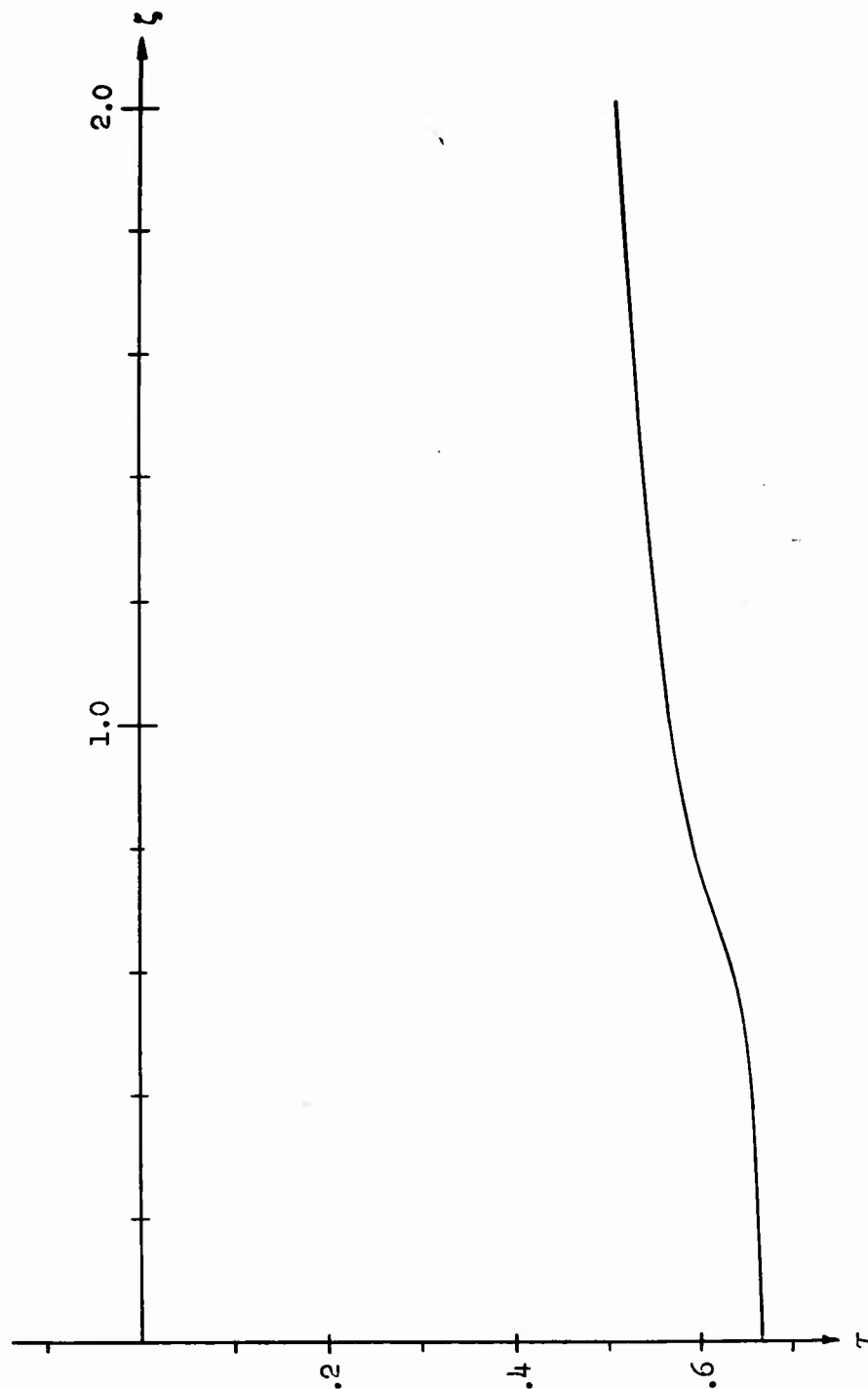


Figure 4.16 - Decay of Maximum Shear in Compressive Front

MRD DIVISION
GENERAL AMERICAN TRANSPORTATION CORPORATION

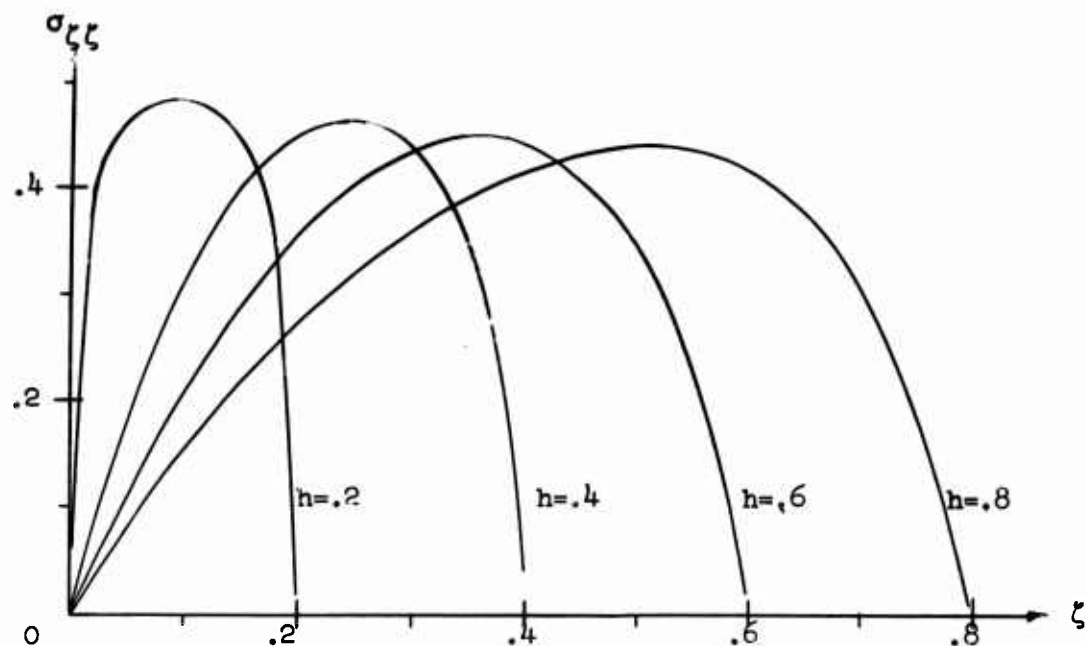


Figure 4.17 - Maximum Vertical Stress vs Depth for Various Plate Thicknesses

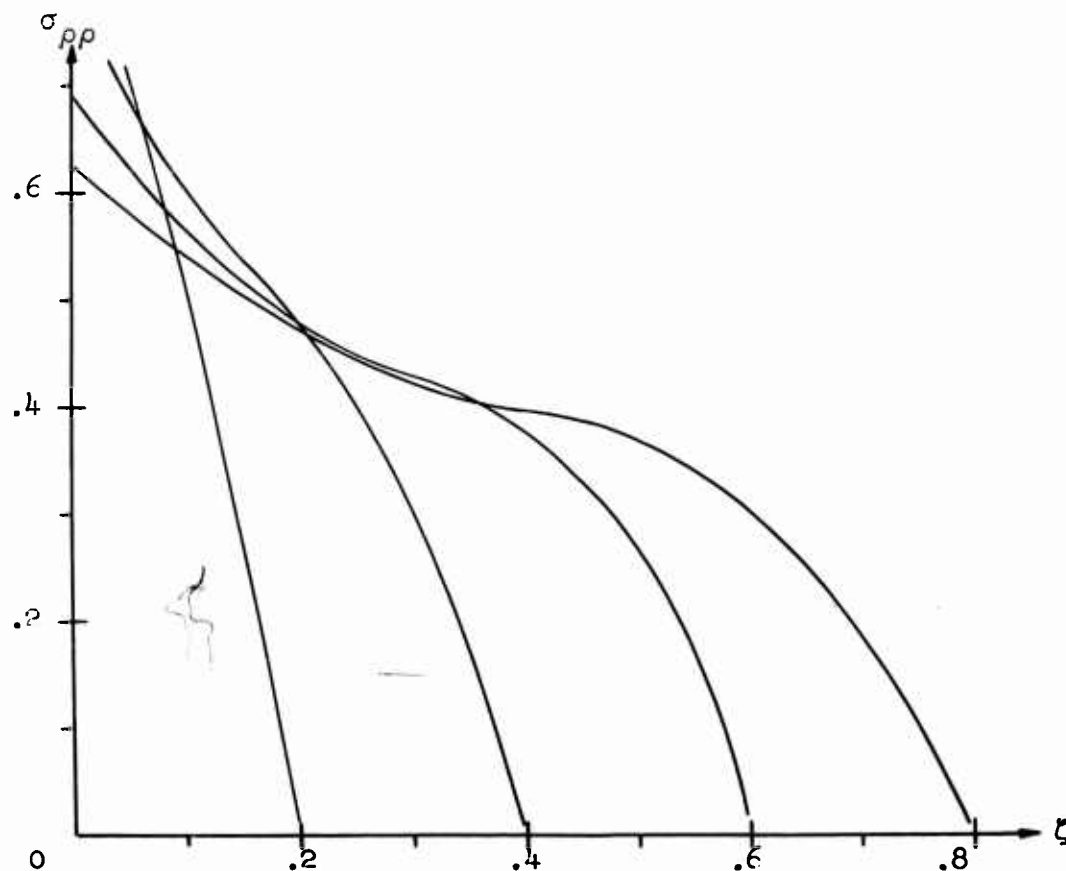


Figure 4.18 - Maximum Radial Stress vs Depth for Various Plate Thicknesses

MRD DIVISION
GENERAL AMERICAN TRANSPORTATION CORPORATION

For each plate thickness the vertical tensile stress has a maximum near the center of the plate. The radial tensile maximum is at the surface near the bullet,

The envelope of the maximum tensile radial and vertical stresses are plotted as a function of the dimensionless thickness h/a (Fig. 4.19.) Also included is twice the maximum shear stress in the compressive wave.

The plate will break if any one of these stresses exceeds the tensile yield stress. The upper curve consists of the radial tensile curve for very small thicknesses and the shear for larger thicknesses. If the plate material is very strong in compression, the upper curve for thicker plates will become the tensile vertical stress envelope.

Denote the upper bound by $f(h/a)$. The stress criteria for failure is (now in dimensional form)

$$\sigma_{cy} = f\left(\frac{h}{a}\right) p = f\left(\frac{h}{a}\right) \frac{\mu_1 c_1 \mu_2 c_2}{\mu_1 c_1 + \mu_2 c_2} v_s$$

or

$$v_{50} \equiv \frac{\mu_1 c_1 + \mu_2 c_2}{\mu_1 c_1 \mu_2 c_2} \frac{\sigma_{cy}}{f(h/a)}$$

The v_{50} as a function of plate thickness is shown in figure 4.20.

The overall reduction in bullet velocity may be calculated very simply from the force on the bullet.

$$\frac{mdv}{dt} = F$$

where $m = \text{Mass of bullet} = \pi a^2 L \mu_2$
 $L = \text{length of bullet}$

$v = \text{velocity of bullet}$

$F = \text{force} = \text{normal stress times area}$

$$\pi a^2 \sigma_2 = \pi a^2 \frac{\mu_1 c_1 \mu_2 c_2}{\mu_1 c_1 + \mu_2 c_2} v_s$$

MRD DIVISION
GENERAL AMERICAN TRANSPORTATION CORPORATION

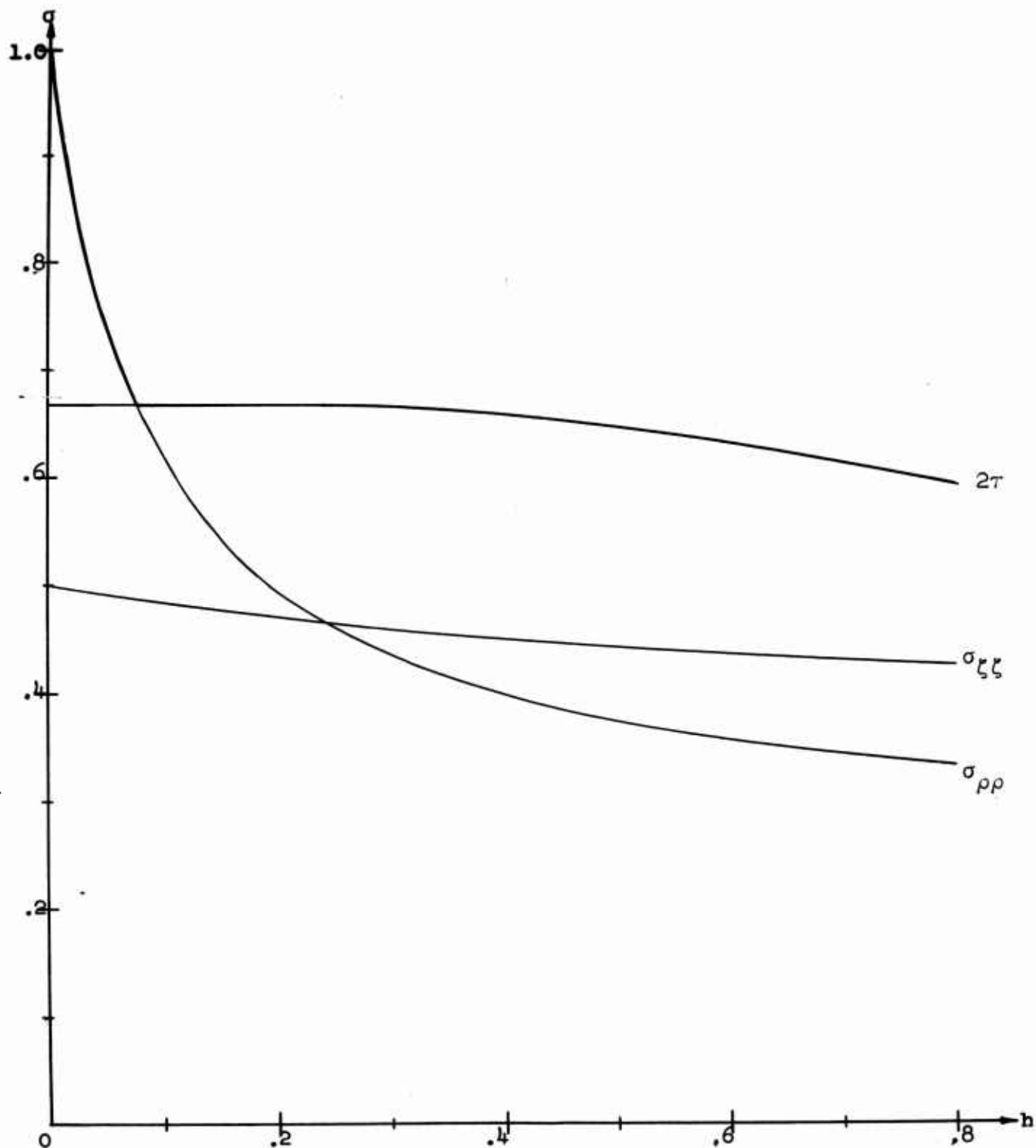


Figure 4.19 - Envelope of Maximum Tensile and Shear Stresses
vs. Plate Thickness

MRD DIVISION
GENERAL AMERICAN TRANSPORTATION CORPORATION

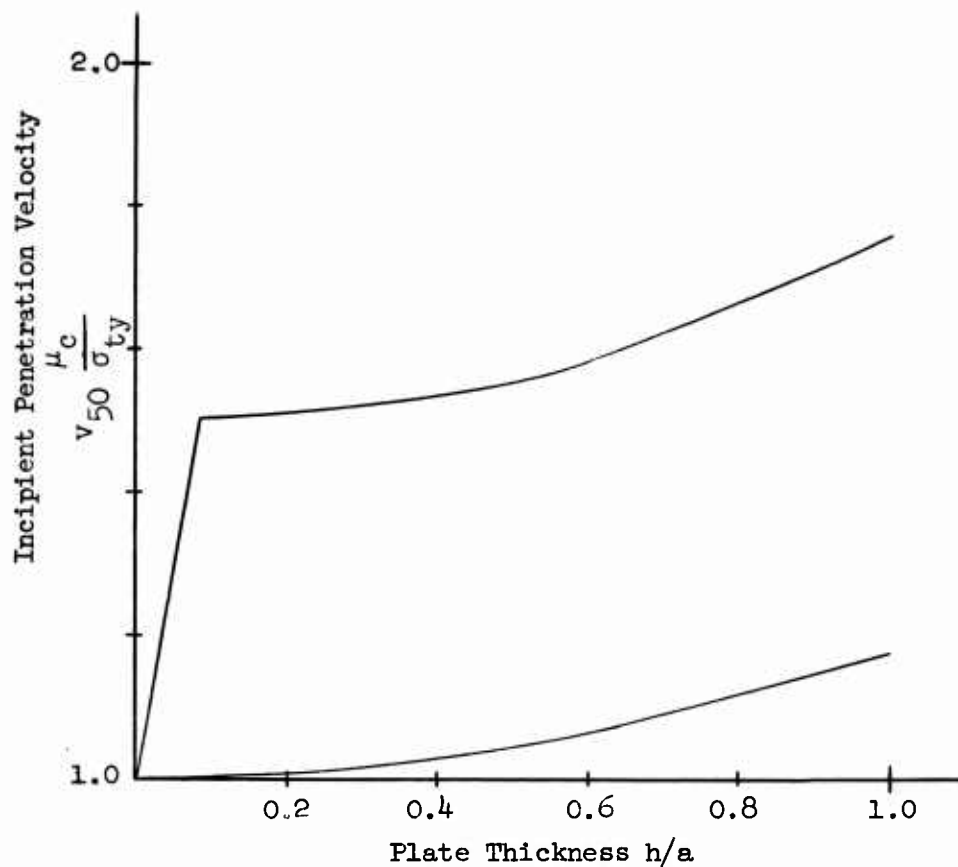


Figure 4,20 - Increase of the v_{50} with Increasing Plate Thickness

MRD DIVISION
GENERAL AMERICAN TRANSPORTATION CORPORATION

The velocity is integrated from its initial velocity V_S to its final velocity v_R and the force term is integrated from zero time until the time that the plate breaks which is the sum of the time to fracture and the transient time of the wave.

$$t_1 = t_{\text{trans.}} + t_f$$

$$V_S \sim v_R = \left(\frac{\mu_1 c_1 c_2}{\mu_1 c_1 + \mu_2 c_2} \right) L V_S t_1$$

For most cases, t_f is negligible compared with $t_{\text{trans.}}$.

$$t_1 \approx t_{\text{trans.}} = \frac{nh}{c_1}$$

and

$$\frac{v_R}{V_S} = 1 - \frac{\mu_1 c_2}{\mu_1 c_2 + \mu_2 c_2} \frac{h}{L}$$

where $n = 1$ if failure by shear stress is direct compressive wave

$n = 2$ if failure by reflected tensile stresses

Thus the v_R versus V_S curve is a straight line which, if extended would pass through the origin. At the lower end of this curve, however, the time to fracture may not be negligible and the v_R vs V_S curve will be slightly below the predicted curve.

The v_{50} values and the maximum v_R/V_S ratios were calculated for several cases for which experimental data is available. The experimental data was supplied by Mr. A. L. Alesi of the Quartermaster Corps Research and Engineering Command, Natick, Massachusetts. The predicted v_{50} values are given in table 4.3. The v_{50} values are evaluated for the compressive stress failure criteria in the

MRD DIVISION
GENERAL AMERICAN TRANSPORTATION CORPORATION

Table 4.3

PARAMETERS FOR RESIDUAL VELOCITY CALCULATION

Case	Thickness/ Radius h/a	Density lbs/in^3	Compressive Yield Stress ($\times 10^{-3}$) psi	High Critical Strain	V_{50} Calc. ft/sec	V_{50} (Exp.) ft/sec	Maximum v_r/v_s
I	1.09	0.286	70 130	.30	705 1310	1850	.7638 .7638
II	0.39	0.286	70 130	.30	385 715	800	.9158 .9158
III	0.077	0.163	160 170 180	.06	1735 1840 1950	1425	.8837 .8837 .8837
IV	1.16	0.163	160 170 180	.06	2480 2630 2790	1825	.8113 .8113 .8113
V	0.675	0.162	120 130 140	.12	1220 1320 1425	1425	.8914 .8914 .8914
VI	0.48	0.162	120 130 140	.12	1070 1120 1210	950	.9293 .9293 .9293
VII	0.90	0.161	110 120 130	.15	1370 1495 1620	1725	.8570 .8570 .8570
VIII	0.70	0.161	110 120 130	.15	1150 1250 1360	1400	.8878 .8878 .8878
IX	0.84	0.163	130 140 150	.10	1595 1715 1840	1700	.8629 .8629 .8629
X	0.425	0.163	130 140 150	.10	1095 1180 1260	850	.9306 .9306 .9306

MRD DIVISION

GENERAL AMERICAN TRANSPORTATION CORPORATION

direct wave. The values of the yield stress used are indicative of the range of yield reported in the literature. The plate descriptions together with the experimental data is classified. The descriptions of the materials and dimensions are given in Appendix B in the same order as Table 4.3. The predicted values of v_{50} are reasonable and reflect the uncertainty of the measured values of the yield strengths.

MRD DIVISION
GENERAL AMERICAN TRANSPORTATION CORPORATION

Section 5

MODEL FOR SHEAR FAILURE OF THE PLATE

The full solution of the equations of motion for impact involve the computation of both elastic and inelastic behavior in at least two dimensions plus time. The linear elastic solution for this problem is devilishly complicated. Only this model allows for an analytic solution.⁽¹⁴⁾ Since the stresses are above the static yield point for most of the deformation process, an approach is desired that will demonstrate the effects of the inelastic behavior.

To increase the mathematical description of the physics involved, and yet retain a fairly reasonably sized problem, the geometrical variations of the problem must be reduced.

To effect this geometric simplification, we note that after the stress wave has reflected at least once the vertical variation in stresses is almost zero. So the vertical variation of the stresses and displacements are approximated by setting

$$\frac{\partial}{\partial z} \equiv 0$$

Further, since most of the motion of the plate and projectile is vertical, we will neglect the radial displacement.

5.1 Historical Background

This type of model has been used by several authors to analyze impact on thin plates. Hopkins and Prager⁽¹⁷⁾ treated the deformation of the plate as pure bending and Craggs treated the problem as pure membrane stresses⁽⁹⁾. Illyushin⁽¹⁹⁾ thought that the deformation was pure shear and the Russian authors Kotchekov⁽²³⁾⁽²⁴⁾ Bakhshian⁽²⁾⁽³⁾, and Sokolov⁽²⁷⁾⁽²⁸⁾ used various visco-elastic and linear visco-plastic materials to carry out explicit calculations.

MRD DIVISION
GENERAL AMERICAN TRANSPORTATION CORPORATION

5.2 Mathematical Model

Assume a cylindrical bullet of radius R , length L approaches a plate of thickness h with an incident velocity v_s . The densities of the bullet and plate are μ_1 and μ_2 , respectively. The bullet strikes the plate. Denote the region of the plate directly under the bullet as the plug, Fig. (5.1) (Assume the propagation velocity for the transient spike stress waves is infinitely fast). Thus the momentum in the bullet is transferred instantaneously to the bullet and plug system.

The mass of the bullet is

$$M = \pi\mu_1 R^2 L \quad (5.1)$$

and the mass of the plug is

$$m = \pi\mu_2 R^2 h \quad (5.2)$$

The momentum in the bullet before impact is

$$p = Mv_s \quad (5.3)$$

The resulting velocity of the mass and plug system is given by the conservation of linear momentum

$$Mv_s = (M+m)v_o \quad (5.4)$$

or

$$v_o = \frac{M}{M+m} v_s \quad (5.5)$$

Assume that the only motion of the plate is in the vertical direction and that the only variation of displacement occurs in the radial direction (i.e. the variations in stress across the thickness of the plate are neglected). Further, assume that the membrane stresses and bending moments are zero.

MRD DIVISION
GENERAL AMERICAN TRANSPORTATION CORPORATION

This resulting deformation is thus a shear deformation. A further assumption is that the plug itself does not undergo any further deformation.

These assumptions have the effect that only the shear deformation near the rim of the bullet will be investigated. At the expense of full geometric detail, the influence of the non-elastic mechanisms of deformation will be brought to light.

Under these assumptions, the equations of motion in the plate reduce to a single equation

$$\mu_2 \frac{\partial v}{\partial t} = \frac{\partial \tau_{rz}}{\partial r} + \frac{\tau_{rz}}{r} \quad (5.6)$$

where

v = particle velocity

$v = \frac{\partial u}{\partial t}$

u = vertical displacement

τ_{rz} = shear stress

The shear strain is defined by

$$\gamma_{rz} = \frac{\partial u}{\partial r} \quad (5.7)$$

The equation of mass continuity in the plate is

$$\frac{\partial v}{\partial r} = \frac{\partial \gamma_{rz}}{\partial t} \quad (5.8)$$

One further relation is needed to complete the description. This equation is the equation of state if the material is conservative or constitutive equation if the material is not conservative. In either case, this equation

MRD DIVISION
GENERAL AMERICAN TRANSPORTATION CORPORATION

is a relation between the stresses and strains.

For the plastically deforming media, this constitutive equation is of the form

$$\dot{\gamma}_{rz} = \dot{\gamma}_{rz}^e + \dot{\gamma}_{rz}^p \quad (5.9)$$

where

$$\dot{(\quad)} = \frac{d}{dt} (\quad)$$

$\dot{\gamma}_{rz}$ = Total strain rate

$\dot{\gamma}_{rz}^e$ = elastic strain rate

$\dot{\gamma}_{rz}^p$ = plastic strain rate

For this problem, the elastic component of strain rate will be given by the differentiated form of Hooke's law.

$$\dot{\gamma}_{rz}^e = \frac{\dot{\tau}_{rz}}{G} \quad (5.10)$$

with G = shear modulus

The plastic strain rate term can be quite involved, depending on the material and boundary condition (see Section 2 for details). For the present derivation, it is assumed that the plastic strain rate is a function of the instantaneous stress only. No explicit terms will be inserted for this until the numerical evaluation.

Then

$$\dot{\gamma}_{rz}^p = \phi(\tau_{rz}) \quad (5.11)$$

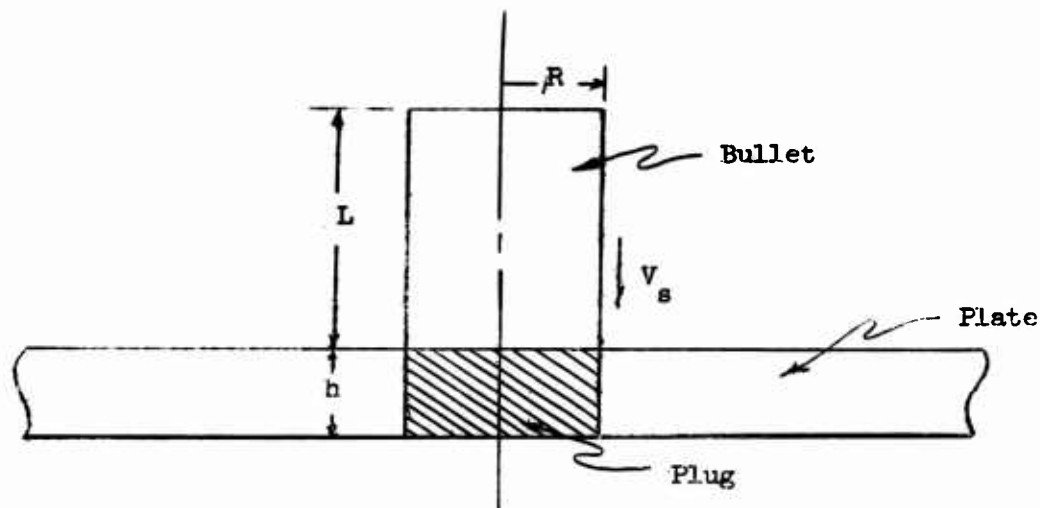


Figure 5.1 - Initial Configuration of Plate and Bullet

The constitutive equation is then

$$\dot{\gamma}_{rz} = \frac{\dot{\tau}_{rz}}{G} + \phi(\tau_{rz}) \quad (5.12)$$

These equations must be solved subject to the following boundary and initial conditions.

$$\left. \begin{array}{l} \text{Initial conditions } v = 0 \\ v = v_0 \end{array} \right\} \begin{array}{l} r > R \\ r = R \end{array} \quad t = 0$$

$$\text{Boundary conditions } (M+m) \frac{\partial v}{\partial t} = 2\pi R h \tau_{rz}, \quad r = R \quad t > 0$$

Introduce the following dimensionless parameters

$$\tau = \frac{\tau_{rz}}{\tau_s} \quad \text{Dimensionless Shear Stress}$$

$$\gamma = \frac{\gamma_{rz}}{\gamma_s} \quad \text{Dimensionless Shear Strain}$$

$$\tau = \frac{ct}{R} \quad \text{Dimensionless Time}$$

MRD DIVISION
GENERAL AMERICAN TRANSPORTATION CORPORATION

$$\rho = \frac{r}{R} \quad \text{Dimensionless Distance}$$

$$U = \frac{u}{\gamma_s R} \quad \text{Dimensionless Displacement}$$

$$V = \frac{v}{\gamma_s c} \quad \text{Dimensionless Velocity}$$

$$C = \sqrt{\frac{G}{\mu_2}} \quad \text{Sonic Velocity in plate}$$

$$\gamma_s = \frac{\tau_s}{G}$$

In these dimensionless variables the equations reduce to:

Momentum conservation

$$\frac{\partial v}{\partial \tau} = \frac{\partial T}{\partial \rho} + \frac{T}{\rho} \quad (5.13)$$

Continuity

$$\frac{\partial V}{\partial \rho} = \frac{\partial \gamma}{\partial t} \quad (5.14)$$

Constitutive equation

$$\frac{\partial \gamma}{\partial \tau} = \frac{\partial T}{\partial \tau} + \psi(T) \quad (5.15)$$

with

$$\psi(T) = \frac{R}{c\gamma_s} \phi\left(\frac{\tau R z}{\tau_s}\right) \quad (5.16)$$

A word of caution should be extended at this point. The form of the function ϕ which describes the plastic flow may or may not be amenable to scaling. The form that shall be used in later numerical calculations is scalable (i.e. it can be written in the form $\phi = \phi(T)$). However, many materials can be envisioned where this does not hold.

The boundary and initial conditions are:

$$\left. \begin{array}{ll} \text{Initial conditions} & v = 0 \quad \rho > 1 \\ & v = v_0 \quad \rho = 1 \end{array} \right\} \tau = 0$$

MRD DIVISION
GENERAL AMERICAN TRANSPORTATION CORPORATION

Boundary conditions $m_o \frac{\partial V}{\partial \tau} = T$

$$\rho = 1 \quad \tau > 0$$

where

$$m_o = \frac{(M+m)c^2}{2\pi R^2 hG} = \frac{M+m}{2M}$$

Even with simple forms of $\psi(\tau)$ analytical solutions are normally impossible, so that numerical equations must be used. However, a partial analytic solution sheds some light on various features of the solution.

The continuity equation is combined with the constitutive equation

$$\frac{\partial V}{\partial \rho} = \frac{\partial T}{\partial \tau} + \psi(T) \quad (5.17)$$

This equation with the momentum equation forms a system of totally hyperbolic partial differential equations. Thus this system can be simplified by the method of Riemann characteristics. The ulterior goal of this analysis is to find a simplified solution for the jump or shock conditions at the wave front that will propagate into the medium.

Add and subtract the momentum equation and continuity equations.

$$\frac{\partial V}{\partial \tau} \pm \frac{\partial V}{\partial \rho} = \frac{\partial T}{\partial \rho} \pm \frac{\partial T}{\partial \tau} + \frac{T}{\rho} \pm \psi(T) \quad (5.18)$$

Define the characteristics coordinates α, β

$$2\alpha = \tau + \rho$$

$$2\beta = \tau - \rho$$

The characteristic $\beta = \text{constant}$ is a line on a sonic wave which propagates outward and the line $\alpha = \text{constant}$ is a line on a sonic wave which propagates inward.

MRD DIVISION
GENERAL AMERICAN TRANSPORTATION CORPORATION

In terms of these characteristics the equations above may be written

$$\frac{dV}{d\alpha} - \frac{dT}{d\alpha} = \frac{T}{\rho} + \psi(T) \quad \text{along } \alpha = \text{constant}$$

$$\frac{dV}{d\beta} + \frac{dT}{d\beta} = \frac{T}{\rho} - \psi(T) \quad \text{along } \beta = \text{constant}$$

The characteristics are the only lines on which the solutions can be discontinuous.

Now consider the β characteristic that passes through the point $\rho=1, T=0$. Ahead of this characteristic the solution is identically zero. By considering the solution to any α -characteristic that crosses this line (in differential form)

$$dT + dV = (T + \psi(T)) d\beta \quad (5.19)$$

however $d\beta = 0$

Thus

$$[T^+ - T^-] = [V^- - V^+]$$

where the plus superscript refers to the values on one side of the β -characteristic and the minus superscript refers to the values on the other side. Thus, at the wave front, the jump in the dimensionless velocity is equal to the negative of the jump in the shear stress.

Along the β -characteristic the characteristic equation is simplified to

$$-2 \frac{dT}{d\alpha} = \left(\frac{T}{\rho} + \psi(T) \right) \quad (5.20)$$

or writing α as a function of ρ only

$$\frac{dT}{d\rho} = - \frac{1}{2} \left[\frac{T}{\rho} + \psi(T) \right] \quad (5.21)$$

Thus, at the wave front a simpler equation giving T as a function of ρ is available together with the relation $T = -V$

MRD DIVISION
GENERAL AMERICAN TRANSPORTATION CORPORATION

5.3 Numerical Method of Solution

The equations to be solved are

$$\frac{\partial V}{\partial \tau} = \frac{\partial T}{\partial \rho} + \frac{T}{\rho} \quad (5.22)$$

$$\frac{\partial V}{\partial \rho} = \frac{\partial T}{\partial \tau} + \psi(T) \quad (5.23)$$

in the region

$$\rho \geq 1$$

$$\tau \geq 0$$

subject to the boundary and initial conditions.

$$\left. \begin{array}{l} \text{Initial conditions } V = 0 \\ V = V_0 \end{array} \right\} \begin{array}{l} \rho > 1 \\ \rho = 1 \end{array} \tau = 0$$

$$\text{Boundary conditions } m_0 \left(\frac{\partial V}{\partial \tau} \right) = T, \quad \rho = 1, \quad \tau > 0 \quad (5.24)$$

The displacement is U and the total strain and particle velocity are defined by

$$V = \frac{\partial U}{\partial \tau} \quad (5.25)$$

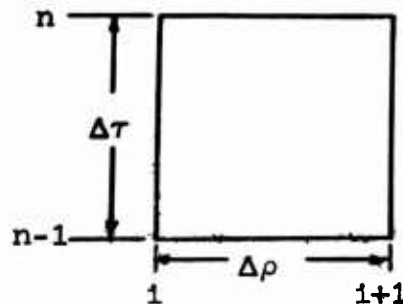
$$\gamma = \frac{\partial U}{\partial \rho}$$

The total plastic strain at any time and position is given by the integral

$$\gamma_p(\rho, \tau) = \int_0^\tau \psi(\rho, \tau') d\tau' \quad (5.26)$$

In addition to these, a simpler equation gives the stresses and particle

MRD DIVISION
GENERAL AMERICAN TRANSPORTATION CORPORATION



velocity at the wave front

$$\left. \begin{aligned} \frac{dT}{d\rho} &= -\frac{1}{2}\left(\frac{T}{\rho} + \psi(T)\right) \\ V &= -T \end{aligned} \right\} \text{ along } \rho = \tau + 1$$

These equations were solved by a finite difference set of equations.

The finite difference scheme is given below.

Form a square mesh work in the ρ, τ plane. The increment of mesh size in τ is $\Delta\tau$ and the increment in ρ is $\Delta\rho$, as shown in the figure. The index i refers to the increments in ρ and the index n refers to the increments in τ .

At some time t^{n-1} the displacements and velocities at the corners of the mesh U_i^{n-1}, v_i^{n-1} are known and the stress and accumulated plastic strain at the midpoint between each pair of mesh points, $T_{i+1/2}^{n-1}, \gamma_{p, i+1/2}^{n-1}$ are known. In addition, the wave front is located at $i = n-1$ and the stress and particle velocity at this point are known. The displacement is zero at the wave front.

First the displacements at time τ^n are computed

$$U_i^n = U_i^{n-1} + v_i^{n-1/2} \Delta\tau, \text{ for the points } 1 \leq i \leq n-1.$$

The displacement at $i = n$ is zero, i.e., $U_n^n = 0$.

The total strain at the midpoint of each cell is computed

$$\gamma_{T, i-1/2}^n = \frac{U_{n+1}^n - U_1^n}{\Delta\rho} \quad (5.27)$$

MRD DIVISION
GENERAL AMERICAN TRANSPORTATION CORPORATION

The increment in plastic strain γ_p^n at $i+1/2$ is computed by a Runge-Kutta integration assuming a constant total strain-rate process in each cell during this time step.

$$\gamma_p^n \text{ at } i+1/2 = \gamma_p^{n-1} \text{ at } i+1/2 + \frac{\Delta\tau}{6} (f_1 + 2f_2 + 2f_3 + f_4) \quad (5.28)$$

where

$$f_1 = \phi(T_{i+1/2}^{n-1}) \quad f_3 = \phi(T_{i+1/2}^{n-1} + \frac{\Delta\tau}{2} f_2)$$

$$f_2 = \phi(T_{i+1/2}^{n-1} + \frac{\Delta\tau}{2} f_1) \quad f_4 = \phi(T_{i+1/2}^{n-1} + \frac{\Delta\tau}{2} f_3)$$

The stress at each midpoint is found by the integrated form of the constitutive equation

$$T_{i+1/2}^n = \gamma_T^n \text{ at } i+1/2 - \gamma_p^n \text{ at } i+1/2 \quad (5.29)$$

The accelerations and particle velocities are computed at each interior point

$$\left. \frac{\partial V}{\partial \tau} \right|_1^n = \frac{T_{i+1/2}^n - T_{i-1/2}^n}{\Delta\rho} + \frac{1}{2} \frac{(T_{i+1/2}^n + T_{i-1/2}^n)}{\rho_1} \quad (5.30)$$

$$V_1^{n+1/2} = V_1^{n-1/2} + \left. \frac{\partial V}{\partial \tau} \right|_1^n \Delta\tau \quad (5.31)$$

The stress and velocity at the wave front are computed by a Runge-Kutta solution of

$$\frac{\partial T}{\partial \rho} = -\frac{1}{2} \left(\frac{T}{\rho} + \psi(T) \right) \quad (5.32)$$

MRD DIVISION
GENERAL AMERICAN TRANSPORTATION CORPORATION

The particle velocity at $i = 1$ is solved by using the boundary condition. Interpolation of the stresses in the first two cells is used to derive the stress at $\rho = 1$.

$$\left. \frac{\partial v}{\partial \tau} \right|_1^n = \frac{1}{m_0} \left(\frac{3}{2} T_1^n - \frac{1}{2} T_2^n \right) \quad (5.33)$$

All the values at T^n have been computed. Now the time is increased and the cycle is repeated.

The computation is continued until one of two things occurs, either the stress at the surface goes below the yield stress, at which time no further flow can occur, or the plastic strain in the first cell exceeds the limit, at which fracture will probably occur, at which time fracture occurs and the plug is free. If the second case occurs then the plate has been perforated.

The difference scheme was checked for stability and convergence by running trial calculations using different sizes of the mesh. The difference scheme was stable, varying roughly as the order of h^4 .

5.4 Results

The calculations were evaluated for several cases of interest. The calculations are divided into two categories. The first category was the determination of the effect of the various parameters on the shape and location of the v_R vs. v_s curve. The second category was the evaluation of certain specific plate and target materials for which experimental values of the v_R-v_s were available. In addition to these cases, one of the cases was evaluated for the stresses, displacements and particle velocities everywhere.

MRD DIVISION
GENERAL AMERICAN TRANSPORTATION CORPORATION

The form of the plastic strain rate term in the constitutive equation was taken as (see Sec. 2)

$$\dot{\epsilon}_p = \dot{\epsilon}_p^0 e^{-A/\tau} = \phi(\tau) \quad (5.34)$$

where

$\dot{\epsilon}_p^0$ is the maximum possible plastic strain rate

A is a constant

This form of the plastic strain rate component is easily rendered into the dimensionless form by appropriate change in A. Since the behavior of this function is almost as sharp as a unit step function, the scaling behavior is dependent on the ratio of $\frac{\tau_{RZ}}{A}$. For values of this number less than 0.5, the behavior is almost entirely elastic. For values of this ratio in the neighborhood of unity or above the behavior is almost that of a perfect fluid.

$\dot{\epsilon}_p^0$ and A were evaluated for typical titanium alloys by assuming the model derived in Section 2, and using the constant strain rate data for various titanium alloys⁽⁷⁾.

Table 5.1 gives the values of A and $\dot{\epsilon}_p^0$. The maximum critical strain was assumed independent of the rate and was chosen as 1/2 of the critical elongation in tension. The most probable value in the literature⁽³⁵⁾ is also shown in the table.

The residual velocity v_R versus the striking velocity v_g was evaluated for two typical titanium alloys which show the influence of one of the parameters. The two alloys were Ti 2.5 Sn 5Al and Ti 4 Mn 4Al which very nearly have the same static compressive yield strength, the same value of A, and the same value of $\dot{\epsilon}_p^0$.

MRD DIVISION
GENERAL AMERICAN TRANSPORTATION CORPORATION

Table 5.1

PLASTIC PROPERTIES OF PLATE MATERIALS IN SHEAR

Alloy	Strain Rate Parameters		Critical Shear Strain	Static Compression Yield Strength
	$\dot{\epsilon}_p = \dot{\epsilon}_p^0 e^{-A/\tau}$	$\dot{\epsilon}_p^0$		
Ti 2.5 Sn 5Al	8.0×10^6 psi	5×10^5 /sec	0.10	140,000 psi
Ti 4 Al 4 Mn	8.5	5×10^5 /sec	0.05	140,000 psi
Mn Fe	8.5	10^6 /sec	0.15	140,000 psi

MRD DIVISION
GENERAL AMERICAN TRANSPORTATION CORPORATION

Table 5.2

MATERIAL PROPERTIES OF PLATE AND PROJECTILE FOR DETAILED CALCULATIONS

<u>Property</u>	<u>Projectile</u>	<u>Plate</u>
Material	4340 Steel	Ti 2.5 Sn 5 Al
Pertinent Dimensions	R = 0.22" L = 0.25"	h = 0.100"
Density	0.283 lbs/in	0.163 lbs/in ³
σ_{cy} static compressive yield strength	150,000 psi	120,00 psi
A coefficient in exponent of strain rate term	_____	8.0 x 10 ⁵ psi
ϵ_p^0 max plastic strain rate		5 x 10 ⁵ /sec
max critical elongation		0.15

MRD DIVISION
GENERAL AMERICAN TRANSPORTATION CORPORATION

The major difference is that the critical permanent strain at fracture in one, Ti 2.5 Sn 5Al, is nearly double that of the other alloy. The v_R vs. v_s curves that were calculated for these two alloys are shown in figures 5.2 - 5.9. The v_{50} point or the velocity of incident perforation is taken as the intercept of the v_R - v_s curve with the v_s axis. This v_{50} is plotted versus \bar{m} for the two alloys. (Fig. 5.10).

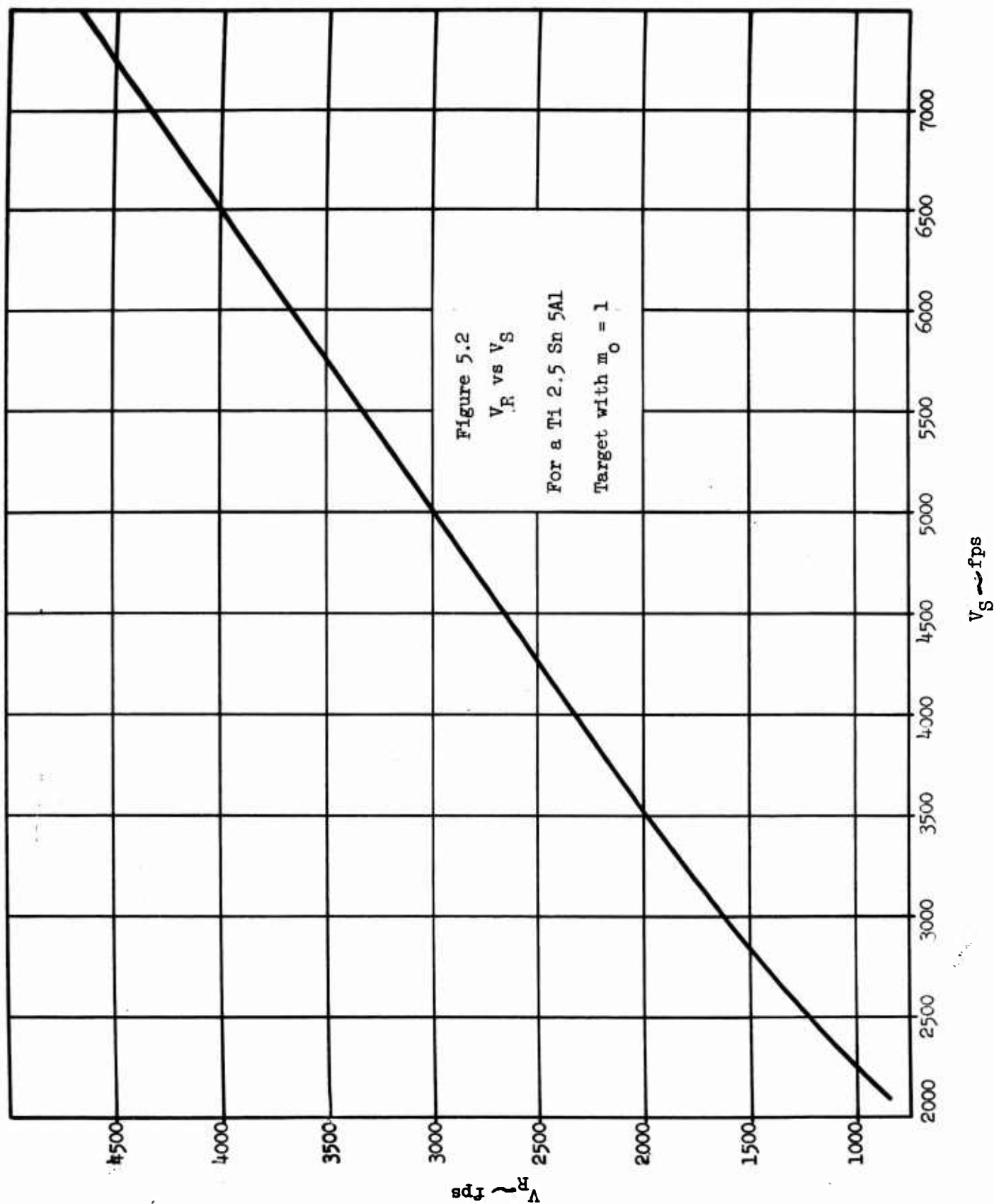
A typical steel was the other case evaluated. The same yield strength as the titanium alloys was used but the maximum strain rate and maximum critical elongation were taken as twice that of the Ti 2.5 Sn 5Al. No good strain rate data is available on steels. This data was chosen since it represents a much more ductile material. The v_R vs. v_s curves are shown in figures 5.11-5.14.

One case was evaluated for all stresses and particle velocities as a function of position and time for several values of the striking velocity. The case chosen for this evaluation was a Ti 2.5 Sn 5Al plate thickness 0.10 inches being struck by a 4340 steel cylindrical projectile 0.22" diameter, 0.25 " length. Material properties of the plate are given in Table 5.2. The vertical particle velocity and the shear stress are shown as a function of position and time for five impacting velocities, ranging from below the elastic limit to 25 times higher, (Fig. 5.15-24). Where the diagrams are incomplete, this means the plate has been perforated and the stresses have gone to zero.

The permanent deformation of the plate as shown for these five cases in Figure 5.25.

Four specific cases of the v_R vs. v_s curves were evaluated to correspond

MRD DIVISION
GENERAL AMERICAN TRANSPORTATION CORPORATION



MRD DIVISION
GENERAL AMERICAN TRANSPORTATION CORPORATION

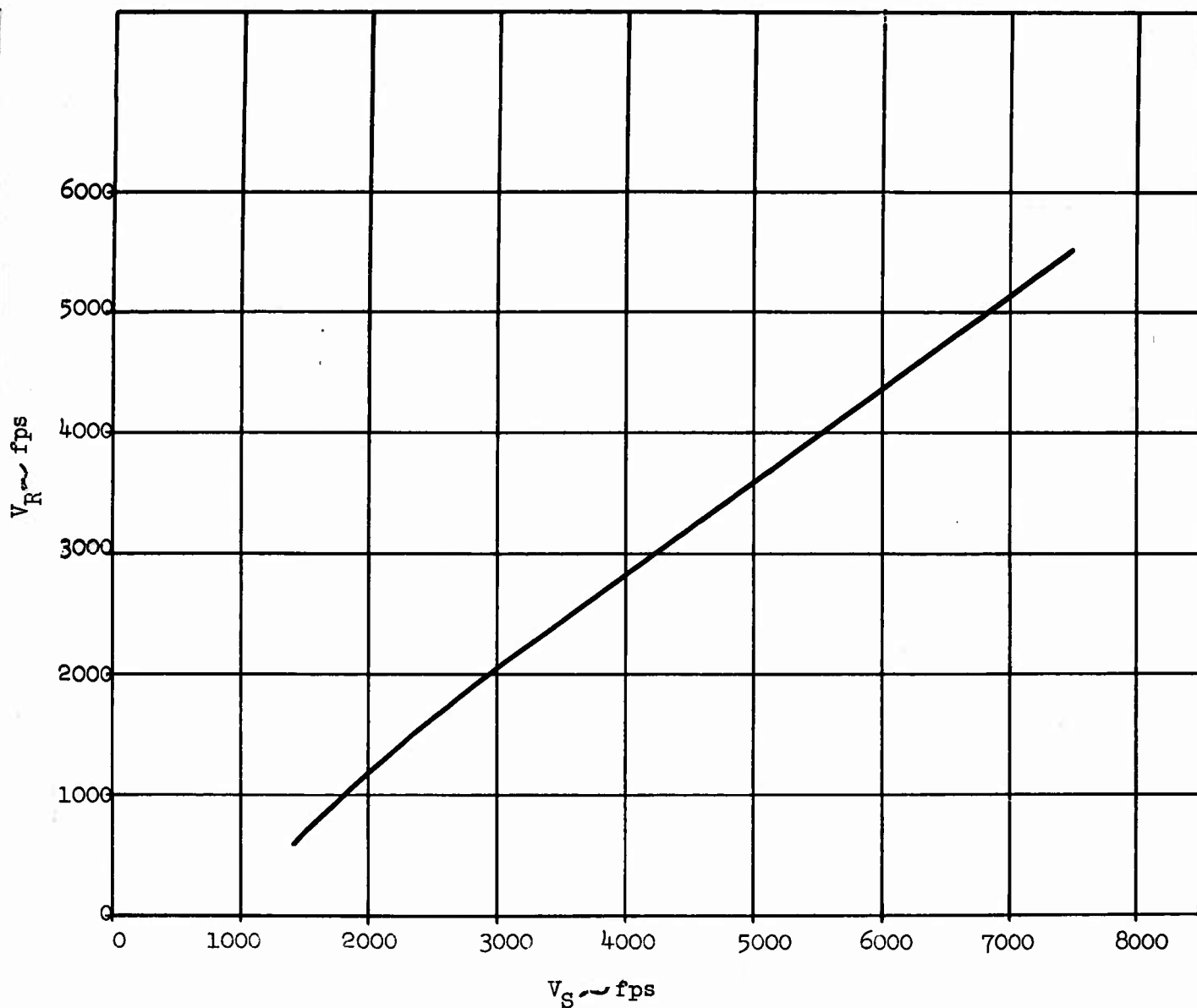


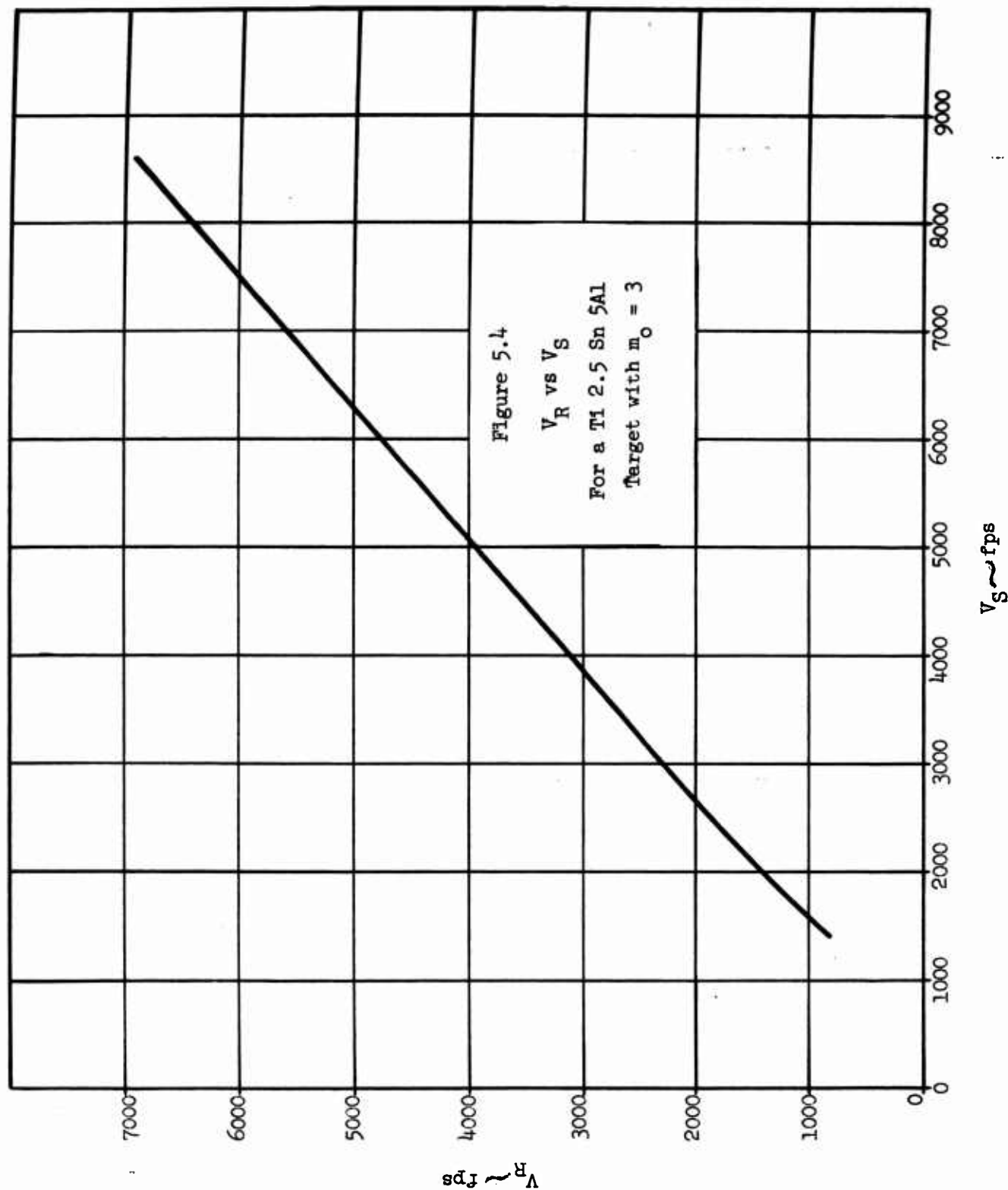
Figure 5.3

V_R vs V_S

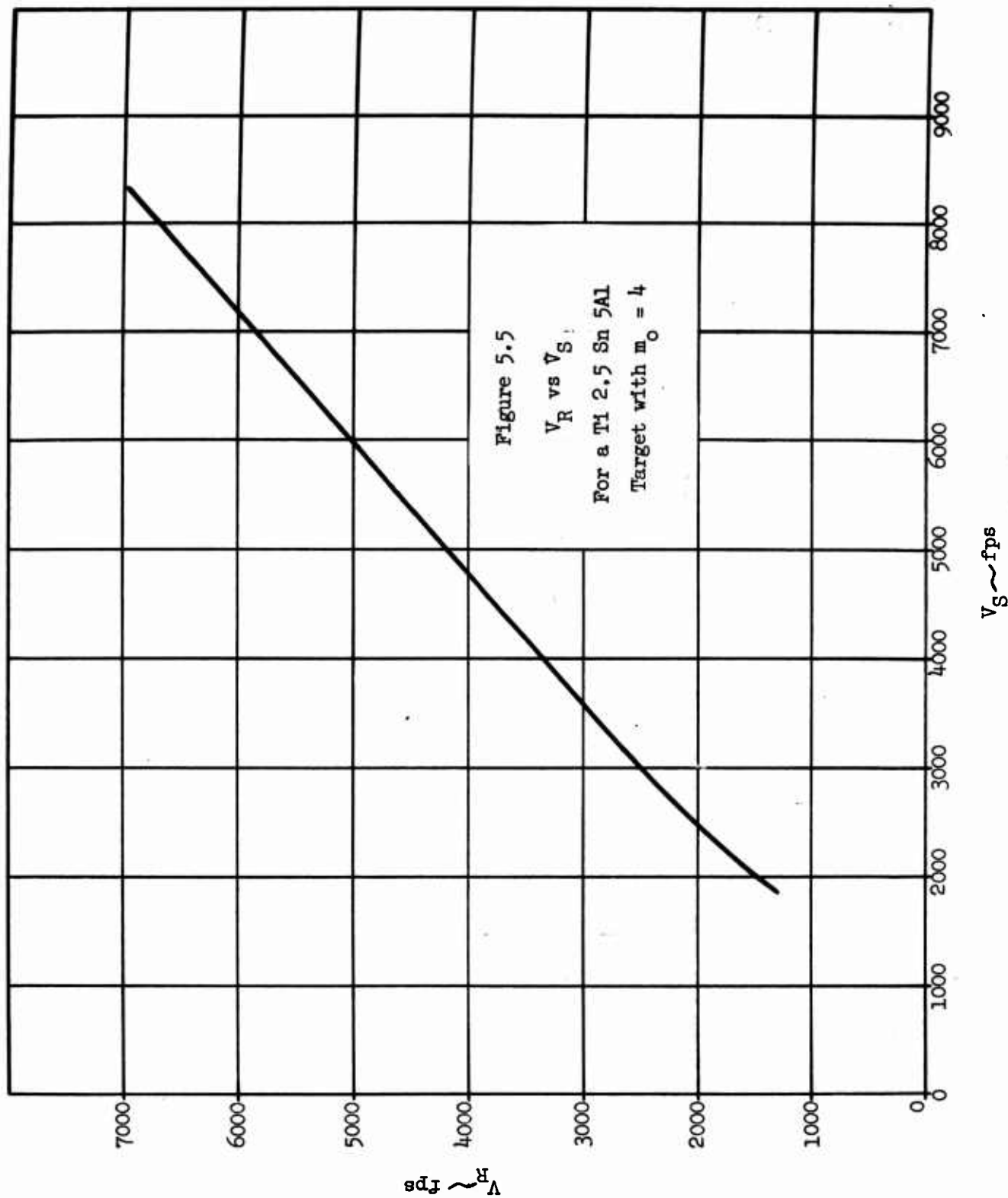
For a Ti 2,5 Sn 5Al Target

with $m_0 = 2$

MRD DIVISION
GENERAL AMERICAN TRANSPORTATION CORPORATION



MRD DIVISION
GENERAL AMERICAN TRANSPORTATION CORPORATION



MRD DIVISION
GENERAL AMERICAN TRANSPORTATION CORPORATION

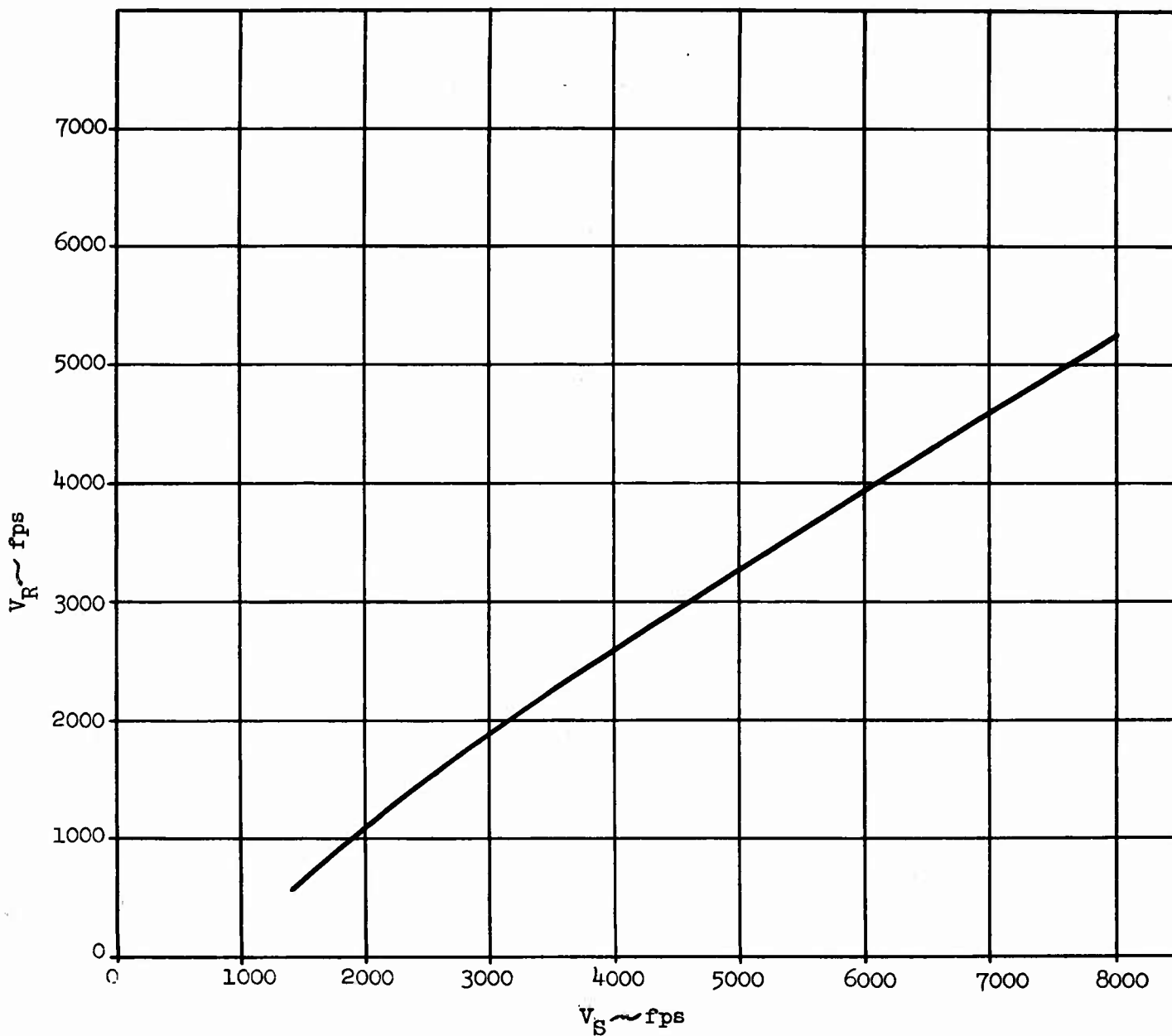


Figure 5,6
 V_R vs V_S For a Ti 4 Mn 4 Al Target
with $m_o = 1$

MRD DIVISION
GENERAL AMERICAN TRANSPORTATION CORPORATION

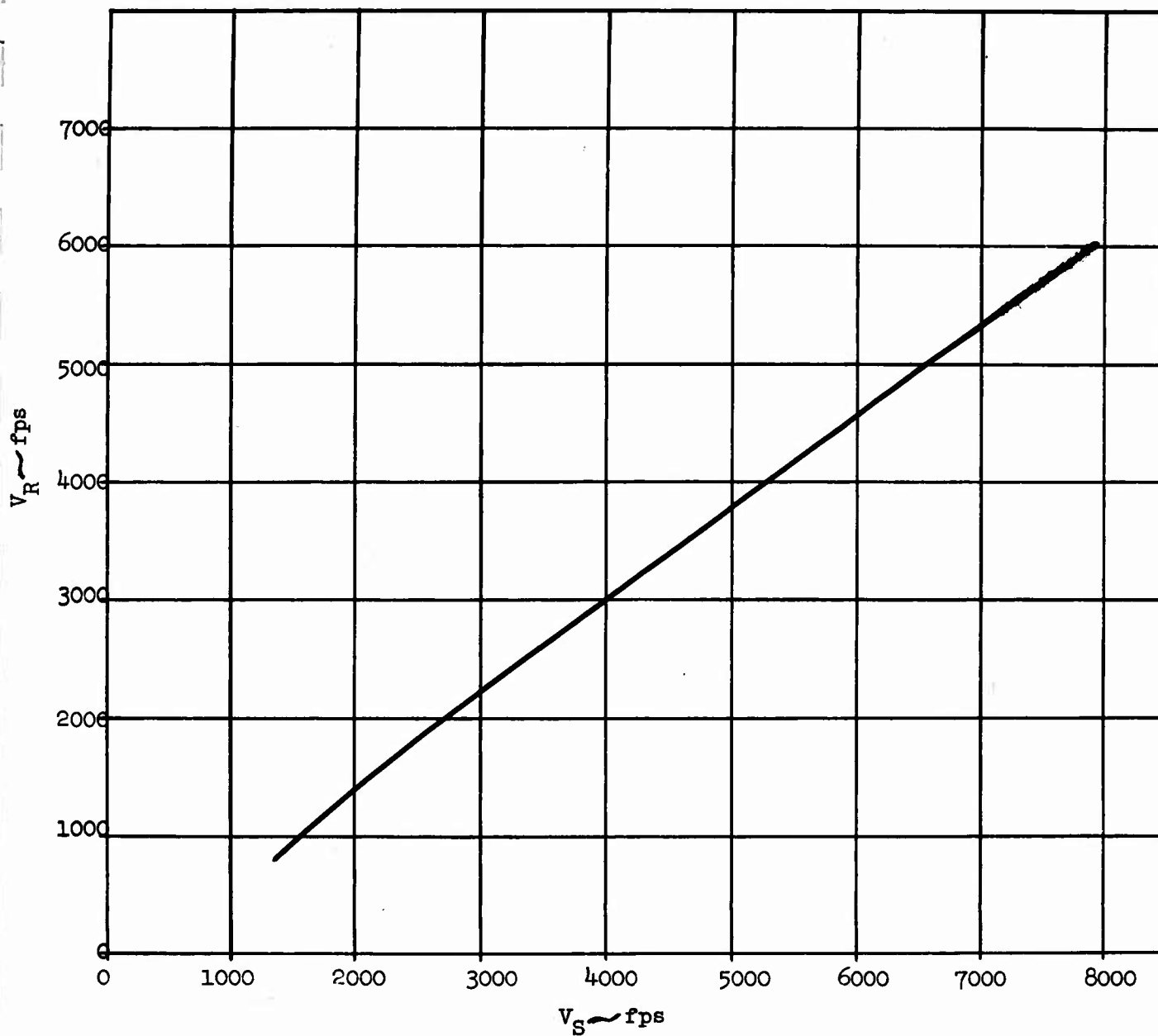


Figure 5.7
 V_R vs V_S For a T1 4 Mn 4 Al Target
 with $m_o = 2$

MRD DIVISION
GENERAL AMERICAN TRANSPORTATION CORPORATION

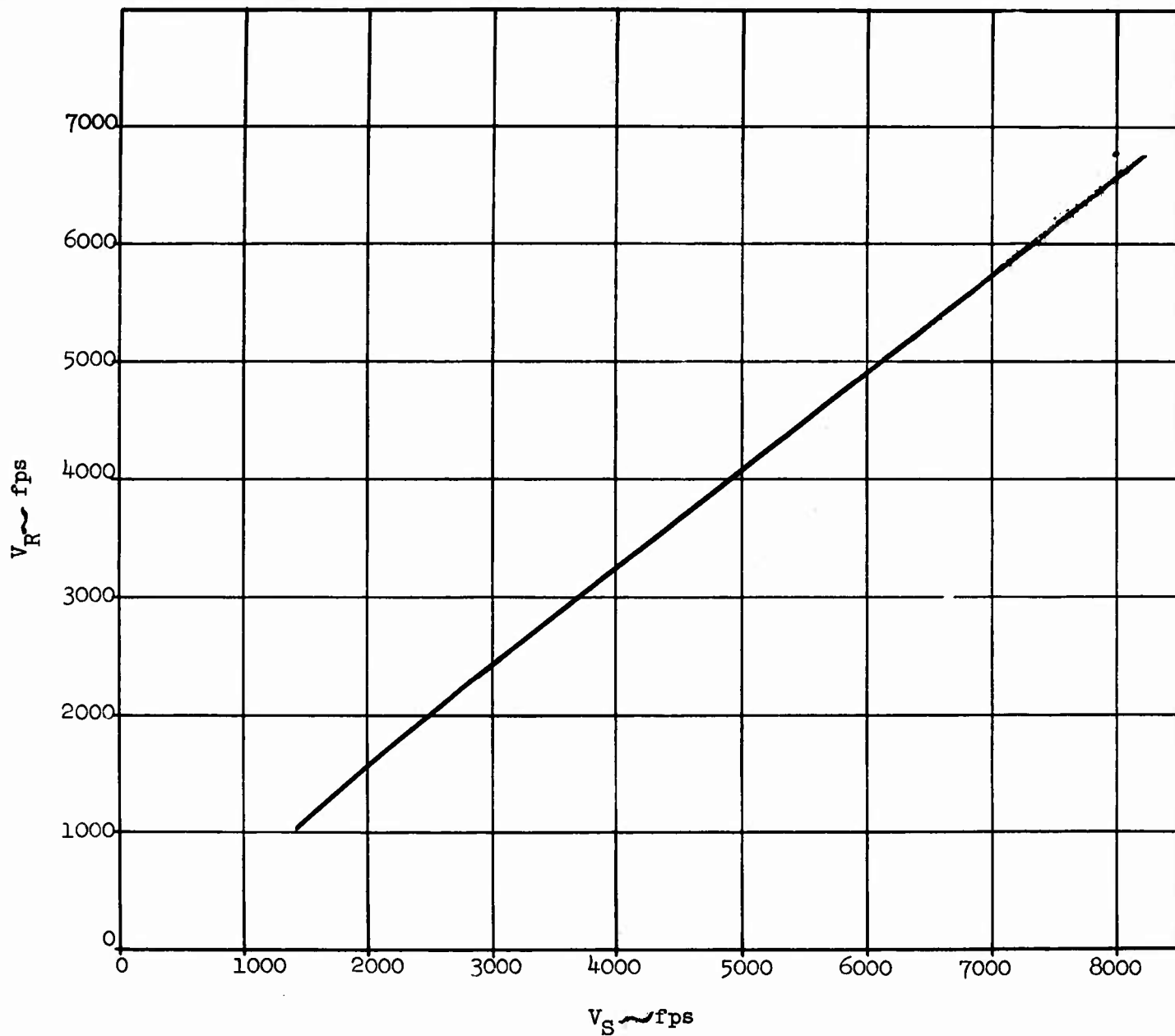
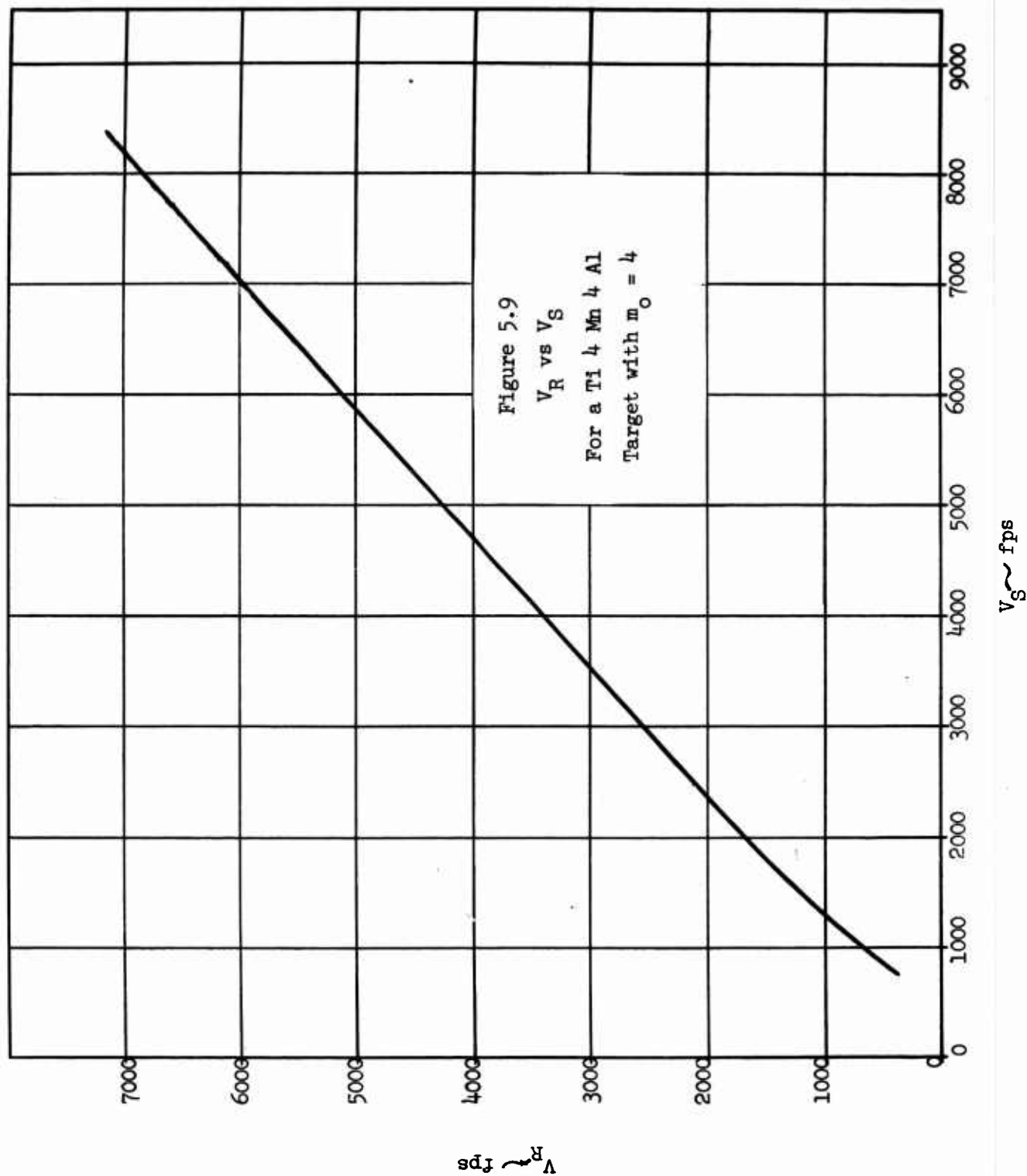


Figure 5.8

V_R vs V_S

For a Ti 4 Mn 4 Al Target with $m_0 = 3$

MRD DIVISION
GENERAL AMERICAN TRANSPORTATION CORPORATION



MRD DIVISION
GENERAL AMERICAN TRANSPORTATION CORPORATION

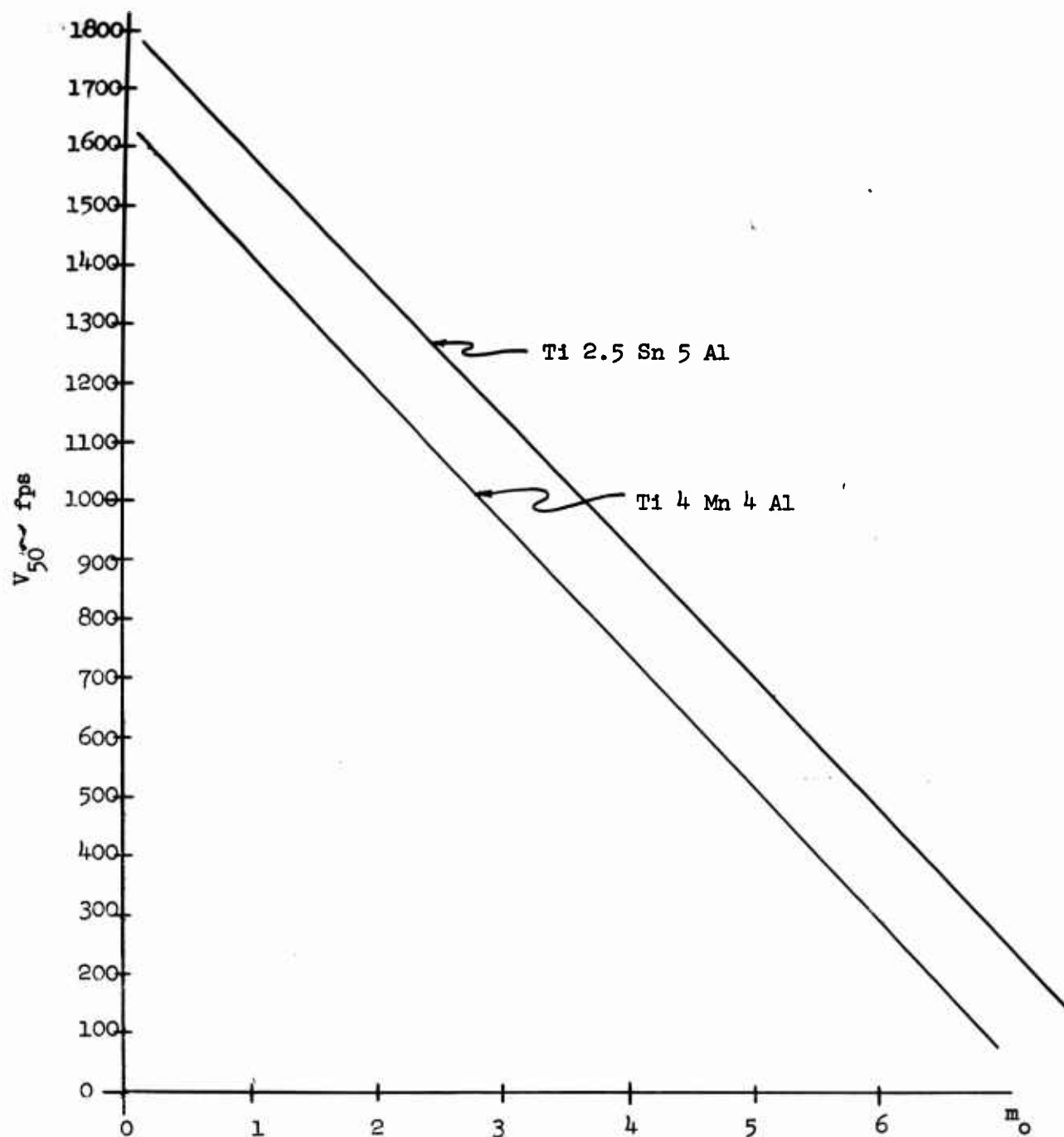
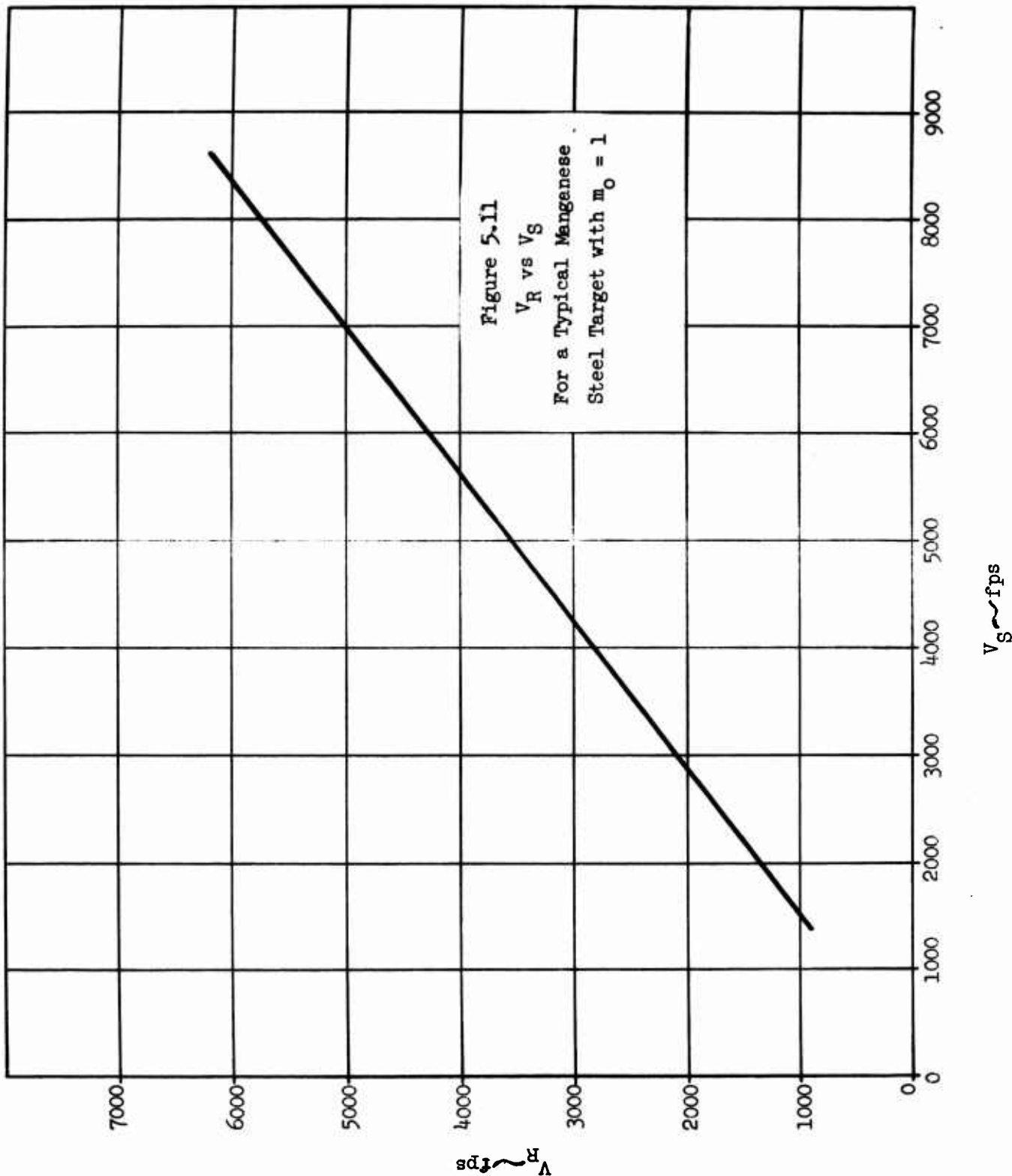
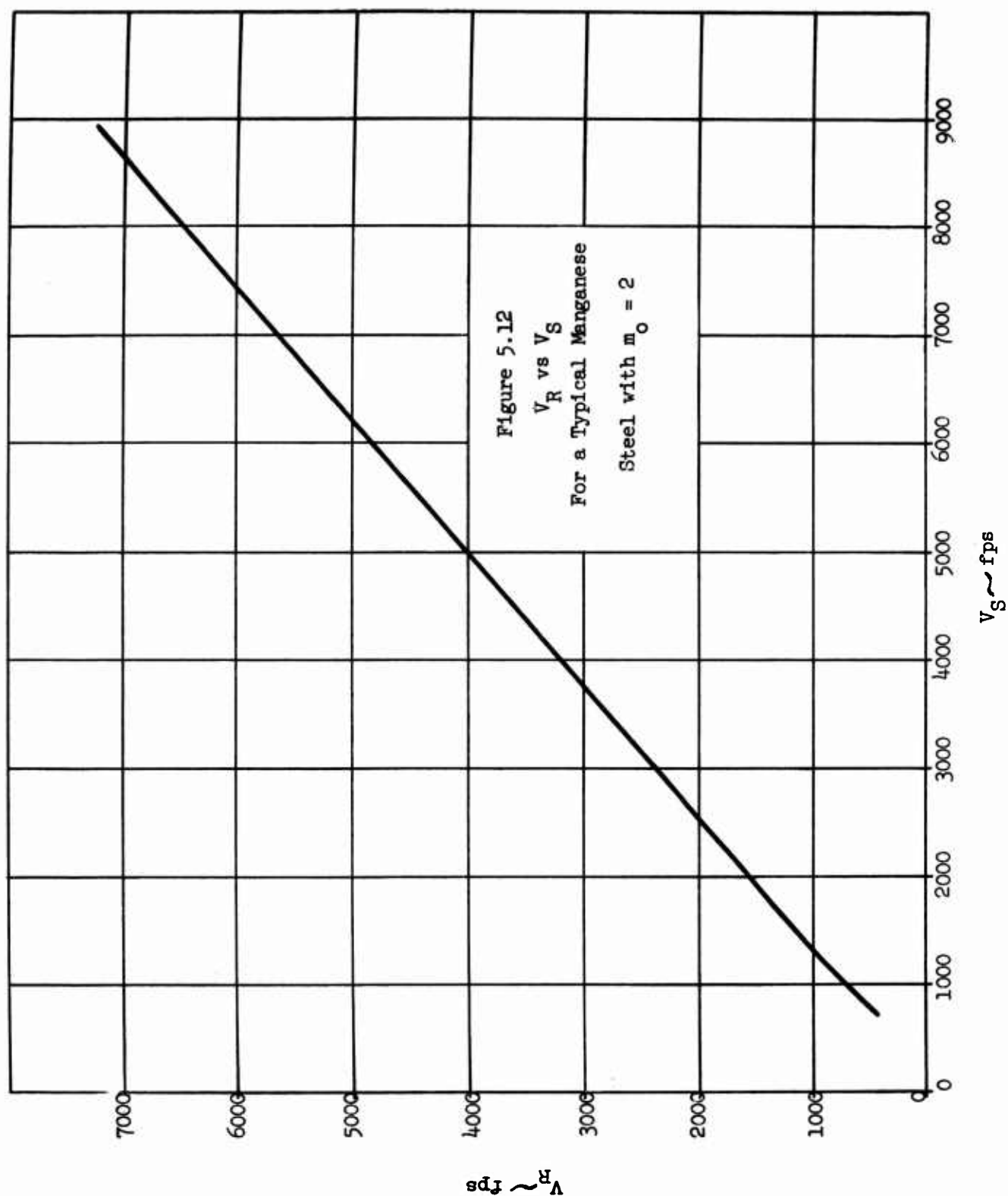


Figure 5,10 - V_{50} vs. m_0 for Two
Titanium Alloy Targets

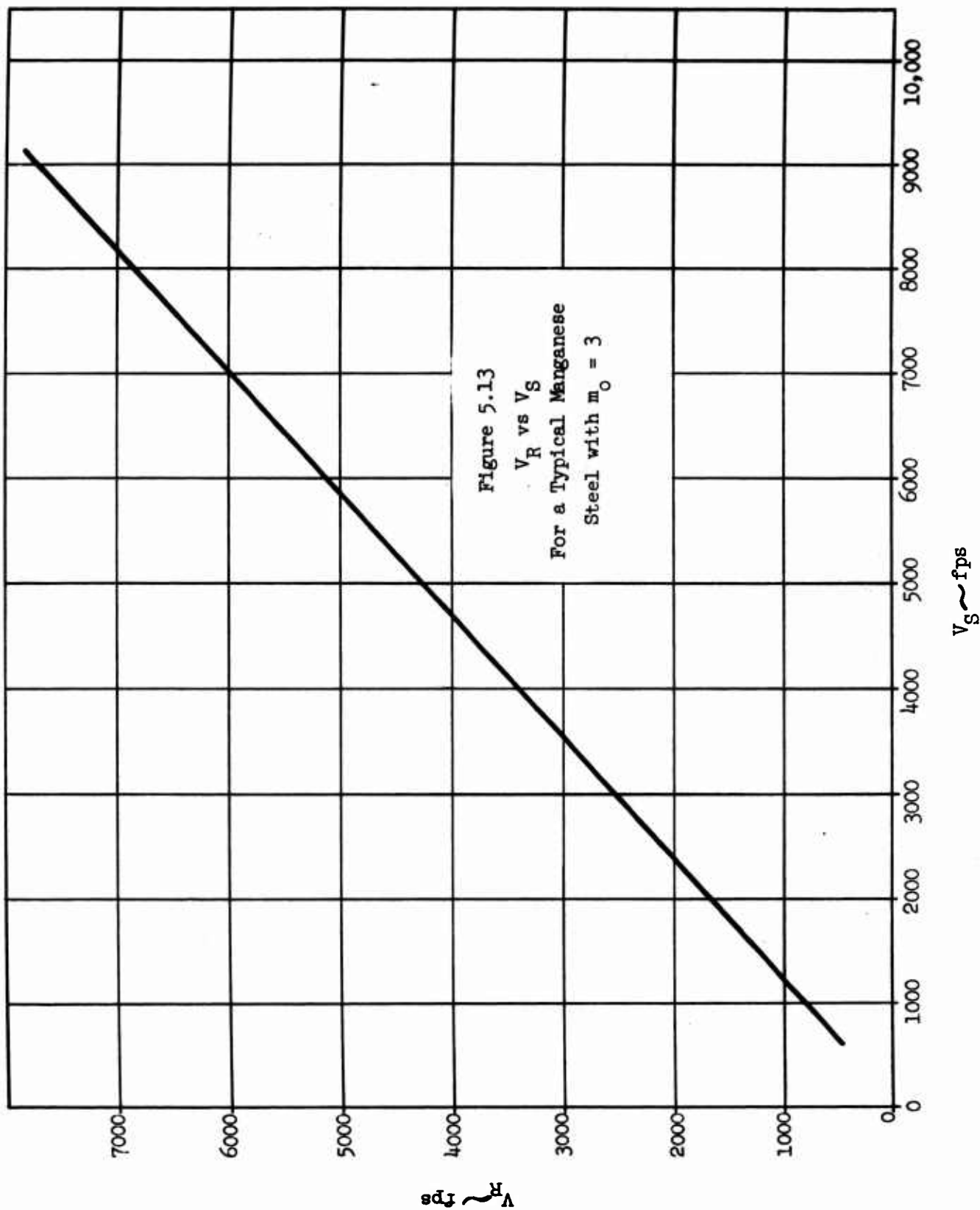
MRD DIVISION
GENERAL AMERICAN TRANSPORTATION CORPORATION



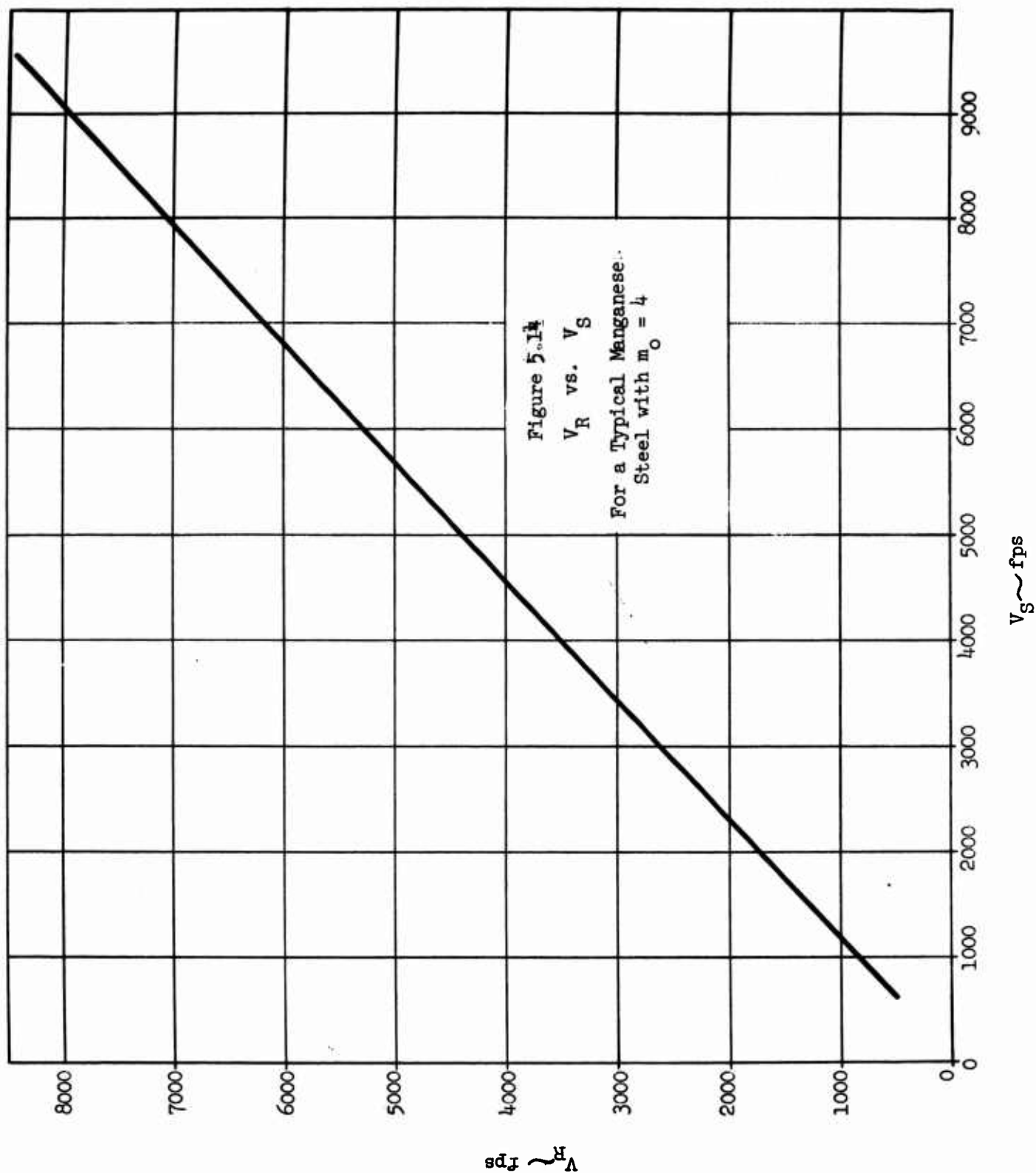
MRD DIVISION
GENERAL AMERICAN TRANSPORTATION CORPORATION



MRD DIVISION
GENERAL AMERICAN TRANSPORTATION CORPORATION



MRD DIVISION
GENERAL AMERICAN TRANSPORTATION CORPORATION



MRD DIVISION
 GENERAL AMERICAN TRANSPORTATION CORPORATION

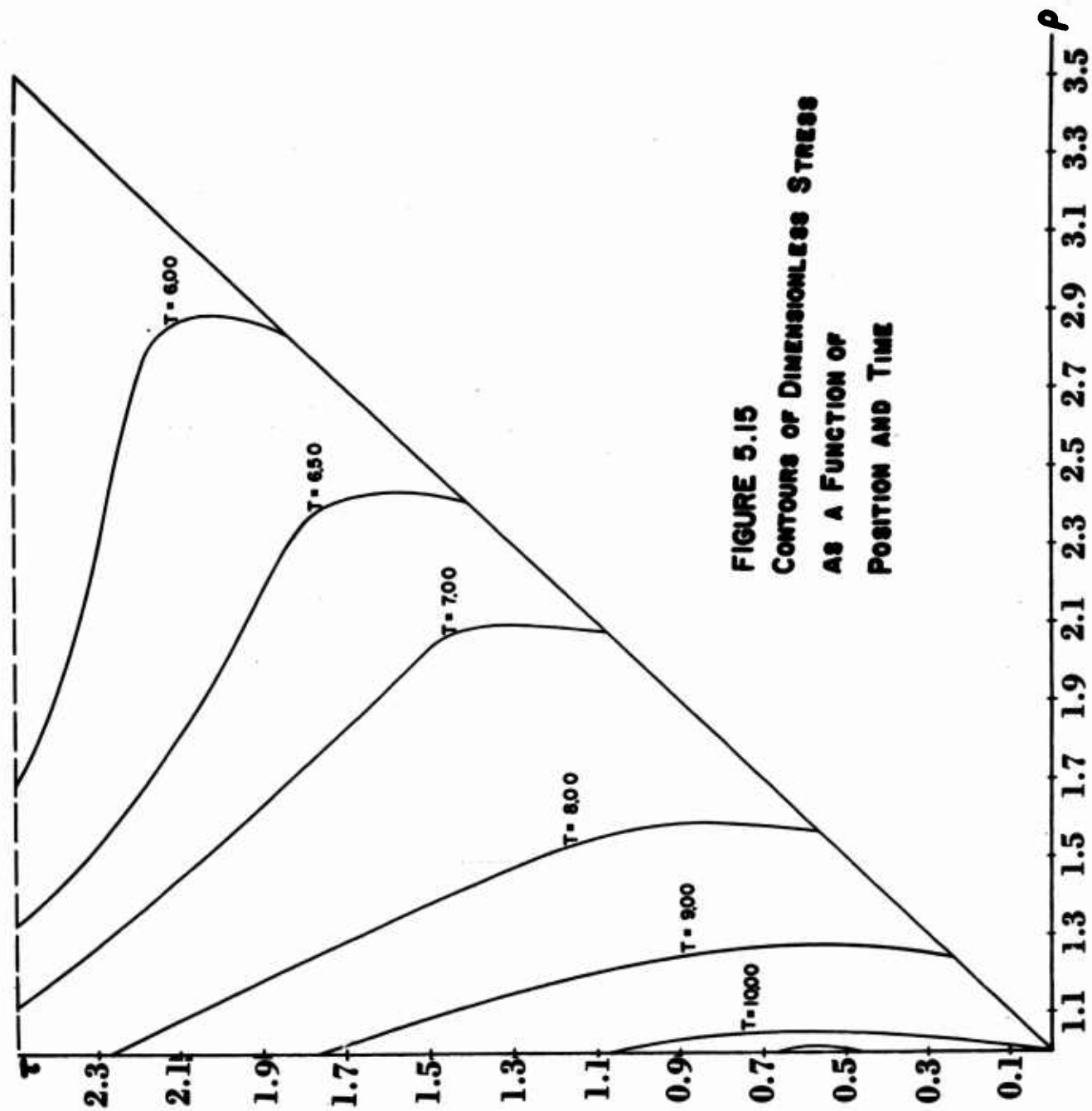


FIGURE 5.15
CONTOURS OF DIMENSIONLESS STRESS
AS A FUNCTION OF
POSITION AND TIME

MRD DIVISION
GENERAL AMERICAN TRANSPORTATION CORPORATION

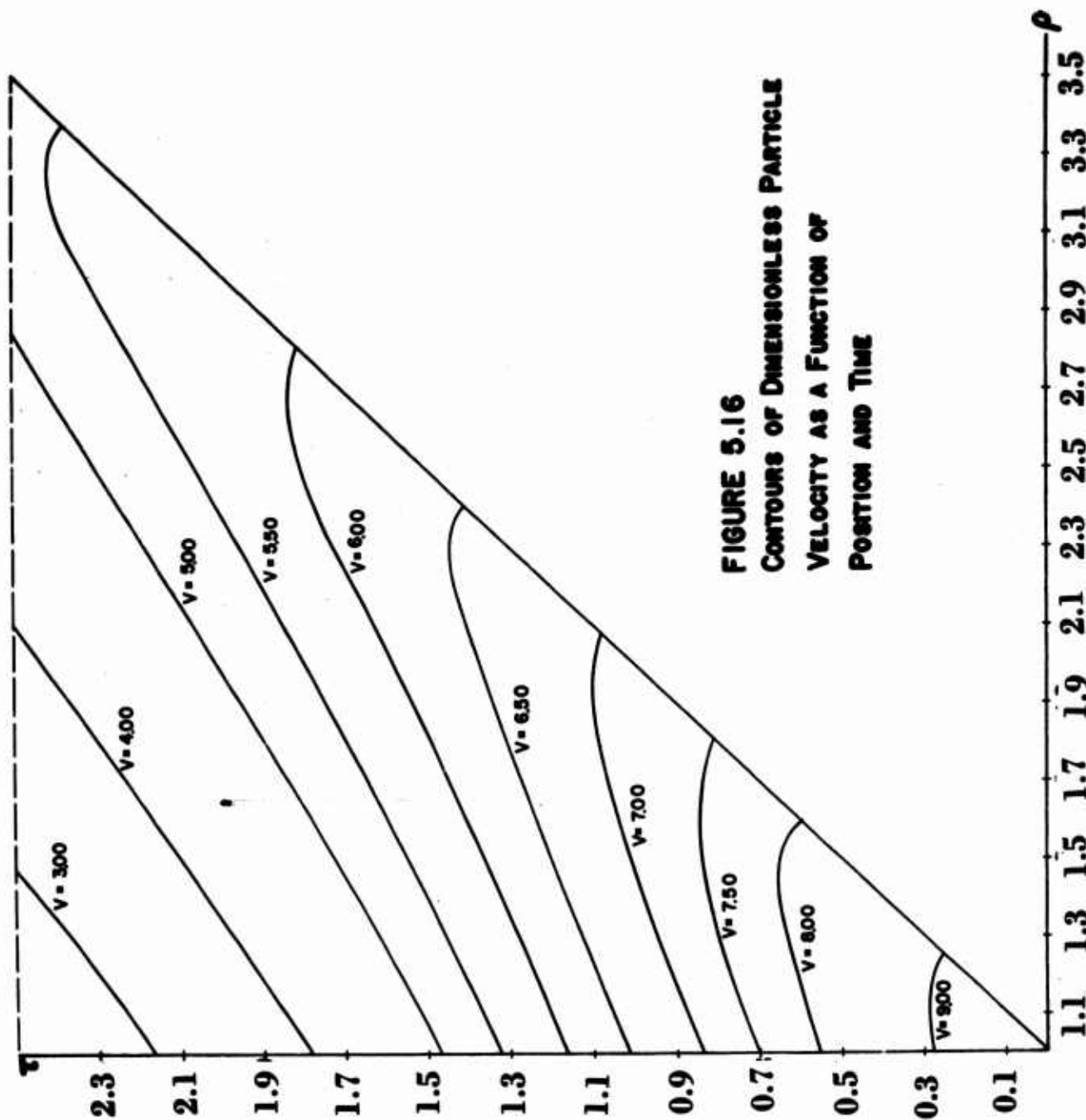


FIGURE 5.16
CONTOURS OF DIMENSIONLESS PARTICLE
VELOCITY AS A FUNCTION OF
POSITION AND TIME

MRD DIVISION
GENERAL AMERICAN TRANSPORTATION CORPORATION

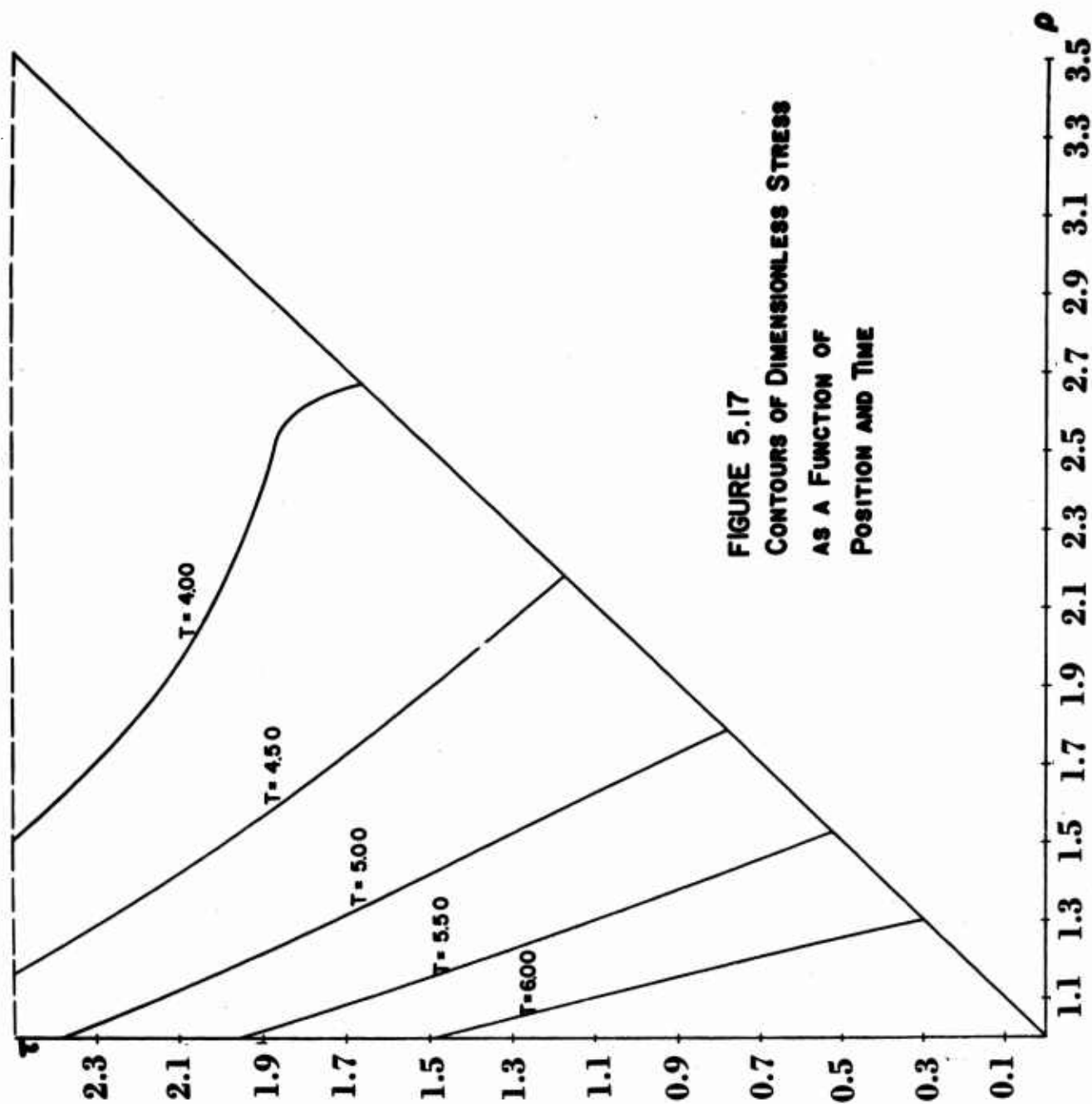


FIGURE 5.17
CONTOURS OF DIMENSIONLESS STRESS
AS A FUNCTION OF
POSITION AND TIME

MRD DIVISION
GENERAL AMERICAN TRANSPORTATION CORPORATION

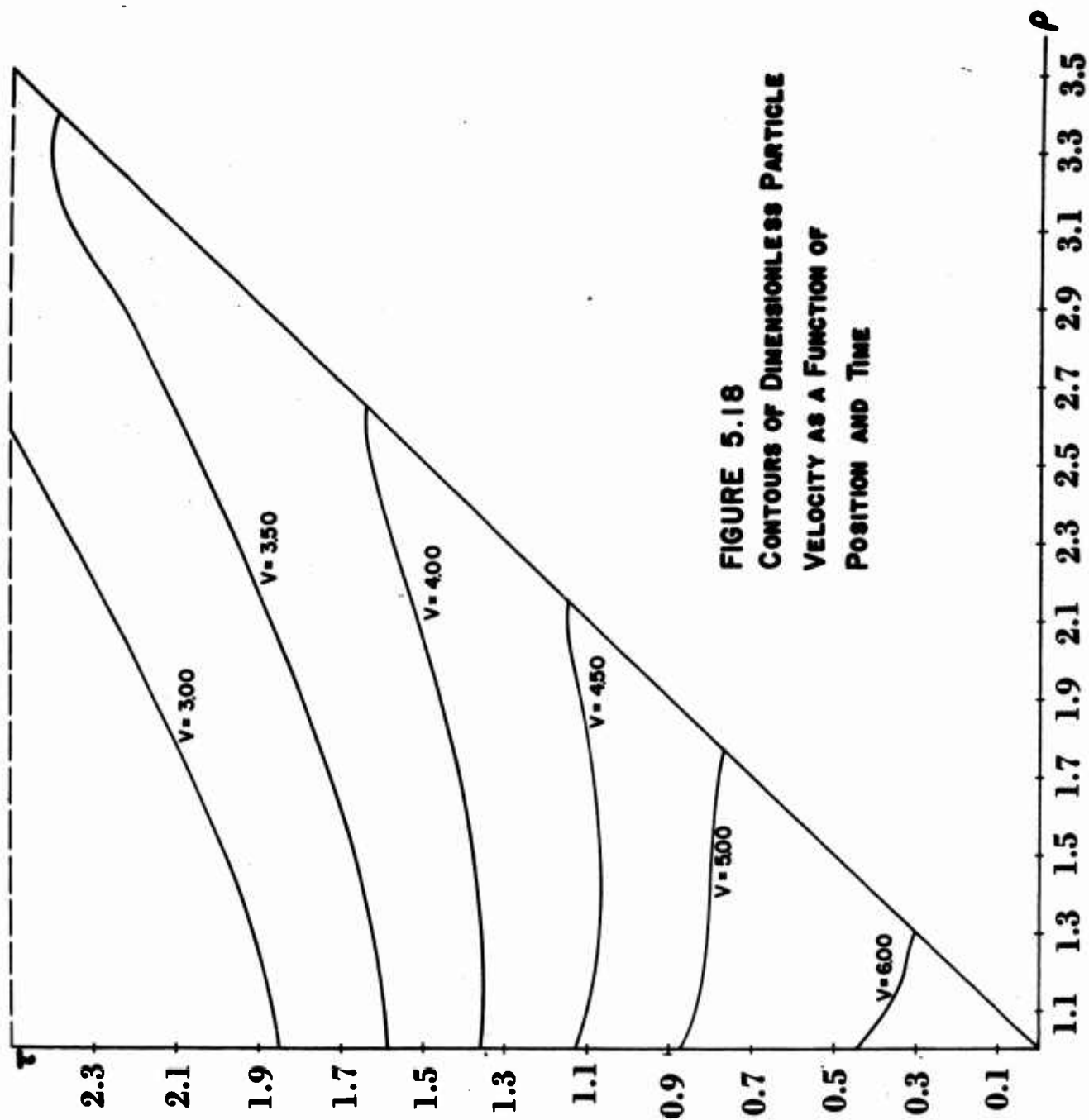


FIGURE 5.18
CONTOURS OF DIMENSIONLESS PARTICLE
VELOCITY AS A FUNCTION OF
POSITION AND TIME

MRD DIVISION
GENERAL AMERICAN TRANSPORTATION CORPORATION

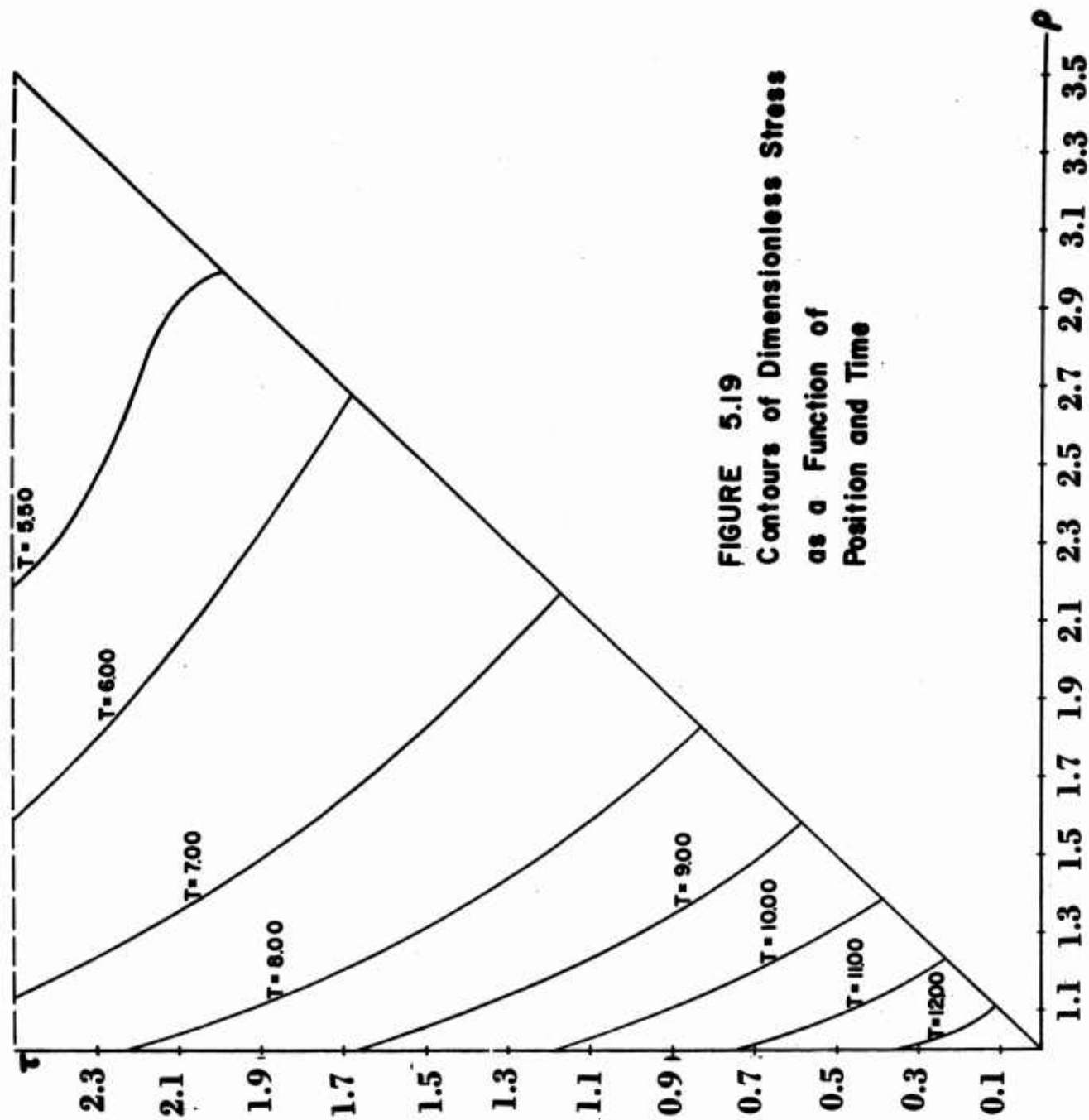


FIGURE 5.19
Contours of Dimensionless Stress
as a Function of
Position and Time

MRD DIVISION
GENERAL AMERICAN TRANSPORTATION CORPORATION

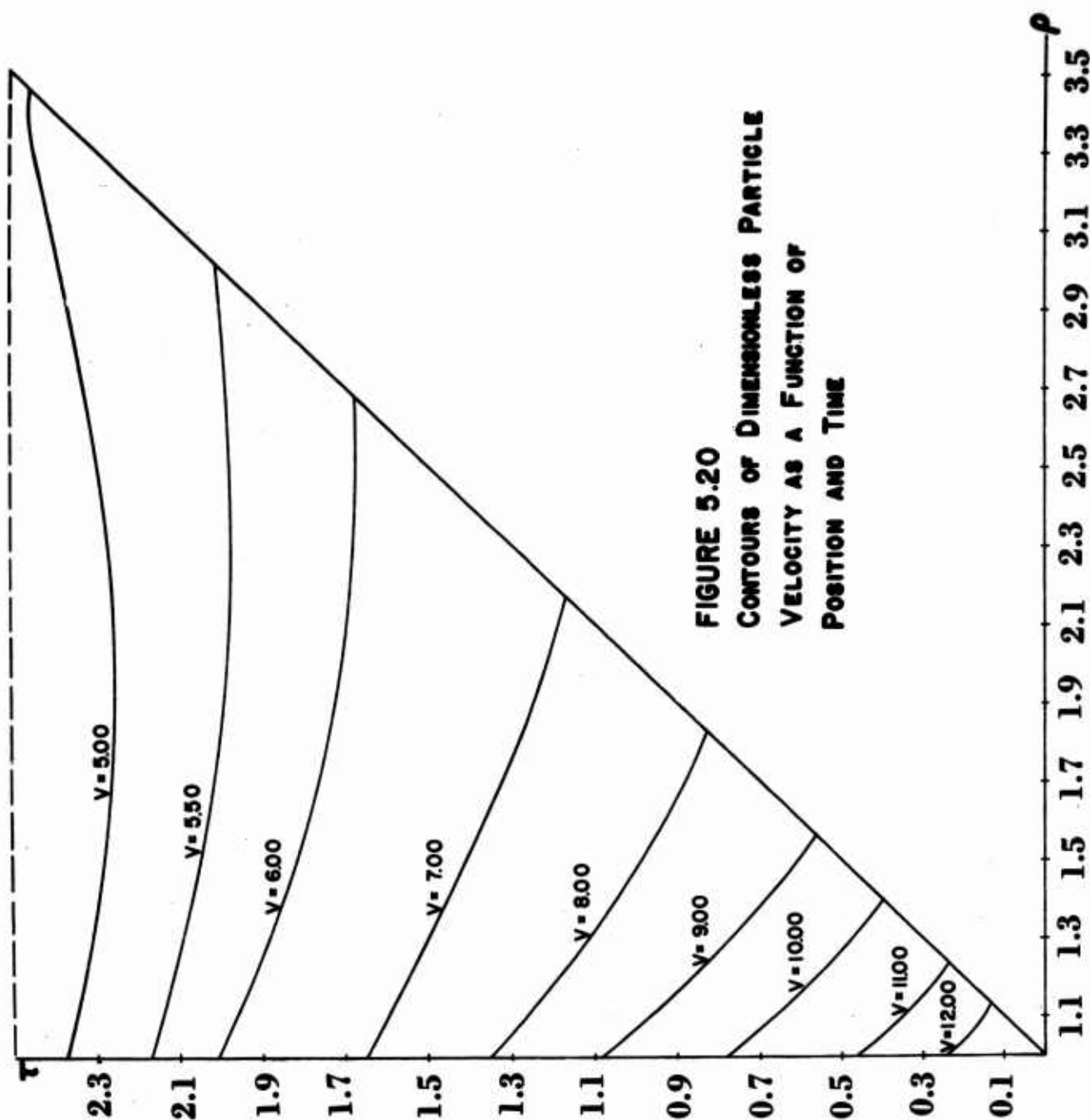


FIGURE 5.20
CONTOURS OF DIMENSIONLESS PARTICLE
VELOCITY AS A FUNCTION OF
POSITION AND TIME

MRD DIVISION
GENERAL AMERICAN TRANSPORTATION CORPORATION

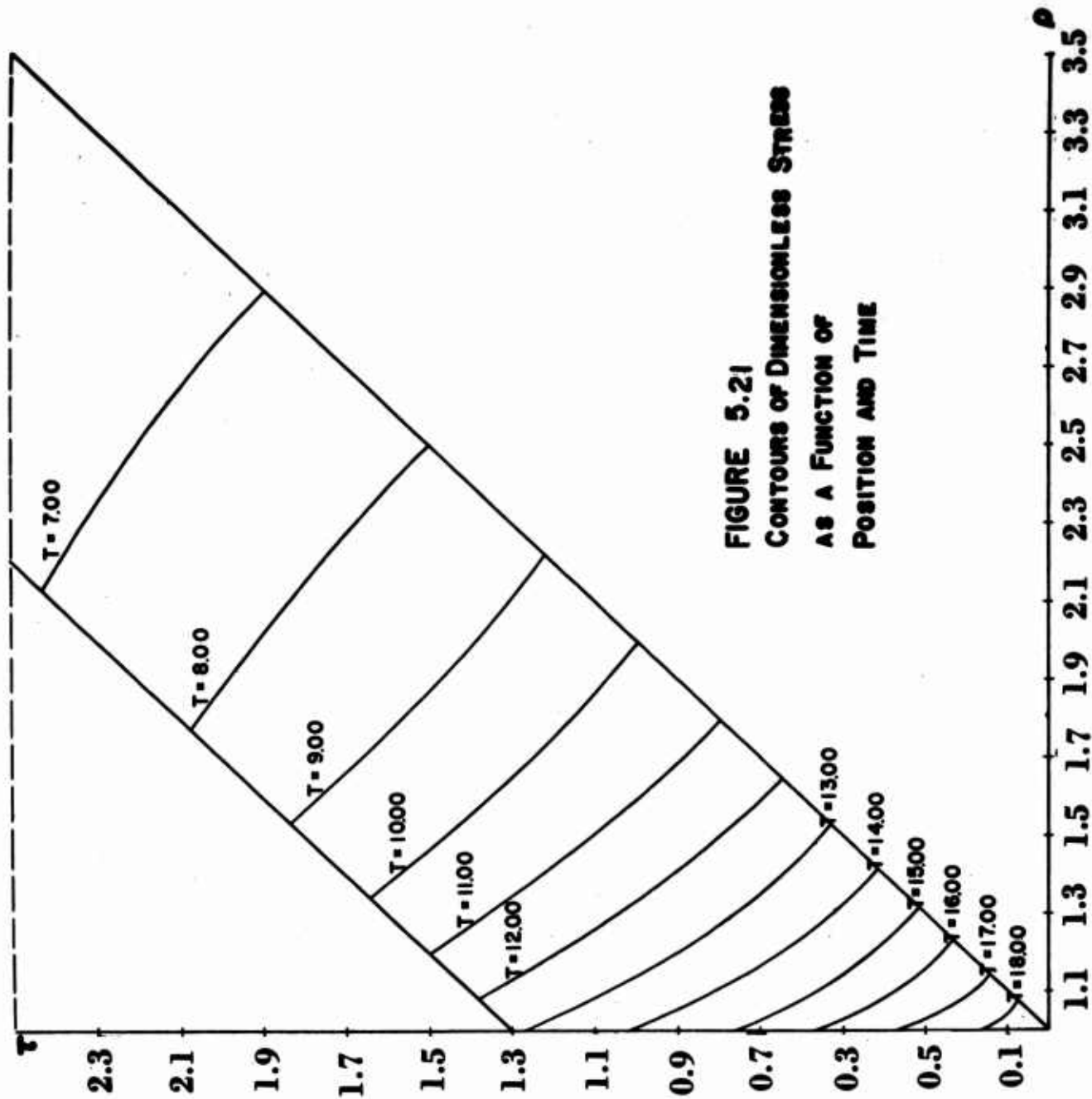


FIGURE 5.21
CONTOURS OF DIMENSIONLESS STRESS
AS A FUNCTION OF
POSITION AND TIME

MRD DIVISION
GENERAL AMERICAN TRANSPORTATION CORPORATION

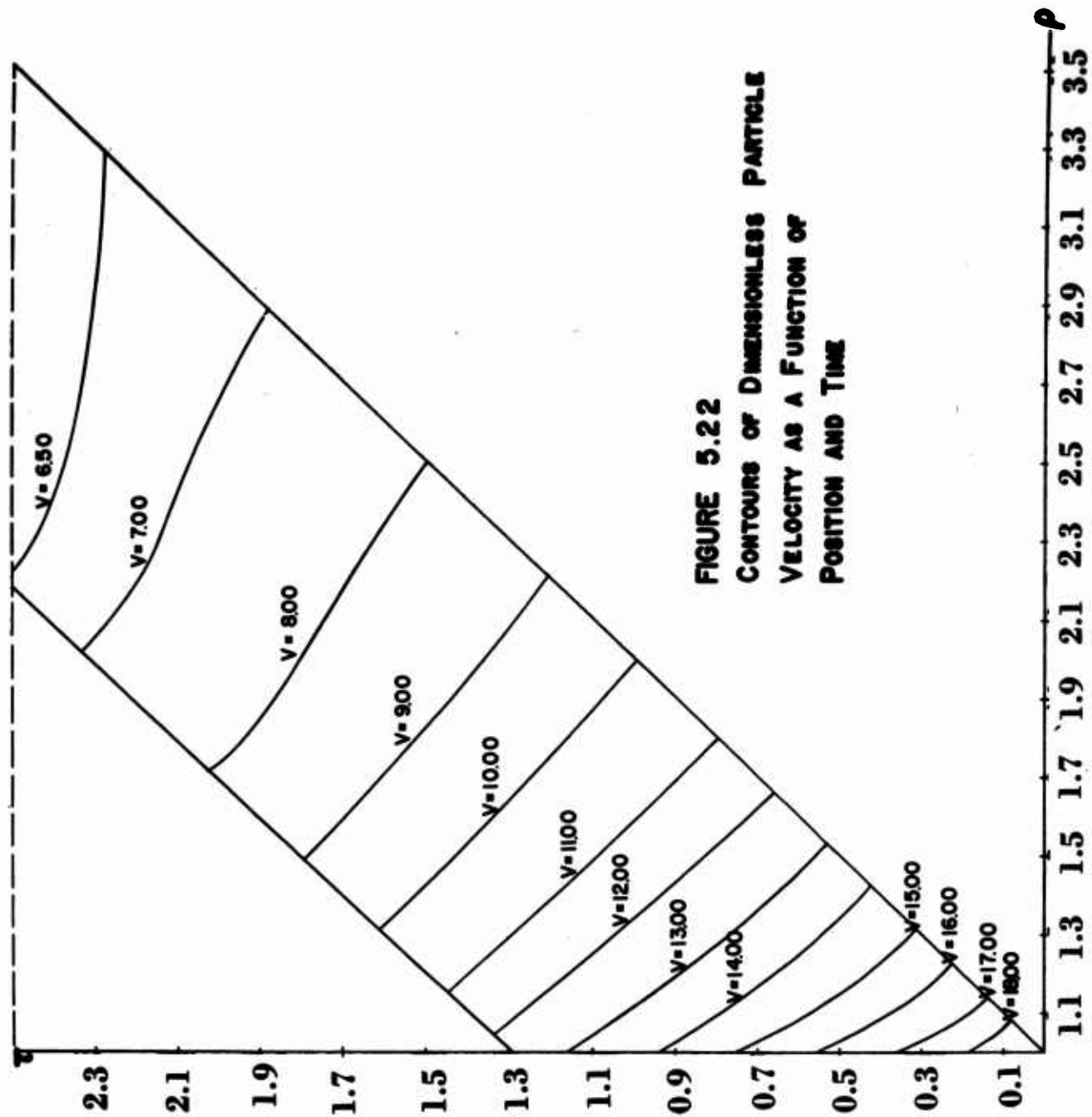


FIGURE 5.22
CONTOURS OF DIMENSIONLESS PARTICLE
VELOCITY AS A FUNCTION OF
POSITION AND TIME

MRD DIVISION
GENERAL AMERICAN TRANSPORTATION CORPORATION

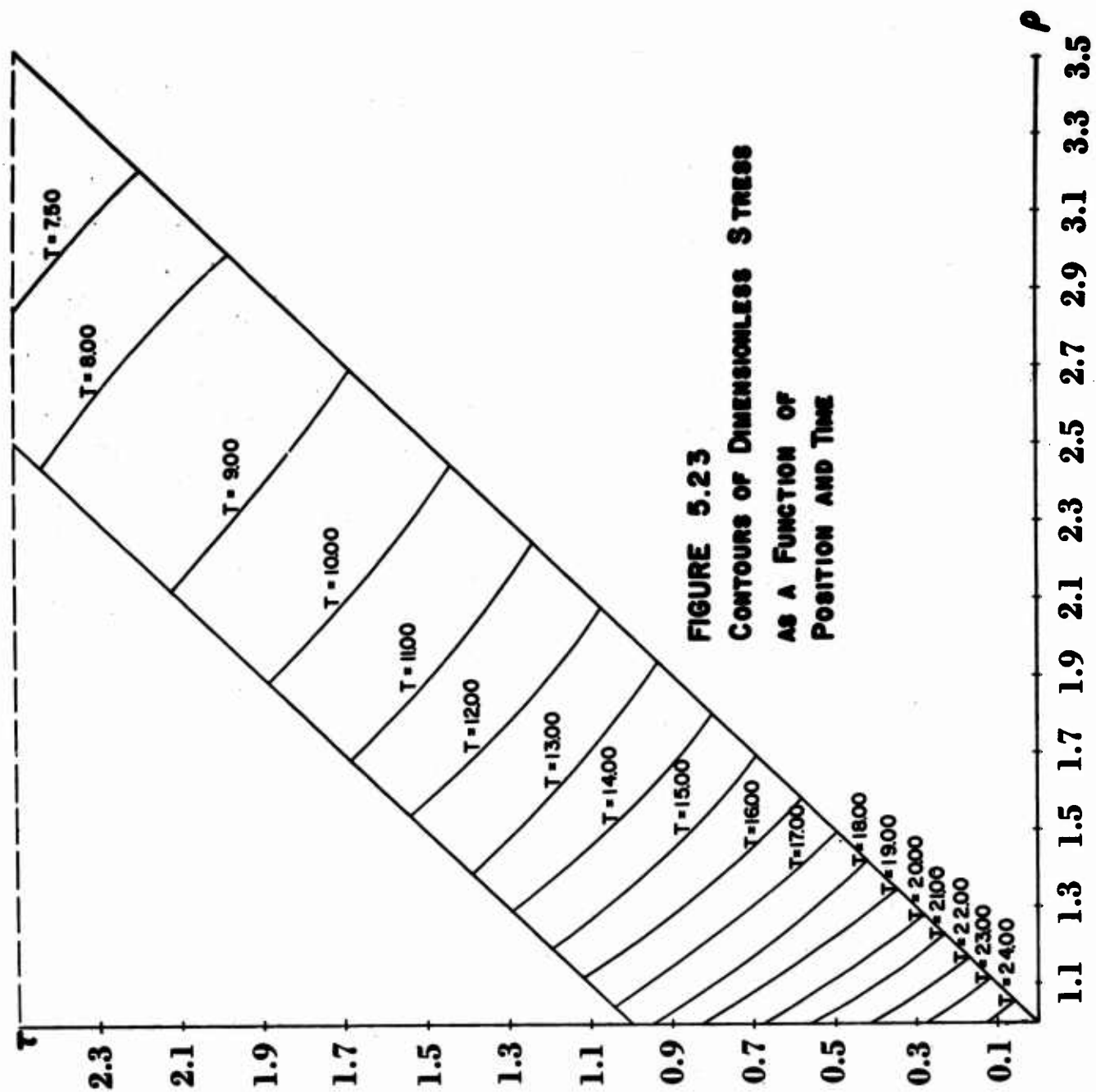
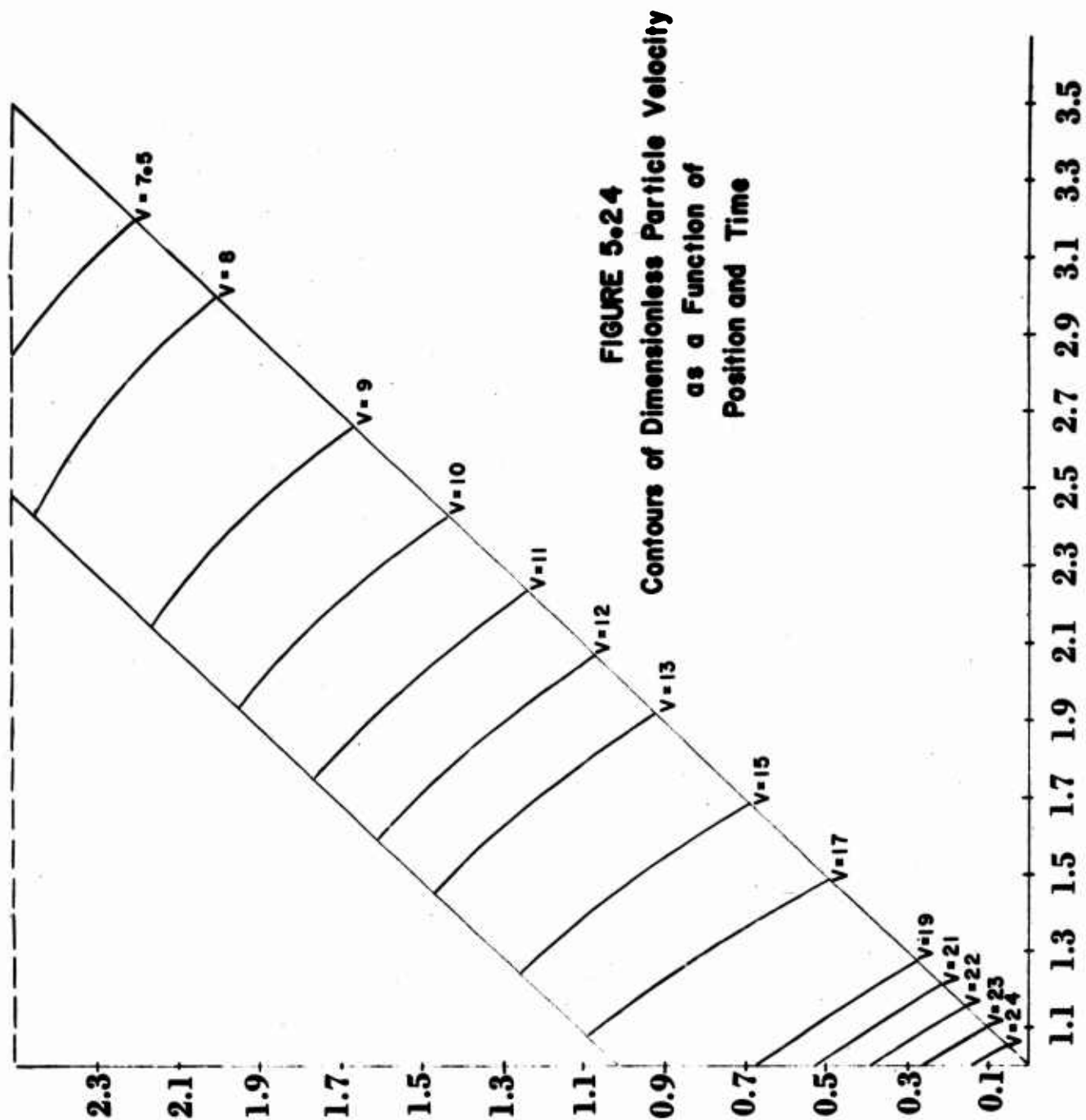


FIGURE 5.23
CONTOURS OF DIMENSIONLESS STRESS
AS A FUNCTION OF
POSITION AND TIME

MRD DIVISION
GENERAL AMERICAN TRANSPORTATION CORPORATION



MRD DIVISION
GENERAL AMERICAN TRANSPORTATION CORPORATION

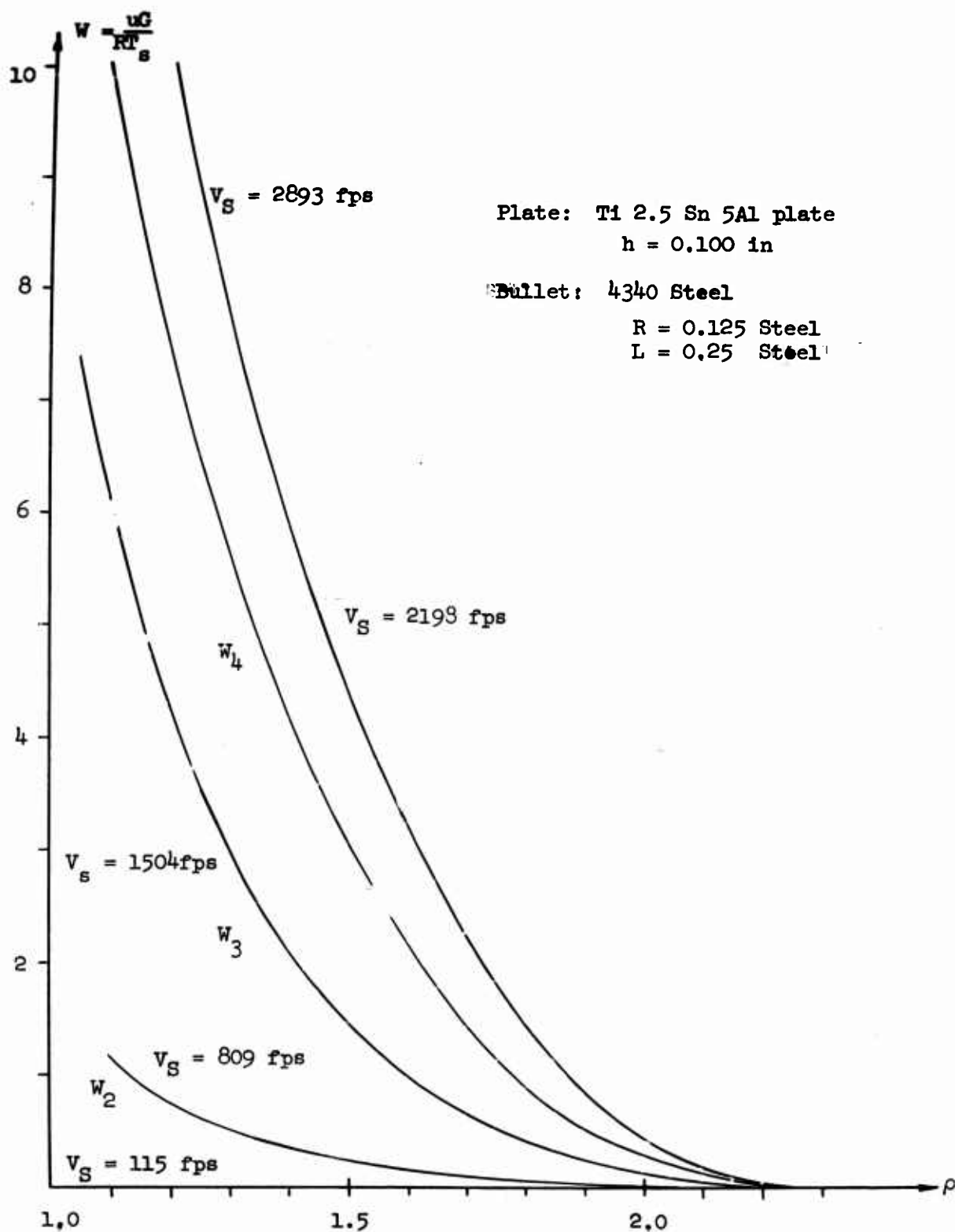


Figure 5.25 - Permanent Vertical Displacement as a Function of Radius and Input Velocity

MRD DIVISION
GENERAL AMERICAN TRANSPORTATION CORPORATION

with experimental measurements of v_R vs. v_s . This experimental data was supplied by Mr. A.L. Alesi of the Quartermaster Corps Research and Engineering Command. The description of the plate and projectile materials in conjunction with the experiments is classified. These descriptions of the plate and projectile materials are given in a classified Appendix B.

The v_R vs. v_s curves together with the experimentally determined points are shown in Fig. 5-26-28. The agreement between the theoretically predicted results and the experimental results is considered good.

5.5 Summary

This section has investigated a simple geometrical model of penetration using a physically nonlinear model of nonelastic behavior,

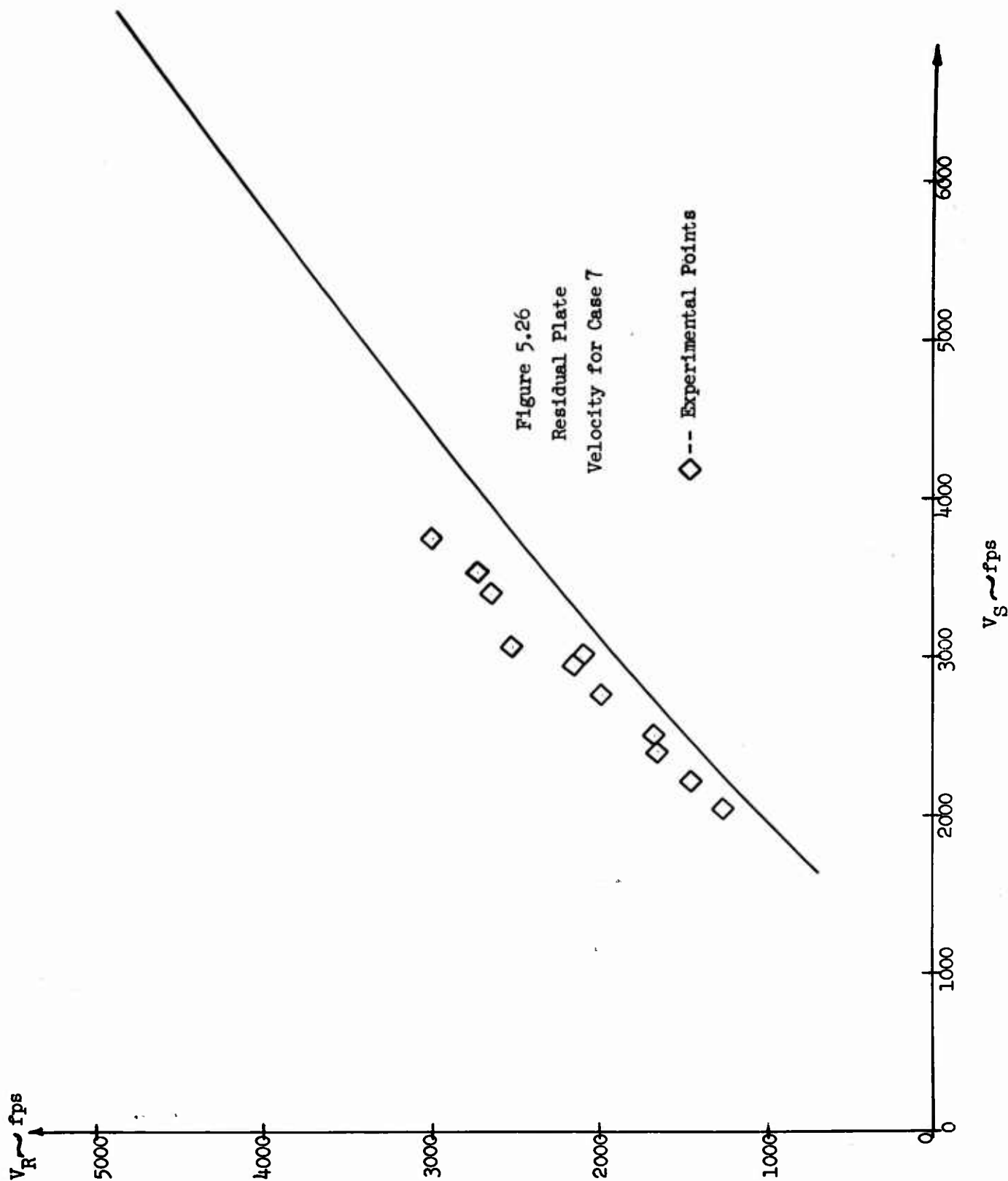
The stress-position-time pattern is altered if there is plastic flow.

There are three basic parameters in the nonelastic model that influence the v_R versus v_s curves.— the exponent coefficient A (which is directly related to the static yield strength), the maximum flow rate and the critical strain for fracture. In addition, there is the geometrical factor of thickness or total mass of the plate under the bullet.

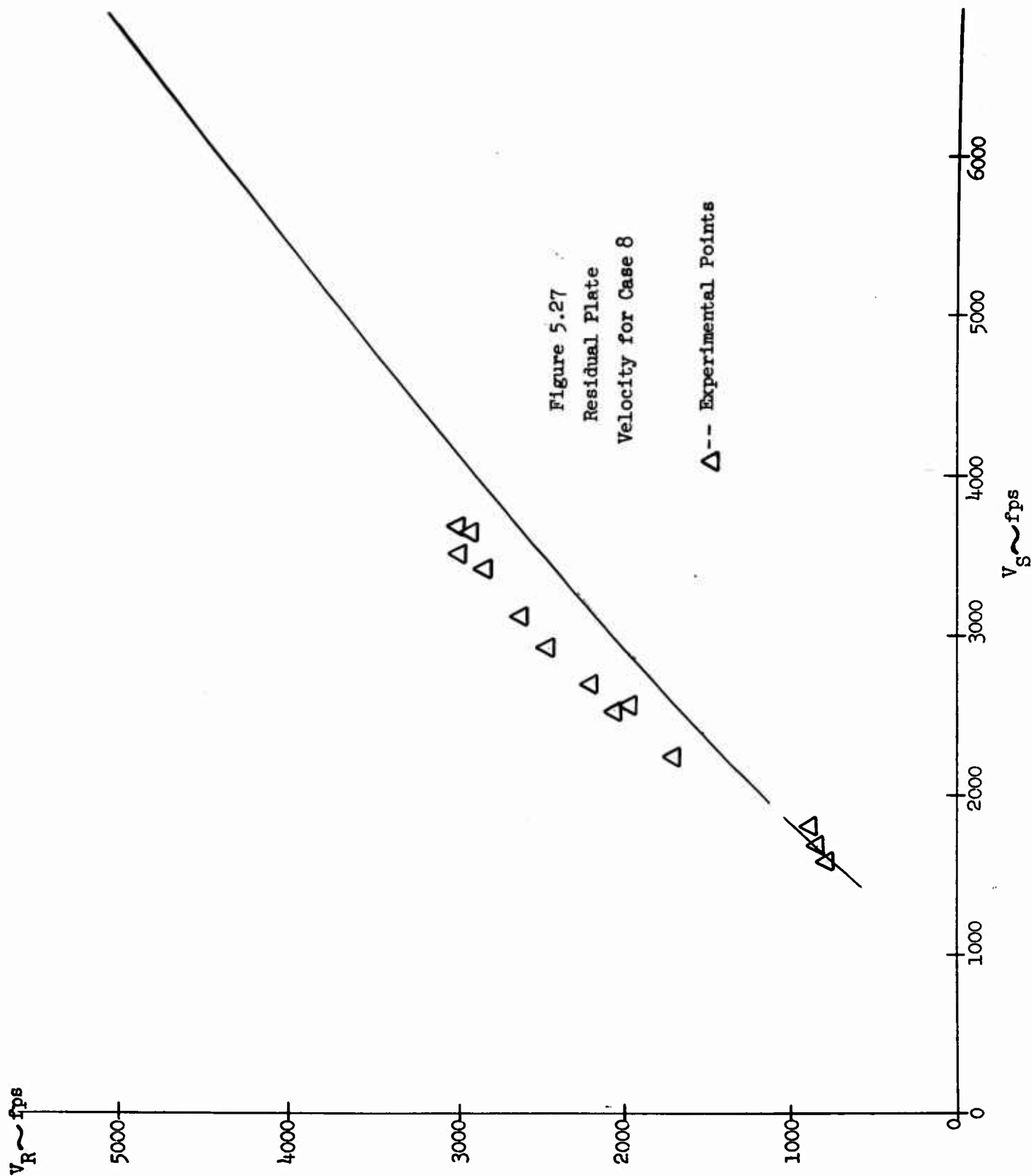
For all the material properties chosen, if these are held constant and only the thickness of the plate is increased the v_{50} decreases almost linearly with $\bar{m}_0 = \frac{M+m}{2m}$.

If the flow rate of the plate is held constant, the v_{50} increases with increasing critical elongations.

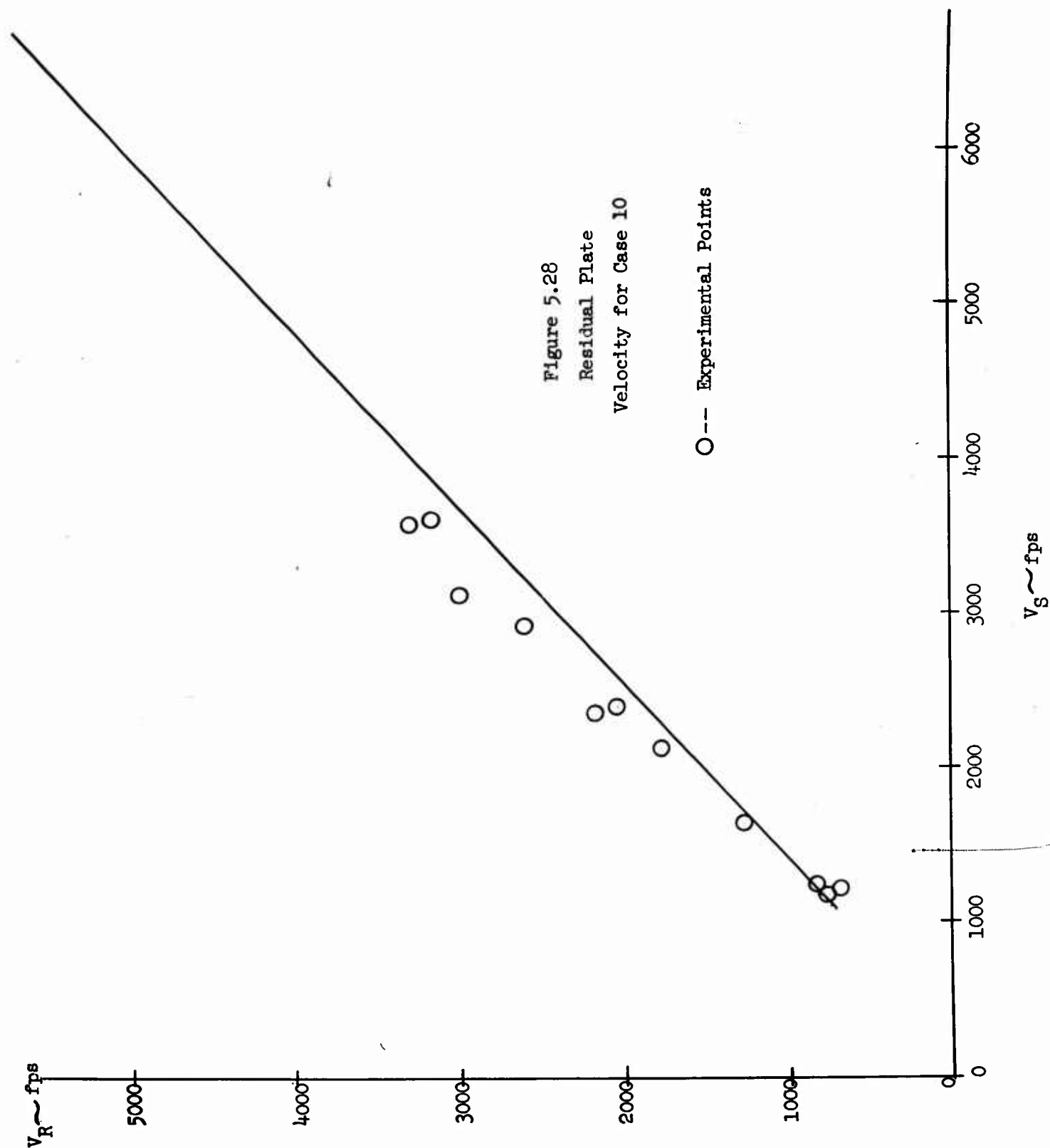
MRD DIVISION
GENERAL AMERICAN TRANSPORTATION CORPORATION



MRD DIVISION
GENERAL AMERICAN TRANSPORTATION CORPORATION



MRD DIVISION
GENERAL AMERICAN TRANSPORTATION CORPORATION



MRD DIVISION
GENERAL AMERICAN TRANSPORTATION CORPORATION

Since in most materials the flow rate and the critical elongation increase together (this combination is most likely), one set of v_R versus v_s curves was evaluated increasing both by the same percentage. In this case the v_{50} or resistance to penetration was significantly reduced. The stresses in the region of a large amount of plastic flow are reduced slower than if there is little flow. Thus the plastic strain at that point will increase faster, thus tending to break the specimens.

The v_R vs V_S curves for high impact velocities are straight which, if extended, would pass through the origin. This reflects the momentum transfer to the plate material proportional to the impact velocity. This momentum transfer occurs over a short duration of time which is the time to fracture at very high stress. At lower impact velocities the stress in the plate is lower, the time to fracture becomes longer, more momentum is transferred in the plate during this longer interval and the v_R vs V_S curve has a greater shape and, if extended, will intersect the V_S axis to the right of zero. The curvature in this bend is not great, but the intercept is shifted by anywhere for 50 fps to 500 fps.

MRD DIVISION
GENERAL AMERICAN TRANSPORTATION CORPORATION

Section 6

COMBINATION OF RESULTS

In the previous two sections, two models describing two critical phenomena in the perforation of metallic plates and metallic laminates have been discussed. The two critical areas are:

1. Transient wave propagation
2. Long time (compared to the transient) plastic flow

The v_R vs V_S curves and the v_{50} points were predicted in each case. In the actual problem both problems must be discussed simultaneously, both mechanisms of perforation of the plate must be considered in determining the resistance of the plate or laminate to ballistic impact.

The simplest way of showing the combined behavior is to assume that each mechanism is entirely independent of the other and then to superpose, the v_R vs V_S curves. The lower v_{50} and the higher v_R over V_S ratios must be used.

This combination of curves is shown schematically in fig. 6.1 for a single plate. From the results of sections 4 and 5 the transient wave is normally the dominant mode of failure,

In the laminated plates, the transient wave may be reduced in the rear plate so that the critical model for failure will be the shear model. This is shown schematically in fig. 6.2.

MRD DIVISION
GENERAL AMERICAN TRANSPORTATION CORPORATION

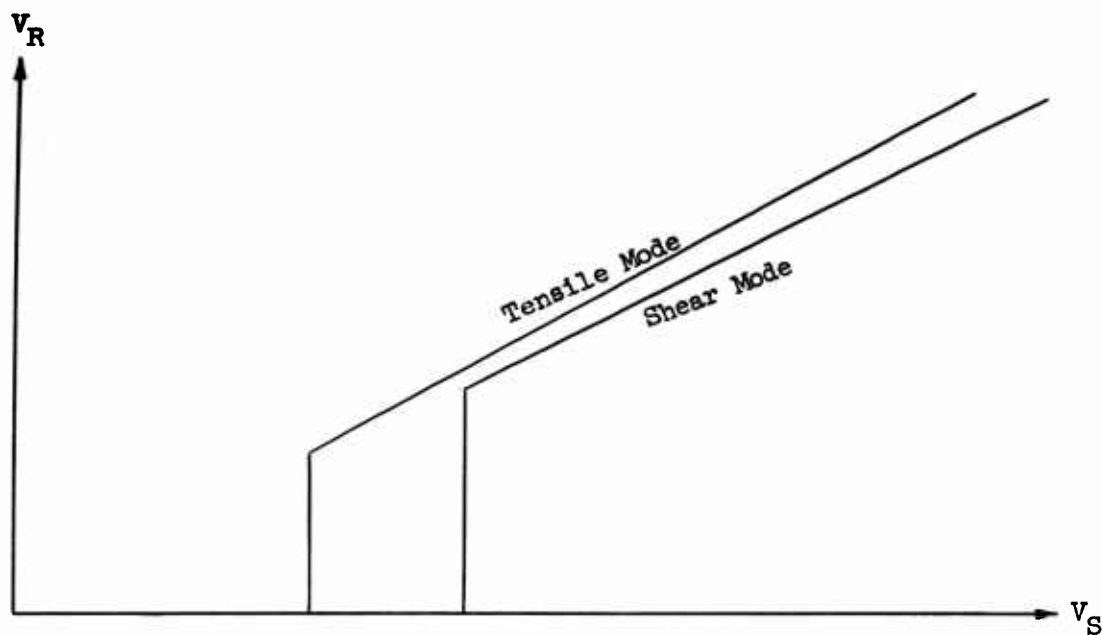


Figure 6.1 - V_R vs V_S for Single Plate (Schematic)

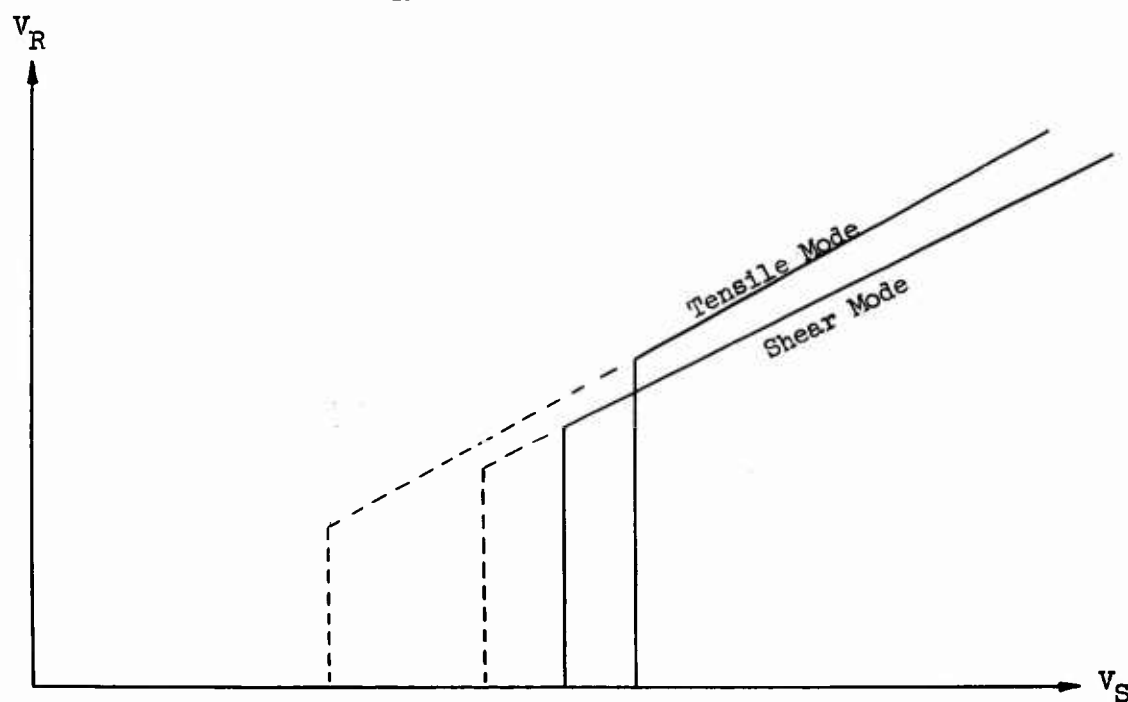


Figure 6.2 - V_R vs V_S for Laminated Plate (Schematic)

MRD DIVISION
GENERAL AMERICAN TRANSPORTATION CORPORATION

Section 7

CONCLUSIONS AND RECOMMENDATIONS

7.1 Survey of Results

The following sequence of events takes place when a bullet or projectile strikes a plate or combination of plates. When the bullet strikes the plate a stress is immediately established at the interface between the two. A stress wave is propagated into the plate and a stress wave is propagated back into the bullet.

The stress wave that propagates into the plate has very high compressive stresses at the wave front. Both the radial and vertical stress are compressive. In a very short time after the wave front has passed, these stresses are altered. The vertical stress is still compressive but reduced in magnitude. The radial stress, however, changes size and becomes tensile.

The stress wave in the plate traverses the plate and is reflected from the back surface. Both of the reflected stresses at the wave front are tensile. These stresses add to the existing stress from the tail of the downward wave. In most cases the vertical stress is very nearly zero since a compressive component and a tensile component are being added. However, the end result is a tensile vertical stress which results in spalling,

On the other hand the radial stress in the tail of the downward wave is tensile and the reflected radial stress at the wave front is also tensile. When these two add, the resulting radial stress is large tensile.

Due to this transient behavior of the propagating stresses the plate

MRD DIVISION
GENERAL AMERICAN TRANSPORTATION CORPORATION

can be broken in three ways:

1. By spalling, due to reflected tensile vertical stress.
2. By radial and tangential fracture due to the large tensile radial stress of the incident and reflected radial stress.
3. By compressive shear fracture as the first wave crosses the plate.

If the plate survives the first wave, the problem of perforation is not over. The bullet has been reduced somewhat in velocity but it is still moving. Now this process of fracture is akin to extrusion or punching. The dominant mechanism is now shear failure at the rim of the projectile.

The laminated plates after the transient stress wave characteristics by internal transmission and reflection of stresses. The proper choice of lamination materials will reduce the critical stresses in the back plate.

The effects of lamination may be summarized by considering the transmission and reflection properties of the lameller. There are two distinct cases, based on the order of the plates. The first case is where the upper plate has a high mechanical impedance and the lower plate has a low mechanical impedance. The second case is where the plate order is reversed.

In either case, the stress wave transmitted to the back plate is lower. The reflected wave is tensile in the first case and compressive in the second. The second reflection of this wave is off the original surface and is compressive and tensile, respectively. In either case large tensile stresses develop in the upper plate. The tensile fracture is delayed a little in the second case,

The effect of lamination may be summed up to reduce the stresses in the

MRD DIVISION
GENERAL AMERICAN TRANSPORTATION CORPORATION

back plate, the stresses in the upper plate will be increased. The upper plate will fracture then at a lower impact velocity. The lower plate's resistance to fracture by the stress spike will be increased.

However, the back plate must now resist fracture by shear deformation. The projectile is moving at a lower velocity. The analysis of Section 5 now applies to the rear plate with a lower incident velocity.

7.2 Design Implications

The objective of this study program is to make a theoretical determination of the phenomena that occur when a projectile strikes a piece of armor. Through a knowledge of such phenomena, the factors which deter the penetration of the armor can be optimized and more effective armor designs can be realized. Although this study does not complete the total theory required to optimize armor design, we can already draw certain conclusions which will help the armor designer.

Results of the study up to this point indicate that there are two effects which must be eliminated or significantly reduced in order to enhance the ability of personnel armor to do its job. These effects are due to transient stress spikes and long-term shear stress.

The effect of a stress-spike perpendicular to the plane of the plate is spallation. The effect of a stress-spike in the plane of the plate (radial stress) is tearing of the plate. These effects may be alleviated by using laminated plates. The degree of alleviation will depend on the materials and geometries that are feasible to use within the limitations imposed (economics, weight, availability, bulk, etc.).

MRD DIVISION
GENERAL AMERICAN TRANSPORTATION CORPORATION

Even if the effects of transient stress spikes are significantly reduced, however, the long-time shear stress is a factor still to be considered. It is well known that the effects of long-time shear stress can be overcome by increasing the thickness of the armor. Since increasing the thickness of present armor designs would also increase their weight, this approach is not desirable.

Thus, the improvement of armor is somewhat dependent on a more adequate use of materials research. With the results of the analytic program to date and with anticipated results of future analytic work, a straight-forward and direct approach should be possible,

7.2.1 Materials

Conclusions reached from the analytic studies to date should be helpful in providing guidance in the search for new materials to use for protective armor. This guidance may be used in two ways.

The capabilities of new materials as protective armor can be assessed by making a theoretical calculation of v_s/v_r . This would eliminate the need for experimenting with materials which offer no hope for improvement.

In the development of new material concepts, the theoretical conclusions may be used to set the direction of research. The qualities which enhance a material's capability to resist penetration become the objects of improvement. Composite materials may be developed which combine the best qualities of two or more materials to produce a generally better armor material. For example, it is known that many ceramic materials possess unusually high compressive strength; however, they are weak in tension. It would seem that a fruitful

MRD DIVISION
GENERAL AMERICAN TRANSPORTATION CORPORATION

avenue of investigation would lie in developing a composite material which would make use of the desirable properties of the ceramic by combining it with such a material as would overcome its weaknesses. Since several material properties are involved in resistance to penetration, the problem will be one of optimization. Such a composite might take the form of a ceramic "slab" reinforced by high tensile strength wire in a suitable configuration.

7.2.2 Geometry

In addition to the improvements that may be obtained solely through materials research, there are indications that improvements are possible through geometry as well. Atkins⁽¹⁾ has reported an experiment wherein three separated thin plates were more effective against penetration by a hypervelocity fragment impact than a single plate of more than 5 times the combined thickness of the spaced plates. A photograph of the results of his experiment shows that the projectile neatly punched through the first plate encountered, ripped a large jagged hole and severely bent the second plate, and bent, but did not penetrate, the third plate. It would seem from these results that the first plate deforms the projectile so that it presents a rather large blunt surface to the second plate. The second plate absorbs much of the energy from the projectile, thus greatly reducing its velocity. The third plate was then able to resist penetration.

Atkins' experiment used a separation of 4 inches between plates. It is felt that this much separation is unnecessary. The only spacing that is

MRD DIVISION
GENERAL AMERICAN TRANSPORTATION CORPORATION

necessary between the first and second plates is that required to allow the projectile to deform before reaching the second plate. The spacing between the second and third plates should be sufficient to allow them to act on the plate independently.

Each of the three plates should be designed of such material as to maximize the effect it is to produce. The first plate should be of a material that will cause greatest deformation of the projectile. The second plate should be designed for maximum energy-absorbing damage to itself in order to reduce the velocity of the deformed projectile as much as possible. The third plate should be designed to withstand the penetration of the deformed, reduced-velocity projectile. In application, the spacing between the plates could be maintained by a suitable light-weight material (e.g. cotton batting).

7.2.3 Local Effects

It should be remembered, in any personnel armor design, that the problem of penetration is local. The static configuration considered as a structure is not of significance. Only those effects which apply to the immediate area of impact should be considered,

MRD DIVISION
GENERAL AMERICAN TRANSPORTATION CORPORATION

BIBLIOGRAPHY

1. Atkins, W. W., Hypervelocity Penetration Studies, Proc. 4th Hypervelocity Symposium, 1960.
2. Bakhshiyani, F. A., Prik. Math. Mech. 12, 47-52, (1948)
3. Bakhshiyani, F. A., Prik. Math. Mech. 12, 281, (1948)
4. Bateman, H., and Pekeris C. L., Jour. Opt. Soc. Amer., 35, 651-657 (1955)
5. Bjork, R. L., Proc. 3rd Hypervelocity Symposium V II (1959)
6. Brekliovskikh, L. M., Waves in Layered Media, Academic Press. (1960)
7. Catlin, J. P., and Wentz, W. W., Effect of Strain Rate on the Mechanical Properties of Titanium Base Materials, WADD Tech. Rept. 53-71. (1953)
8. Cinelli, G., and Fugelso, L. E., Theoretical Study of Ground Motion Due to a Nuclear Burst, Final Tech. Rept. Contract AF 29(601)-1132 (1960)
9. Craggs, J. W., Proc. Roy. Soc. Edinburgh, 53, 359 (1952)
10. Eason, G., Noble, B., and Sneddon, I. N., Proc. Roy. Soc. Series A 247, 559 (1955)
11. Eichelberger, R. J., and Gehring, J. W., Effects of Meteoroid Impacts in Space Vehicles, BRL Rept. 1155 (1961)
12. Fugelso, L. E., Analytical Study of Early Deformation From an Underground Explosion, Final Tech. Rept. Contract DA-49-146-XZ-088 (1962)
13. Fugelso, L. E., Proc. Symp. on Properties of Earth Materials, Kirtland AFB, (1962)
14. Fugelso, L. E., Arentz, A. A., and Poczatek, J. J., Mechanics of Penetration I, Final Tech. Rept. Contract DA-19-129-QM-1542 (1961)
15. Griffith, A. A., Phil. Trans. Roy. Soc. London Ser. A 221, 163-198 (1920)
16. Harkin, J. B., Theoretical Study of Ground Motion Due to a Nuclear Burst, Final Tech. Rept. Contract AF 29(601)-2832 (1962)
17. Hopkins, H. G., and Kolsky, H., Mechanics of Hypervelocity Impact in Solids, Proc. 4th Hypervelocity Symposium, 1960.
18. Hopkins, H. G., and Prager, W., J. Mech. Phys. Solids 2, 1 (1953)
19. Illyushin, A. A., Proc. Conf. on Plastic Deformation (1938)(in Russia)

MRD DIVISION
GENERAL AMERICAN TRANSPORTATION CORPORATION

20. Irwin, G. R., "Fracture" in Handbuch der Physik B.6, (1958)
21. Irwin, G. R., "Fracture Dynamics" in ASM Symposium on Fracturing of Metals, (1948)
22. Kolsky, H., Stress Waves in Solids, Oxford U.P. (1955)
23. Kotchetchov, A. M., Prik. Math. Mech., 14, 203 (1950)
24. Kotchetchov, A. M., Prik. Math. Mech., 14, 433-438, (1950)
25. Mura, T., Theory of the Continuous Dislocation, Final Tech. Rept. Contract AF 49(638)-780, (1961)
26. Sneddon, I. N., Proc. Phys. Soc. of London, 187, 229, (1946)
27. Sokolovsky, V. V., Doklady Akadameia Nauk SSR, 60, 775-778 (1948)
28. Sokolovsky, V. V., Prik. Math. Mech. 12, 261-280 (1948)
29. Thompson N., Wadsworth, N., and Louet, N., Phil. Mag., 1, 113-126 (1956)
30. Westergaard, H. M., J. Appl. Mech., 6, 2 (1939)
31. Zener, C., "Micromechanism of Fracture" in Fracturing of Metals, ASM Symposium, (1908)
32. Zhurkov, S. N. and Sanfirova, T. P., Soviet Physics Solid State 2, 933-935 (1960)
33. Zhurkov, S. N. and Sanfirova, T. P., Soviet Physics Technical Physics 2, 1586-1592 (1958)
34. Davies, R. M., Proc. Roy. Soc. Ser. A 197, 116 (1947)
35. ASM Metals Handbook

MRD DIVISION
GENERAL AMERICAN TRANSPORTATION CORPORATION

APPENDIX A
FORMAL INTEGRAL SOLUTION FOR STRESSES
IN A LAMINATED PLATE

by
J. D. Stein and P. G. Boekhoff

MRD DIVISION
GENERAL AMERICAN TRANSPORTATION CORPORATION

A.I Introduction

The problem of finding formal expressions for the stresses in a laminated plate will be investigated. It is assumed herein that both the material properties of the plate and the otherwise arbitrary load on the plate are axially symmetric. The plate will be loaded dynamically with an arbitrary pressure $p(r,t)$, and a method for finding the stresses in the plate in terms of the loading function and the plate characteristics will be developed.

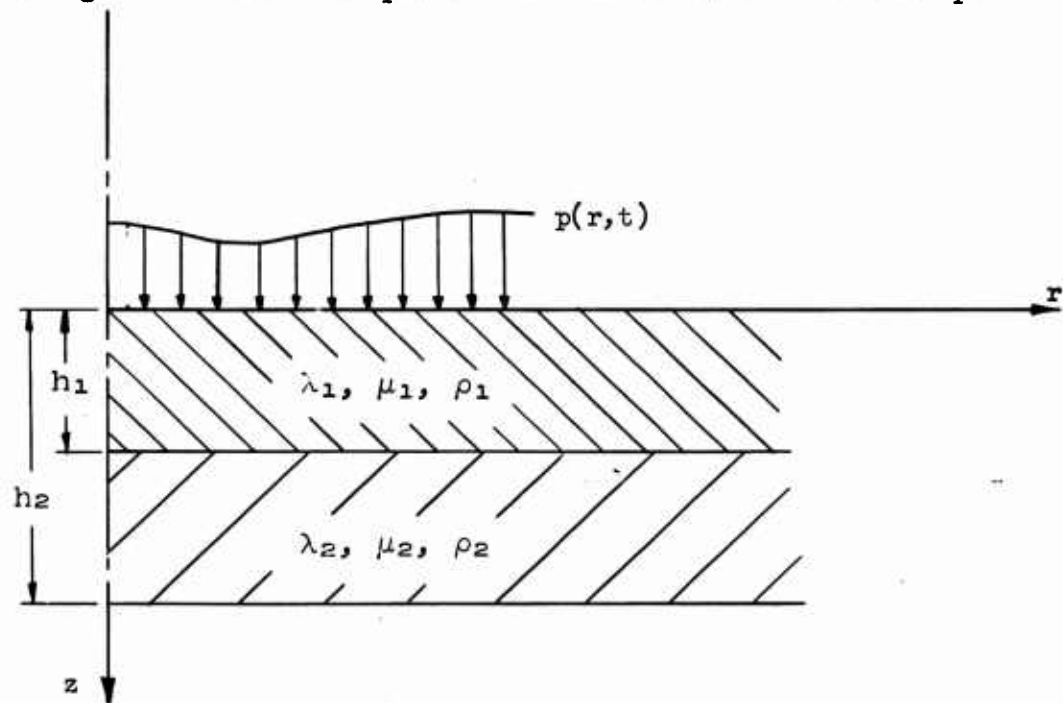


Figure A.1 - CONFIGURATION OF LAMINATED PLATE

First, the potential functions ϕ and θ are defined and the partial-differential potential equations are presented. To these equations and the appropriate boundary conditions, Hankel-Laplace transforms are applied. A set of equations in the transform space is developed which, when solved by determinants, yields expressions for the transformed potential functions

MRD DIVISION
GENERAL AMERICAN TRANSPORTATION CORPORATION

ϕ and θ . Inversion formulae are given by which ϕ and θ can be found, and the stresses finally appear as explicit functions of the potentials ϕ and θ .

A.II Equations of Motion

Under the assumption of axial symmetry, the equations of motion can be written as

$$\rho \frac{\partial^2 u_r}{\partial t^2} = \frac{\partial \sigma_r}{\partial r} + \frac{\partial \tau_{rz}}{\partial z} + \frac{\sigma_r - \sigma_\theta}{r}$$

$$\rho \frac{\partial^2 u_z}{\partial t^2} = \frac{\partial \tau_{rz}}{\partial r} + \frac{\partial \sigma_z}{\partial z} + \frac{\tau_{rz}}{r}$$

where u_r and u_z are the radial and vertical (axial) components of displacement and σ_r , σ_θ , σ_z , and τ_{rz} are the radial, tangential, axial, and shear stresses respectively, and ρ is the plate density. The stresses are then given by

$$\sigma_r = (\lambda + 2\mu) \left(\frac{\partial u_r}{\partial r} + \frac{u_r}{r} + \frac{\partial u_z}{\partial z} \right) - 2\mu \left(\frac{u_r}{r} + \frac{\partial u_z}{\partial z} \right)$$

$$\sigma_\theta = (\lambda + 2\mu) \left(\frac{\partial u_r}{\partial r} + \frac{u_r}{r} + \frac{\partial u_z}{\partial z} \right) - 2\mu \left(\frac{\partial u_r}{\partial r} + \frac{\partial u_z}{\partial z} \right)$$

$$\sigma_z = (\lambda + 2\mu) \left(\frac{\partial u_r}{\partial r} + \frac{u_r}{r} + \frac{\partial u_z}{\partial z} \right) - 2\mu \left(\frac{\partial u_r}{\partial r} + \frac{u_r}{r} \right)$$

$$\tau_{rz} = \mu \left(\frac{\partial u_r}{\partial z} + \frac{\partial u_z}{\partial r} \right)$$

where λ and μ are the Lamé numbers of the plate material.

MRD DIVISION
GENERAL AMERICAN TRANSPORTATION CORPORATION

A.III Boundary Conditions

At the surfaces of the laminated plate, the boundary conditions may be simply formulated and are not dependent on the characteristics of the plate; at the interface, however, some assumption must be made regarding the characteristics of the bond. At one extreme, the bond may be considered infinitely strong, in which case we have

$$u_r^{(1)} = u_r^{(2)} \quad z = h_1$$

$$u_z^{(1)} = u_z^{(2)} \quad z = h_1$$

$$\frac{\partial u_r^{(1)}}{\partial r} = \frac{\partial u_r^{(2)}}{\partial r} \quad z = h_1$$

$$\frac{\partial u_z^{(1)}}{\partial r} = \frac{\partial u_z^{(2)}}{\partial r} \quad z = h_1$$

where the superscripts (1) and (2) denote the top and bottom plates respectively.

At the other extreme, taking the bond strength to be zero gives

$$\tau_{rz}^{(1)} = \tau_{rz}^{(2)} = 0 \quad z = h_1$$

$$\sigma_z^{(1)} \leq 0 \quad z = h_1$$

$$\sigma_z^{(2)} < 0 \quad z = h_1, \sigma_z^{(1)} < 0$$

$$\sigma_z^{(2)} = 0 \quad z = h_1, \sigma_z^{(1)} = 0$$

$$u_z^{(1)} = u_z^{(2)} \quad z = h_1, \sigma_z^{(1)} < 0$$

$$\frac{\partial u_z^{(1)}}{\partial r} = \frac{\partial u_z^{(2)}}{\partial r} \quad z = h_1, \sigma_z^{(1)} < 0$$

MRD DIVISION
GENERAL AMERICAN TRANSPORTATION CORPORATION

We shall assume here a bond such that the vertical stresses and displacements are equal across the interface and the rz-shear stress is zero at each side of the interface. Then if $p(r,t)$ is the pressure on the top surface, the boundary conditions are:

$$\sigma_z^{(1)} = -p(r,t) \quad z = 0$$

$$\sigma_z^{(1)} = \sigma_z^{(2)} \quad z = h_1$$

$$\sigma_z^{(2)} = 0 \quad z = h_2$$

$$\tau_{rz}^{(1)} = 0 \quad z = 0$$

$$\tau_{rz}^{(1)} = 0 \quad z = h_1$$

$$\tau_{rz}^{(2)} = 0 \quad z = h_1$$

$$\tau_{rz}^{(2)} = 0 \quad z = h_2$$

$$u_z^{(1)} = u_z^{(2)} \quad z = h_1$$

A. IV The Potential Equations

The partial-differential equations which must be solved subject to the above boundary conditions are

$$\nabla^2 \phi_1 = \frac{1}{\alpha_1^2} \frac{\partial^2 \phi_1}{\partial t^2} \quad i = 1, 2 \quad (A.1)$$

MRD DIVISION
GENERAL AMERICAN TRANSPORTATION CORPORATION

$$\nabla^2 \theta_1 - \frac{\theta_1}{r^2} = \frac{1}{\beta_1^2} \frac{\partial^2 \theta_1}{\partial t^2} \quad 1 = 1, 2 \quad (\text{A.2})$$

where

$$\nabla^2 = \frac{\partial^2}{\partial r^2} + \frac{1}{r} \frac{\partial}{\partial r} + \frac{\partial^2}{\partial z^2}$$

$$\alpha_1^2 = \frac{\lambda_1 + 2\mu_1}{\rho_1}$$

$$\beta_1^2 = \frac{\mu_1}{\rho_1}$$

ϕ_1 and θ_1 are defined by

$$u_r^{(1)} = \frac{\partial \phi_1}{\partial r} - \frac{\partial \theta_1}{\partial z} \quad (\text{A.3})$$

$$u_z^{(1)} = \frac{\partial \phi_1}{\partial z} + \frac{\theta_1}{r} + \frac{\partial \theta_1}{\partial r} \quad (\text{A.4})$$

and the stresses are given in terms of ϕ_1 and θ_1 by

$$\sigma_r^{(1)} = (\lambda_1 + 2\mu_1) \nabla^2 \phi_1 - 2\mu_1 \left(\frac{\partial^2 \phi_1}{\partial z^2} + \frac{1}{r} \frac{\partial \phi_1}{\partial r} + \frac{\partial^2 \theta_1}{\partial r \partial z} \right) \quad (\text{A.5})$$

$$\sigma_\theta^{(1)} = (\lambda_1 + 2\mu_1) \nabla^2 \phi_1 - 2\mu_1 \left(\frac{\partial^2 \phi_1}{\partial r^2} + \frac{\partial^2 \phi_1}{\partial z^2} + \frac{1}{r} \frac{\partial \theta_1}{\partial z} \right) \quad (\text{A.6})$$

$$\sigma_z^{(1)} = (\lambda_1 + 2\mu_1) \nabla^2 \phi_1 - 2\mu_1 \left(\frac{\partial^2 \phi_1}{\partial r^2} + \frac{1}{r} \frac{\partial \phi_1}{\partial r} - \frac{1}{r} \frac{\partial \theta_1}{\partial z} - \frac{\partial^2 \theta_1}{\partial r \partial z} \right) \quad (\text{A.7})$$

$$\tau_{rz}^{(1)} = \mu_1 \left(2 \frac{\partial^2 \phi_1}{\partial r \partial z} - \frac{\partial^2 \theta_1}{\partial z^2} + \frac{\partial^2 \theta_1}{\partial r^2} + \frac{1}{r} \frac{\partial \theta_1}{\partial r} - \frac{\theta_1}{r^2} \right) \quad (\text{A.8})$$

MRD DIVISION
GENERAL AMERICAN TRANSPORTATION CORPORATION

If we make the substitutions

$$\tau = \alpha_1 t$$

$$\gamma_1 = 1$$

$$\gamma_2 = \frac{\alpha_1}{\alpha_2}$$

$$\nu_1 = \frac{\alpha_1}{\beta_1}$$

$$\nu_2 = \frac{\alpha_1}{\beta_2}$$

$$p_0(r, \tau) = p(r, t)$$

equations (A.1) and (A.2) become

$$\nabla^2 \phi_1 = \gamma_1^2 \frac{\partial^2 \phi_1}{\partial \tau^2} \quad (\text{A.9})$$

$$\nabla^2 \theta_1 - \frac{\theta_1}{r^2} = \nu_1^2 \frac{\partial^2 \theta_1}{\partial \tau^2} \quad (\text{A.10})$$

A.V Transformation of the Differential Equations

We shall denote by $\bar{\phi}_{1,0}$ the Hankel (order zero) -Laplace transform of ϕ_1 , and by $\bar{\theta}_{1,1}$ the Hankel (order one) -Laplace transform of θ_1 . Multiplying equation (A.9) by $r J_0(\xi r) e^{-s\tau}$ and integrating over τ and r from 0 to ∞ , we obtain:

$$-\xi^2 \bar{\phi}_{1,0} + \frac{d^2 \bar{\phi}_{1,0}}{dz^2} = \gamma_1^2 s^2 \bar{\phi}_{1,0} \quad (\text{A.11})$$

MRD DIVISION
GENERAL AMERICAN TRANSPORTATION CORPORATION

Multiplying (A.10) by $r J_1(\xi r) e^{-sr}$ and integrating:

$$-\xi^2 \bar{\theta}_{1,1} + \frac{d^2 \bar{\theta}_{1,1}}{dz^2} = \nu_1^2 s^2 \bar{\theta}_{1,1} \quad (\text{A.12})$$

Now we let

$$m_1^2 = \xi^2 + \gamma_1^2 s^2$$

$$n_1^2 = \xi^2 + \nu_1^2 s^2$$

so that (A.11) and (A.12) become

$$\frac{d^2 \bar{\phi}_{1,0}}{dz^2} - m_1^2 \bar{\phi}_{1,0} = 0 \quad (\text{A.13})$$

$$\frac{d^2 \bar{\theta}_{1,1}}{dz^2} - n_1^2 \bar{\theta}_{1,1} = 0 \quad (\text{A.14})$$

and we obtain the following equations in the transform space:

$$\bar{\phi}_{1,0} = A_1 e^{m_1 z} + A_2 e^{-m_1 z} \quad (\text{A.15})$$

$$\bar{\phi}_{2,0} = A_3 e^{m_2 z} + A_4 e^{-m_2 z} \quad (\text{A.16})$$

$$\bar{\theta}_{1,1} = A_5 e^{n_1 z} + A_6 e^{-n_1 z} \quad (\text{A.17})$$

$$\bar{\theta}_{2,1} = A_7 e^{n_2 z} + A_8 e^{-n_2 z} \quad (\text{A.18})$$

A.VI Boundary Conditions in the Transform Space

To evaluate the constants in these last four equations, the boundary conditions must be transformed. Since these involve only $\sigma_z^{(1)}, \tau_{rz}^{(1)}$ and

MRD DIVISION
GENERAL AMERICAN TRANSPORTATION CORPORATION

$u_z^{(1)}$, we can confine ourselves to equations (A.4), (A.7), and (A.8).

Multiplying (A.4) by $r J_0(\xi r) e^{-s\tau}$ and integrating over r and τ from 0 to ∞ , we have:

$$\bar{u}_{z,0}^{(1)} = \frac{d\bar{\phi}_{1,0}}{dz} + \xi \bar{\theta}_{1,1} \quad (A.19)$$

Multiplying (A.7) by $r J_0(\xi r) e^{-s\tau}$ and integrating

$$\bar{\sigma}_{z,0}^{(1)} = [(\lambda_1 + 2\mu_1) \gamma_1^2 s^2 + 2\mu_1 \xi^2] \bar{\phi}_{1,0} + 2\mu_1 \xi \frac{d\bar{\theta}_{1,1}}{dz} \quad (A.20)$$

Multiplying (A.8) by $r J_1(\xi r) e^{-s\tau}$ and integrating

$$\bar{\tau}_{rz,1}^{(1)} = -\mu_1 (2\xi \frac{d\bar{\phi}_{1,0}}{dz} + \frac{d^2\bar{\theta}_{1,1}}{dz^2} + \xi^2 \bar{\theta}_{1,1}) \quad (A.21)$$

Now let

$$p_1 = (\lambda_1 + 2\mu_1) \gamma_1^2 s^2 + 2\mu_1 \xi^2$$

$$q_1 = 2\mu_1 \xi$$

so that equations (A.19) - (A.21) become

$$\bar{u}_{z,0}^{(1)} = \frac{d\bar{\phi}_{1,0}}{dz} + \xi \bar{\theta}_{1,1} \quad (A.22)$$

$$\bar{\sigma}_{z,0}^{(1)} = p_1 \bar{\phi}_{1,0} + q_1 \frac{d\bar{\theta}_{1,1}}{dz} \quad (A.23)$$

$$\bar{\tau}_{rz,1}^{(1)} = -q_1 \frac{d\bar{\phi}_{1,0}}{dz} - \mu_1 \frac{d^2\bar{\theta}_{1,1}}{dz^2} - \mu_1 \xi^2 \bar{\theta}_{1,1} \quad (A.24)$$

Denoting by $\bar{p}_{0,0}(\xi, s)$ the Hankel (order zero) -Laplace transform of $p_0(r, \tau)$, we have for the transformed boundary conditions:

MRD DIVISION
GENERAL AMERICAN TRANSPORTATION CORPORATION

$$\bar{\sigma}_{z,0}^{(1)} = -\bar{p}_{o,o}(\xi, s)$$

$$z = 0$$

$$\bar{\sigma}_{z,0}^{(1)} = \bar{\sigma}_{z,0}^{(2)}$$

$$z = h_1$$

$$\bar{\sigma}_{z,0}^{(2)} = 0$$

$$z = h_2$$

$$\bar{\tau}_{rz,1}^{(1)} = 0$$

$$z = 0$$

$$\bar{\tau}_{rz,1}^{(1)} = \bar{\tau}_{rz,1}^{(2)} = 0$$

$$z = h_1$$

$$\bar{\tau}_{rz,1}^{(2)} = 0$$

$$z = h_2$$

$$\bar{u}_{z,0}^{(1)} = \bar{u}_{z,0}^{(2)}$$

$$z = h_1$$

Substitution of equations (A.13) - (A.18) and (A.22) - (A.24) into the above conditions gives us the following system:

$$p_1 A_1 + p_1 A_2 + q_1 n_1 A_5 - q_1 n_1 A_6 = -\bar{p}_{o,o}(\xi, s) \quad (A.25)$$

$$p_1 e^{m_1 h_1} A_1 + p_1 e^{-m_1 h_1} A_2 + q_1 n_1 e^{n_1 h_1} A_5 - q_1 n_1 e^{-n_1 h_1} A_6 =$$

$$p_2 e^{m_2 h_2} A_3 + p_2 e^{-m_2 h_2} A_4 + q_2 n_2 e^{n_2 h_2} A_7 - q_2 n_2 e^{-n_2 h_2} A_8 \quad (A.26)$$

$$p_2 e^{m_2 h_2} A_3 + p_2 e^{-m_2 h_2} A_4 + q_2 n_2 e^{n_2 h_2} A_7 - q_2 n_2 e^{-n_2 h_2} A_8 = 0 \quad (A.27)$$

$$q_1 m_1 A_1 - q_1 m_1 A_2 + \mu_1 (n_1^2 + \xi^2) A_5 + \mu_1 (n_1^2 + \xi^2) A_6 = 0 \quad (A.28)$$

$$q_1 m_1 e^{m_1 h_1} A_1 - q_1 m_1 e^{-m_1 h_1} A_2 + \mu_1 (n_1^2 + \xi^2) e^{n_1 h_1} A_5 + \mu_1 (n_1^2 + \xi^2) e^{-n_1 h_1} A_6 = 0 \quad (A.29)$$

MRD DIVISION
GENERAL AMERICAN TRANSPORTATION CORPORATION

$$q_2 m_2 e^{m h} A_3 - q_2 m_2 e^{-m h} A_4 + \mu_2 (n_2^2 + \xi^2) e^{n h} A_7 + \mu_2 (n_2^2 + \xi^2) e^{-n h} A_8 = 0 \quad (A.30)$$

$$q_2 m_2 e^{m h} A_3 - q_2 m_2 e^{-m h} A_4 + \mu_2 (n_2^2 + \xi^2) e^{n h} A_7 + \mu_2 (n_2^2 + \xi^2) e^{-n h} A_8 = 0 \quad (A.31)$$

$$m_1 e^{m h} A_1 - m_1 e^{-m h} A_2 + \xi e^{n h} A_5 + \xi e^{-n h} A_6 = m_2 e^{m h} A_3 - m_2 e^{-m h} A_4 + \xi e^{n h} A_7 + \xi e^{-n h} A_8 \quad (A.32)$$

A.VII Solution of the Equations in the Transform Space

Let us introduce the following notation:

$$a_{11} = p_1 \quad a_{33} = p_2 e^{m h}$$

$$a_{15} = q_1 n_1 \quad a_{34} = p_2 e^{-m h}$$

$$a_{21} = p_1 e^{m h} \quad a_{37} = q_2 n_2 e^{n h}$$

$$a_{22} = p_1 e^{-m h} \quad a_{38} = q_2 n_2 e^{-n h}$$

$$a_{23} = p_2 e^{m h} \quad a_{41} = q_1 m$$

$$a_{24} = p_2 e^{-m h} \quad a_{45} = \mu_1 (n_1^2 + \xi^2)$$

$$a_{25} = q_1 n_1 e^{n h} \quad a_{51} = q_1 m e^{m h}$$

$$a_{26} = q_1 n_1 e^{-n h} \quad a_{52} = q_1 m e^{-m h}$$

$$a_{27} = q_2 n_2 e^{n h} \quad a_{55} = \mu_1 (n_1^2 + \xi^2) e^{n h}$$

$$a_{28} = q_2 n_2 e^{-n h} \quad a_{56} = \mu_1 (n_1^2 + \xi^2) e^{-n h}$$

MRD DIVISION
GENERAL AMERICAN TRANSPORTATION CORPORATION

$$a_{63} = q_2 m_2 e^{m h_1}$$

$$a_{64} = q_2 m_2 e^{-m h_1}$$

$$a_{67} = \mu_2 (n_2^2 + \xi^2) e^{n h_1}$$

$$a_{68} = \mu_2 (n_2^2 + \xi^2) e^{-n h_1}$$

$$a_{73} = q_2 m_2 e^{m h_2}$$

$$a_{74} = q_2 m_2 e^{-m h_2}$$

$$a_{77} = \mu_2 (n_2^2 + \xi^2) e^{n h_2}$$

$$a_{78} = \mu_2 (n_2^2 + \xi^2) e^{-n h_2}$$

$$a_{81} = m_1 e^{m h_1}$$

$$a_{82} = m_1 e^{-m h_1}$$

$$a_{83} = m_2 e^{m h_1}$$

$$a_{84} = m_2 e^{-m h_1}$$

$$a_{85} = \xi e^{n h_1}$$

$$a_{86} = \xi e^{-n h_1}$$

$$a_{87} = \xi e^{n h_2}$$

$$a_{88} = \xi e^{-n h_2}$$

Now let Γ denote the 8×8 matrix.

$$\begin{bmatrix} a_{11} & a_{11} & 0 & 0 & a_{15} & -a_{15} & 0 & 0 \\ a_{21} & a_{22} & -a_{23} & -a_{24} & a_{25} & -a_{26} & -a_{27} & a_{28} \\ 0 & 0 & a_{33} & a_{34} & 0 & 0 & a_{37} & -a_{38} \\ a_{41} & -a_{41} & 0 & 0 & a_{45} & a_{45} & 0 & 0 \\ a_{51} & -a_{52} & 0 & 0 & a_{55} & a_{56} & 0 & 0 \\ 0 & 0 & a_{63} & -a_{64} & 0 & 0 & a_{67} & a_{68} \\ 0 & 0 & a_{73} & -a_{74} & 0 & 0 & a_{77} & a_{78} \\ a_{81} & -a_{82} & -a_{83} & a_{84} & a_{85} & a_{86} & -a_{87} & -a_{88} \end{bmatrix}$$

MRD DIVISION
GENERAL AMERICAN TRANSPORTATION CORPORATION

and Δ the column matrix

$$\begin{bmatrix} -\bar{p}_{0,0}(\xi, s) \\ 0 \\ 0 \\ 0 \\ 0 \\ 0 \\ 0 \\ 0 \end{bmatrix}$$

and Γ_j the 8×8 matrix formed by substituting Δ for the j th column of Γ .

Then if $||\Gamma||$ and $||\Gamma_j||$ represent the determinants of Γ and Γ_j respectively, we have

$$A_j = ||\Gamma_j|| / ||\Gamma|| \quad j = 1, \dots, 8 \quad (A.33)$$

The determinants are evaluated by standard matrix manipulations; the following sample evaluation will give an indication of the method and of the form and the degree of complexity of the coefficients A_j :

$$||\Gamma|| = \begin{vmatrix} a_{11} & a_{11} & a_{15} & -a_{15} & 0 & 0 & 0 & 0 \\ a_{41} & -a_{41} & a_{45} & a_{45} & 0 & 0 & 0 & 0 \\ a_{51} & -a_{52} & a_{55} & a_{56} & 0 & 0 & 0 & 0 \\ a_{21} & a_{22} & a_{25} & -a_{26} & -a_{23} & -a_{24} & -a_{27} & a_{28} \\ a_{81} & -a_{82} & a_{85} & a_{86} & -a_{83} & a_{84} & -a_{87} & -a_{88} \\ 0 & 0 & 0 & 0 & a_{33} & a_{34} & a_{37} & -a_{38} \\ 0 & 0 & 0 & 0 & a_{73} & -a_{74} & a_{77} & a_{78} \\ 0 & 0 & 0 & 0 & a_{63} & -a_{64} & a_{67} & a_{68} \end{vmatrix}$$

MRD DIVISION
GENERAL AMERICAN TRANSPORTATION CORPORATION

$$\begin{array}{cccccccc}
 a_{11} & 0 & 0 & 0 & 0 & 0 & 0 & 0 \\
 0 & -2a_{41} & \left[a_{45} - \frac{a_{15}a_{41}}{a_{11}} \right] & 2a_{45} & 0 & 0 & 0 & 0 \\
 0 & -a_{52} - a_{51} & \left[a_{55} - \frac{a_{15}a_{51}}{a_{11}} \right] & a_{55} + a_{56} & 0 & 0 & 0 & 0 \\
 0 & a_{22} - a_{21} & \left[a_{25} - \frac{a_{15}a_{21}}{a_{11}} \right] & a_{25} - a_{26} & \left[-a_{23} - \frac{a_{63}a_{23}}{a_{68}} \right] & \left[-a_{24} + \frac{a_{64}a_{23}}{a_{68}} \right] & \left[-a_{27} - \frac{a_{67}a_{23}}{a_{68}} \right] & 0 \\
 0 & -a_{32} - a_{31} & \left[a_{35} - \frac{a_{15}a_{31}}{a_{11}} \right] & a_{35} + a_{36} & \left[-a_{33} + \frac{a_{63}a_{33}}{a_{68}} \right] & \left[a_{34} + \frac{a_{64}a_{33}}{a_{68}} \right] & \left[-a_{37} + \frac{a_{67}a_{33}}{a_{68}} \right] & 0 \\
 0 & 0 & 0 & 0 & \left[a_{33} + \frac{a_{63}a_{33}}{a_{68}} \right] & \left[a_{34} - \frac{a_{64}a_{33}}{a_{68}} \right] & \left[a_{37} + \frac{a_{67}a_{33}}{a_{68}} \right] & 0 \\
 0 & 0 & 0 & 0 & \left[a_{73} + \frac{a_{63}a_{73}}{a_{68}} \right] & \left[-a_{74} + \frac{a_{64}a_{73}}{a_{68}} \right] & \left[a_{77} - \frac{a_{67}a_{73}}{a_{68}} \right] & 0 \\
 0 & 0 & 0 & 0 & 0 & 0 & 0 & a_{68}
 \end{array}$$

$$\begin{array}{cccccccc}
 a_{11} & 0 & 0 & 0 & 0 & 0 & 0 & 0 \\
 0 & -2a_{41} & 0 & 0 & 0 & 0 & 0 & 0 \\
 0 & 0 & b_{55} & b_{56} & 0 & 0 & 0 & 0 \\
 0 & 0 & b_{25} & b_{26} & b_{23} & b_{24} & 0 & 0 \\
 0 & 0 & b_{35} & b_{36} & b_{33} & b_{34} & 0 & 0 \\
 0 & 0 & 0 & 0 & b_{33} & b_{34} & 0 & 0 \\
 0 & 0 & 0 & 0 & 0 & 0 & b_{77} & 0 \\
 0 & 0 & 0 & 0 & 0 & 0 & 0 & a_{68}
 \end{array}$$

MRD DIVISION
GENERAL AMERICAN TRANSPORTATION CORPORATION

where

$$b_{25} = a_{25} - \frac{a_{15}}{a_{11}} a_{21} + \left[\frac{a_{45} - \frac{(a_{15}/a_{11})a_{41}}{2a_{41}}}{2a_{41}} \right] (a_{22} - a_{21})$$

$$b_{26} = a_{25} - a_{26} + \frac{a_{45}}{a_{41}} (a_{22} - a_{21})$$

$$b_{23} = -a_{23} - \frac{a_{63}}{a_{68}} a_{28} + \left[\frac{a_{73} - \frac{(a_{63}/a_{68})a_{78}}{a_{67}/a_{68}}}{a_{77} - \frac{(a_{67}/a_{68})a_{78}}{a_{67}/a_{68}}} \right] (a_{27} + \frac{a_{67}}{a_{68}} a_{28})$$

$$b_{24} = -a_{24} + \frac{a_{64}}{a_{68}} a_{28} - \left[\frac{a_{74} - \frac{(a_{64}/a_{68})a_{78}}{a_{67}/a_{68}}}{a_{77} - \frac{(a_{67}/a_{68})a_{78}}{a_{67}/a_{68}}} \right] (a_{27} + \frac{a_{67}}{a_{68}} a_{28})$$

$$b_{33} = a_{33} + \frac{a_{63}}{a_{68}} a_{38} - \left[\frac{a_{73} - \frac{(a_{63}/a_{68})a_{78}}{a_{67}/a_{68}}}{a_{77} - \frac{(a_{67}/a_{68})a_{78}}{a_{67}/a_{68}}} \right] (a_{37} + \frac{a_{67}}{a_{68}} a_{38})$$

$$b_{34} = a_{34} - \frac{a_{64}}{a_{68}} a_{38} + \left[\frac{a_{74} - \frac{(a_{64}/a_{68})a_{78}}{a_{67}/a_{68}}}{a_{77} - \frac{(a_{67}/a_{68})a_{78}}{a_{67}/a_{68}}} \right] (a_{37} + \frac{a_{67}}{a_{68}} a_{38})$$

$$b_{55} = a_{55} - \frac{a_{15}}{a_{11}} a_{51} - \left[\frac{a_{45} - \frac{(a_{15}/a_{11})a_{41}}{2a_{41}}}{2a_{41}} \right] (a_{51} + a_{52})$$

$$b_{56} = a_{55} + a_{56} - \frac{a_{45}}{a_{41}} (a_{51} + a_{52})$$

$$b_{83} = -a_{83} + \frac{a_{63}}{a_{68}} a_{88} - \left[\frac{a_{73} - \frac{(a_{63}/a_{68})a_{78}}{a_{67}/a_{68}}}{a_{77} - \frac{(a_{67}/a_{68})a_{78}}{a_{67}/a_{68}}} \right] (a_{87} - \frac{a_{67}}{a_{68}} a_{88})$$

$$b_{84} = a_{84} - \frac{a_{64}}{a_{68}} a_{88} - \left[\frac{a_{74} - \frac{(a_{64}/a_{68})a_{78}}{a_{67}/a_{68}}}{a_{77} - \frac{(a_{67}/a_{68})a_{78}}{a_{67}/a_{68}}} \right] (a_{87} - \frac{a_{67}}{a_{68}} a_{88})$$

$$b_{85} = a_{85} - \frac{a_{15}}{a_{11}} a_{81} - \left[\frac{a_{45} - \frac{(a_{15}/a_{11})a_{41}}{2a_{41}}}{2a_{41}} \right] (a_{81} + a_{82})$$

$$b_{86} = a_{85} + a_{86} - \frac{a_{45}}{a_{41}} (a_{81} + a_{82})$$

$$b_{77} = a_{77} - \frac{a_{67}}{a_{68}} a_{78}$$

MRD DIVISION
GENERAL AMERICAN TRANSPORTATION CORPORATION

$$= \begin{vmatrix} a_{11} & 0 & 0 & 0 & 0 & 0 & 0 & 0 \\ 0 & -2a_{41} & 0 & 0 & 0 & 0 & 0 & 0 \\ 0 & 0 & b_{55} & 0 & 0 & 0 & 0 & 0 \\ 0 & 0 & 0 & b_{26} \frac{b_{56}b_{25}}{b_{55}} & b_{23} \frac{b_{33}b_{24}}{b_{34}} & 0 & 0 & 0 \\ 0 & 0 & 0 & b_{86} \frac{b_{56}b_{85}}{b_{55}} & b_{83} \frac{b_{33}b_{84}}{b_{34}} & 0 & 0 & 0 \\ 0 & 0 & 0 & 0 & 0 & b_{34} & 0 & 0 \\ 0 & 0 & 0 & 0 & 0 & 0 & b_{77} & 0 \\ 0 & 0 & 0 & 0 & 0 & 0 & 0 & a_{68} \end{vmatrix}$$

$$\Gamma = -2a_{11}a_{41}a_{68}b_{34}b_{55}b_{77} \left[\left(b_{26} \frac{b_{56}b_{25}}{b_{55}} \right) \left(b_{83} \frac{b_{33}b_{84}}{b_{34}} \right) - \left(b_{23} \frac{b_{33}b_{24}}{b_{34}} \right) \left(b_{86} \frac{b_{56}b_{85}}{b_{55}} \right) \right]$$

By a similar diagonalization process, we can find each of the $\|\Gamma_j\|$; e.g., (A.34)

$$\|\Gamma\| = \begin{vmatrix} -\bar{p}_{0,0} & a_{11} & 0 & 0 & a_{15} & -a_{15} & 0 & 0 \\ 0 & a_{22} & -a_{23} & -a_{24} & a_{25} & -a_{26} & -a_{27} & a_{28} \\ 0 & 0 & a_{33} & a_{34} & 0 & 0 & a_{37} & -a_{38} \\ 0 & -a_{41} & 0 & 0 & a_{45} & a_{45} & 0 & 0 \\ 0 & -a_{52} & 0 & 0 & a_{55} & a_{56} & 0 & 0 \\ 0 & 0 & a_{63} & -a_{64} & 0 & 0 & a_{67} & a_{68} \\ 0 & 0 & a_{73} & -a_{74} & 0 & 0 & a_{77} & a_{78} \\ 0 & -a_{82} & -a_{83} & a_{84} & a_{85} & a_{86} & -a_{87} & -a_{88} \end{vmatrix}$$

MRD DIVISION
GENERAL AMERICAN TRANSPORTATION CORPORATION

Proceeding just as before, we find

$$\| \Gamma \| = \begin{vmatrix} -\bar{p}_{0,0} & 0 & 0 & 0 & 0 & 0 & 0 & 0 & 0 \\ 0 & -a_{41} & 0 & 0 & 0 & 0 & 0 & 0 & 0 \\ 0 & 0 & c_{55} & 0 & 0 & 0 & 0 & 0 & 0 \\ 0 & 0 & 0 & c_{26} & b_{23} - \frac{b_{33}b_{24}}{b_{34}} & 0 & 0 & 0 & 0 \\ 0 & 0 & 0 & c_{86} & b_{83} - \frac{b_{33}b_{84}}{b_{34}} & 0 & 0 & 0 & 0 \\ 0 & 0 & 0 & 0 & 0 & b_{34} & 0 & 0 & 0 \\ 0 & 0 & 0 & 0 & 0 & 0 & b_{77} & 0 & 0 \\ 0 & 0 & 0 & 0 & 0 & 0 & 0 & 0 & a_{68} \end{vmatrix}$$

where

$$c_{55} = a_{55} - \frac{a_{45}}{a_{41}} a_{52}$$

$$c_{26} = -a_{26} + \frac{a_{45}}{a_{41}} a_{22} - \left(\frac{a_{56} - (a_{45}/a_{41})a_{52}}{a_{55} - (a_{45}/a_{41})a_{52}} \right) (a_{25} + \frac{a_{45}}{a_{41}} a_{22})$$

$$c_{86} = a_{86} - \frac{a_{45}}{a_{41}} a_{82} - \left(\frac{a_{56} - (a_{45}/a_{41})a_{52}}{a_{55} - (a_{45}/a_{41})a_{52}} \right) (a_{85} - \frac{a_{45}}{a_{41}} a_{82})$$

or

$$\| \Gamma \| = \bar{p}_{0,0} a_{41} a_{68} b_{34} c_{55} b_{77} [c_{26} (b_{83} - \frac{b_{33}b_{84}}{b_{34}}) - c_{86} (b_{23} - \frac{b_{33}b_{24}}{b_{34}})] \quad (A.35)$$

Thus after simplifying we find from equations (A.33) - (A.35) that

$$A_1 = - \frac{\bar{p}_{0,0} c_{55} [c_{26} (b_{83} b_{34} - b_{33} b_{84}) - c_{86} (b_{23} b_{34} - b_{33} b_{24})]}{2a_{11} [(b_{26} b_{55} - b_{56} b_{25}) (b_{83} b_{34} - b_{33} b_{84}) - (b_{86} b_{55} - b_{56} b_{85}) (b_{23} b_{34} - b_{33} b_{24})]}$$

(A.36)

MRD DIVISION
GENERAL AMERICAN TRANSPORTATION CORPORATION

Substituting into the definitions of the b and c coefficients the values of the a_{ij} , we have:

$$b_{23} = -p_2 e^{m h_1} - \frac{q_2^2 m n}{\mu_2 (n_2^2 + \xi^2)} \left[e^{m h_1} - 2 \frac{e^{m h_2} - e^{(m_2 + n_2) h_1 - n_2 h_2}}{n_2 (h_2 - h_1) - e^{n_2 (h_1 - h_2)}} \right]$$

$$b_{24} = -p_2 e^{-m h_1} - \frac{q_2^2 m n}{\mu_2 (n_2^2 + \xi^2)} \left[e^{-m h_1} + 2 \frac{e^{-m h_2} - e^{(n_2 - m_2) h_1 - n_2 h_2}}{n_2 (h_2 - h_1) - e^{n_2 (h_1 - h_2)}} \right]$$

$$b_{25} = q_1 (n_1 e^{n h_1} - m_1 e^{m h_1}) - \left(\frac{p_1 \mu_1 (n_1^2 + \xi^2) - q_1^2 m n}{2 q_1 m_1} \right) (e^{n h_1} - e^{m h_1})$$

$$b_{26} = q_1 n_1 (e^{n h_1} - e^{n h_1}) - \frac{p_1 \mu_1 (n_1^2 + \xi^2)}{q_1 m_1} (e^{n h_1} - e^{m h_1})$$

$$b_{33} = p_2 e^{m h_2} + \frac{q_2^2 m n}{\mu_2 (n_2^2 + \xi^2)} \left[e^{(m_2 + n_2) h_1 - n_2 h_2} - \frac{e^{m h_2} - e^{(n_2 + m_2) h_1 - n_2 h_2}}{n_2 h_2 - e^{2 n h_1 - n h_2}} (e^{n h_2} + e^{2 n h_1 - n h_2}) \right]$$

$$b_{34} = p_2 e^{-m h_2} - \frac{q_2^2 m n}{\mu_2 (n_2^2 + \xi^2)} \left[e^{(n_2 - m_2) h_1 - n_2 h_2} - \frac{e^{-m h_2} - e^{(n_2 - m_2) h_1 - n_2 h_2}}{n_2 h_2 - e^{2 n h_1 - n h_2}} (e^{n h_2} + e^{2 n h_1 - n h_2}) \right]$$

$$b_{55} = \mu_1 (n_1^2 + \xi^2) (e^{n h_1} - e^{m h_1} - e^{m h_1}) - \frac{q_1^2 m n}{2 p_1} (e^{n h_1} - e^{m h_1})$$

$$b_{56} = \mu_1 (n_1^2 + \xi^2) (e^{n h_1} + e^{n h_1} - e^{m h_1} - e^{m h_1})$$

$$b_{77} = \mu_2 (n_2^2 + \xi^2) (e^{n h_2} - e^{2 n h_1 - n h_2})$$

$$b_{83} = m_2 \left[\frac{q_2 \xi}{\mu_2 (n_2^2 + \xi^2)} - 1 \right] e^{m h_1}$$

$$b_{84} = m_2 \left[1 - \frac{q_2 \xi}{\mu_2 (n_2^2 + \xi^2)} \right] e^{-m h_1}$$

MRD DIVISION
GENERAL AMERICAN TRANSPORTATION CORPORATION

$$\begin{aligned}
b_{55} &= \xi e^{\frac{n h}{1}} - \frac{q_1 m n}{2 p_1} e^{\frac{m h}{1}} - \frac{\mu_1 (n^2 + \xi^2)}{2 q_1} (e^{\frac{m h}{1}} + e^{-\frac{m h}{1}}) \\
b_{56} &= \xi (e^{\frac{n h}{1}} + e^{-\frac{n h}{1}}) - \frac{\mu_1 (n^2 + \xi^2)}{q_1} (e^{\frac{m h}{1}} + e^{-\frac{m h}{1}}) \\
c_{26} &= \frac{p_1 \mu_1 (n^2 + \xi^2)}{q_1 m_1} \left[\frac{e^{\frac{(n-m_1) h_1}{1}} - e^{\frac{(-n-m_1) h_1}{1}}}{e^{\frac{n h}{1}} - e^{-\frac{m h}{1}}} \right] - q_1 n_1 \left[\frac{2 - e^{\frac{(n-m_1) h_1}{1}} - e^{\frac{(-n-m_1) h_1}{1}}}{e^{\frac{n h}{1}} - e^{-\frac{m h}{1}}} \right] \\
c_{55} &= \mu_1 (n^2 + \xi^2) (e^{\frac{n h}{1}} - e^{-\frac{m h}{1}}) \\
c_{56} &= \left[\xi - \frac{\mu_1 (n^2 + \xi^2)}{q_1} \right] \left[\frac{e^{\frac{(n-m_1) h_1}{1}} - e^{\frac{(-n-m_1) h_1}{1}}}{e^{\frac{n h}{1}} - e^{-\frac{m h}{1}}} \right]
\end{aligned}
\tag{A.37}$$

Substituting (A.37) into (A.36):

$$\begin{aligned}
A_1 &= -\bar{p}_{0,0} \mu_1 (n^2 + \xi^2) (e^{\frac{n h}{1}} - e^{-\frac{m h}{1}}) \times \\
&\quad \left\{ \left[\frac{p_1 \mu_1 (n^2 + \xi^2)}{q_1 m_1} \left(\frac{e^{\frac{(n-m_1) h_1}{1}} - e^{\frac{(-n-m_1) h_1}{1}}}{e^{\frac{n h}{1}} - e^{-\frac{m h}{1}}} \right) - q_1 n_1 \left(\frac{2 - e^{\frac{(n-m_1) h_1}{1}} - e^{\frac{(-n-m_1) h_1}{1}}}{e^{\frac{n h}{1}} - e^{-\frac{m h}{1}}} \right) \right] \right. \\
&\quad \left. \left[m_2 \left(\frac{q_2 \xi}{\mu_2 (n^2 + \xi^2)} - 1 \right) e^{\frac{m h}{2}} \right] \right\} \\
&\quad \left[p_2 e^{-\frac{m h}{2}} - \frac{q_2^2 m n}{\mu_2 (n^2 + \xi^2)} \left(e^{\frac{(n-m_2) h_1 - n h_2}{2}} - \frac{e^{-\frac{m h}{2}} - e^{\frac{(n-m_2) h_1 - n h_2}{2}}}{e^{\frac{n h}{2}} - e^{-\frac{m h}{2}}} \right) (e^{\frac{n h}{2}} + e^{\frac{2n h - n h_2}{2}}) \right] \\
&\quad - \left[m_2 \left(1 - \frac{q_2 \xi}{\mu_2 (n^2 + \xi^2)} \right) e^{-\frac{m h}{2}} \right] \left[\right]
\end{aligned}$$

MRD DIVISION
GENERAL AMERICAN TRANSPORTATION CORPORATION

$$\begin{aligned}
& \left[p_2 e^{\frac{m_2 h_2}{2}} + \frac{q_2^2 m_2 n_2}{\mu_2 (n_2^2 + \xi^2)} \left(e^{\frac{(n_2 + m_2) h_1 - n_2 h_2}{2}} \frac{(e^{\frac{m_2 h_2}{2}} - e^{\frac{(n_2 + m_2) h_1 - n_2 h_2}{2}})(e^{\frac{n_2 h_2}{2}} + e^{\frac{2n_2 h_1 - n_2 h_2}{2}})}{e^{\frac{n_2 h_2}{2}} - e^{\frac{2n_2 h_1 - n_2 h_2}{2}}} \right) \right] \\
& - \left[\left(\xi - \frac{\mu_1 (n_1^2 + \xi^2)}{q_1} \right) \cdot \left(\frac{e^{\frac{(n_1 - m_1) h_1}{2}} - e^{\frac{(-n_1 - m_1) h_1}{2}}}{e^{\frac{n_1 h_1}{2}} - e^{\frac{-m_1 h_1}{2}}} \right) \right] \\
& \left[-p_2 e^{\frac{m_2 h_1}{2}} - \frac{q_2^2 m_2 n_2}{\mu_2 (n_2^2 + \xi^2)} \left(e^{\frac{m_2 h_1 - 2}{2}} \frac{e^{\frac{m_2 h_2}{2}} - e^{\frac{(m_2 + n_2) h_1 - n_2 h_2}{2}}}{e^{\frac{n_2 (h_2 - h_1)}{2}} - e^{\frac{n_2 (h_1 - h_2)}{2}}} \right) \right] \\
& \left[p_2 e^{-\frac{m_2 h_2}{2}} - \frac{q_2^2 m_2 n_2}{\mu_2 (n_2^2 + \xi^2)} \left(e^{\frac{(n_2 - m_2) h_1 - n_2 h_2}{2}} \frac{(e^{-\frac{m_2 h_2}{2}} - e^{\frac{(n_2 - m_2) h_1 - n_2 h_2}{2}})(e^{\frac{n_2 h_2}{2}} + e^{\frac{2n_2 h_1 - n_2 h_2}{2}})}{e^{\frac{n_2 h_2}{2}} - e^{\frac{2n_2 h_1 - n_2 h_2}{2}}} \right) \right] \\
& - \left[p_2 e^{\frac{m_2 h_2}{2}} + \frac{q_2^2 m_2 n_2}{\mu_2 (n_2^2 + \xi^2)} \left(e^{\frac{(m_2 + n_2) h_1 - n_2 h_2}{2}} \frac{(e^{\frac{m_2 h_2}{2}} - e^{\frac{(m_2 + n_2) h_1 - n_2 h_2}{2}})(e^{\frac{n_2 h_2}{2}} + e^{\frac{2n_2 h_1 - n_2 h_2}{2}})}{e^{\frac{n_2 h_2}{2}} - e^{\frac{2n_2 h_1 - n_2 h_2}{2}}} \right) \right] \\
& \left[-p_2 e^{-\frac{m_2 h_1}{2}} - \frac{q_2^2 m_2 n_2}{\mu_2 (n_2^2 + \xi^2)} \left(e^{-\frac{m_2 h_1 + 2}{2}} \frac{e^{-\frac{m_2 h_2}{2}} - e^{\frac{(n_2 - m_2) h_1 - n_2 h_2}{2}}}{e^{\frac{n_2 (h_2 - h_1)}{2}} - e^{\frac{n_2 (h_1 - h_2)}{2}}} \right) \right] \Bigg\} / \\
& 2p_1 \left\{ \left[\left[q_1 n_1 (e^{\frac{n_1 h_1}{2}} - e^{\frac{-n_1 h_1}{2}}) - \frac{p_1 \mu_1 (n_1^2 + \xi^2)}{q_1 m_1} (e^{\frac{m_1 h_1}{2}} - e^{\frac{-m_1 h_1}{2}}) \right] \right. \right. \\
& \left[\mu_1 (n_1^2 + \xi^2) (e^{\frac{n_1 h_1}{2}} - e^{\frac{m_1 h_1}{2}} - e^{\frac{-m_1 h_1}{2}}) - \frac{q_1^2 m_1 n_1}{2p_1} (e^{\frac{m_1 h_1}{2}} - e^{\frac{-m_1 h_1}{2}}) \right] \\
& \left. - \left[q_1 (n_1 e^{\frac{n_1 h_1}{2}} - m_1 e^{\frac{m_1 h_1}{2}}) - \frac{p_1 \mu_1 (n_1^2 + \xi^2) - q_1^2 m_1 n_1}{2q_1 m_1} (e^{\frac{m_1 h_1}{2}} - e^{\frac{-m_1 h_1}{2}}) \right] \right. \\
& \left. \left[\mu_1 (n_1^2 + \xi^2) (e^{\frac{n_1 h_1}{2}} + e^{\frac{-n_1 h_1}{2}} - e^{\frac{m_1 h_1}{2}} - e^{\frac{-m_1 h_1}{2}}) \right] \right] \\
& \left[\left[p_2 e^{-\frac{m_2 h_2}{2}} - \frac{q_2^2 m_2 n_2}{\mu_2 (n_2^2 + \xi^2)} \left(e^{\frac{(n_2 - m_2) h_1 - n_2 h_2}{2}} \frac{(e^{-\frac{m_2 h_2}{2}} - e^{\frac{(n_2 - m_2) h_1 - n_2 h_2}{2}})(e^{\frac{n_2 h_2}{2}} + e^{\frac{2n_2 h_1 - n_2 h_2}{2}})}{e^{\frac{n_2 h_2}{2}} - e^{\frac{2n_2 h_1 - n_2 h_2}{2}}} \right) \right] \right]
\end{aligned}$$

MRD DIVISION
GENERAL AMERICAN TRANSPORTATION CORPORATION

$$\begin{aligned}
& \left[\left(\frac{q_2 \xi}{\mu_2 (n_2^2 + \xi^2)} - 1 \right) m_2 e^{m_2 h_1} \right] - \left[\left(1 - \frac{q_2 \xi}{\mu_2 (n_2^2 + \xi^2)} \right) m_2 e^{-m_2 h_1} \right] \\
& \left[p_2 e^{m_2 h_2} + \frac{q_2^2 m_2 n_2}{\mu_2 (n_2^2 + \xi^2)} \left(e^{(m_2 + n_2) h_1 - n_2 h_2} \frac{e^{m_2 h_2} - e^{(n_2 + m_2) h_1 - n_2 h_2}}{n_2 h_2 - e^{2n_2 h_1} - n_2 h_2} \right) \right] \\
& - \left[\left[\xi (e^{n_1 h_1 + e^{-n_1 h_1}}) - \frac{\mu_1 (n_1^2 + \xi^2)}{q_1} (e^{m_1 h_1 + e^{-m_1 h_1}}) \right] \right. \\
& \quad \left[\mu_1 (n_1^2 + \xi^2) (e^{n_1 h_1} - e^{m_1 h_1} - e^{-m_1 h_1}) - \frac{q_1^2 m_1 n_1}{2p_1} (e^{m_1 h_1} - e^{-m_1 h_1}) \right] \\
& \quad - \left[\mu_1 (n_1^2 + \xi^2) (e^{n_1 h_1 + e^{-n_1 h_1}} - e^{m_1 h_1} - e^{-m_1 h_1}) \right] \\
& \quad \left. \left[\xi e^{n_1 h_1} - \frac{q_1 m_1 n_1}{2p_1} e^{m_1 h_1} - \frac{\mu_1 (n_1^2 + \xi^2)}{2q_1} (e^{m_1 h_1} + e^{-m_1 h_1}) \right] \right] \\
& \left[\left[-p_2 e^{m_2 h_1} - \frac{q_2^2 m_2 n_2}{\mu_2 (n_2^2 + \xi^2)} \left(e^{m_2 h_1 - 2} \frac{e^{m_2 h_2} - e^{(n_2 + m_2) h_1 - n_2 h_2}}{n_2 (h_2 - h_1) - e^{2n_2 h_1} - n_2 h_2} \right) \right] \right. \\
& \quad \left[p_2 e^{-m_2 h_2} - \frac{q_2^2 m_2 n_2}{\mu_2 (n_2^2 + \xi^2)} \left(e^{(n_2 - m_2) h_1 - n_2 h_2} \frac{e^{-m_2 h_2} - e^{(n_2 - m_2) h_1 - n_2 h_2}}{n_2 h_2 - e^{2n_2 h_1} - n_2 h_2} \right) \right] \\
& \quad - \left[p_2 e^{m_2 h_2} + \frac{q_2^2 m_2 n_2}{\mu_2 (n_2^2 + \xi^2)} \left(e^{(m_2 + n_2) h_1 - n_2 h_2} \frac{e^{m_2 h_2} - e^{(n_2 + m_2) h_1 - n_2 h_2}}{n_2 h_2 - e^{2n_2 h_1} - n_2 h_2} \right) \right] \\
& \quad \left. \left[-p_2 e^{-m_2 h_1} - \frac{q_2^2 m_2 n_2}{\mu_2 (n_2^2 + \xi^2)} \left(e^{-m_2 h_1 + 2} \frac{e^{-m_2 h_2} - e^{(n_2 - m_2) h_1 - n_2 h_2}}{n_2 (h_2 - h_1) - e^{2n_2 h_1} - n_2 h_2} \right) \right] \right] \Bigg\}
\end{aligned}$$

(A.38)

MRD DIVISION
GENERAL AMERICAN TRANSPORTATION CORPORATION

Similar expressions can be found for A_2, \dots, A_8 .

The substitution variables m_1, n_1, p_1, q_1 can be expressed in terms of the original material parameters λ_1, μ_1, ρ_1 and the variables ξ, s by

$$\begin{aligned}
 m_1 &= \sqrt{\xi^2 + s^2} \\
 m_2 &= \sqrt{\xi^2 + \frac{\rho_2(\lambda_1 + 2\mu_1)}{\rho_1(\lambda_2 + 2\mu_2)} s^2} \\
 n_1 &= \sqrt{\xi^2 + \frac{\lambda_1 + 2\mu_1}{\mu_1} s^2} \\
 n_2 &= \sqrt{\xi^2 + \frac{\rho_2(\lambda_1 + 2\mu_1)}{\rho_1 \mu_2} s^2} \\
 p_1 &= 2\mu_1 \xi^2 + (\lambda_1 + 2\mu_1) s^2 \\
 p_2 &= 2\mu_2 \xi^2 + \frac{\rho_2}{\rho_1} (\lambda_1 + 2\mu_1) s^2 \\
 q_1 &= 2\mu_1 \xi \\
 q_2 &= 2\mu_2 \xi
 \end{aligned} \tag{A.39}$$

The coefficients A_j can then be evaluated and $\bar{\phi}_{1,0}, \bar{\phi}_{2,0}, \bar{\theta}_{1,1}, \bar{\theta}_{2,1}$ can be immediately determined from equations (A.15) - (A.18).

A.VIII Inversion and Stress Solution

Once $\bar{\phi}_{1,0}$ and $\bar{\theta}_{1,1}$ are known, ϕ_1 and θ_1 are obtained through application of the inversion formulae

$$\phi_1 = \frac{1}{2\pi i} \int_{Br_1} \int_0^\infty \xi \bar{\phi}_{1,0} J_0(r\xi) e^{s\tau} ds d\xi \tag{A.40}$$

MRD DIVISION
GENERAL AMERICAN TRANSPORTATION CORPORATION

$$\theta_1 = \frac{1}{2\pi i} \int_{\Gamma} \int_0^{\infty} \xi \bar{\theta}_{1,1} J_1(r\xi) e^{s\tau} ds d\xi \quad (\text{A.41})$$

The stresses $\sigma_r^{(1)}, \sigma_{\theta}^{(1)}, \sigma_z^{(1)}, \tau_{rz}^{(1)}$ can then be obtained directly from ϕ_1 and θ_1 by equations (A.5) - (A.8).

MRD DIVISION
GENERAL AMERICAN TRANSPORTATION CORPORATION

BIBLIOGRAPHY

1. W. M. Ewing, W. S. Jardetzky, and F. Press, "Elastic Waves in Layered Media", 1957; McGraw Hill
2. C. M. Ablow, R. Alverson, F. C. Gair, and F. M. Sauer, "Theoretical Study of Ground Motion Induced in Nonhomogeneous Media by Nuclear Explosions", 1960; Stanford Research Institute under Contract AF 29(601)-1948 with AFSWC.
3. G. Cinelli and L. E. Fugelso, "Theoretical Study of Ground Motion Produced by Nuclear Bursts", 1959; Mechanics Research Division, American Machine and Foundry Company under Contract AF 29(601)-1190 with AFSWC.
4. J. B. Harkin, "Theoretical Study of Energy Distribution in a Half-Space Under Dynamic Loads", 1962; Mechanics Research Division, General American Transportation Corporation under Contract AF 29(601)-2832 with AFSWC.
5. L. E. Fugelso, A. A. Arentz, Jr., and J. J. Poczatek, "Mechanics of Penetration", Volume I, 1961; Mechanics Research Division, American Machine and Foundry Company under Contract DA-19-129-QM-1542.

MRD DIVISION
GENERAL AMERICAN TRANSPORTATION CORPORATION

UNCLASSIFIED

UNCLASSIFIED